

Appendix 1

国内外の学会等での事業成果発表 [投稿ポスターおよび論文]

- Appendix-1_1** Framework of probabilistic and deterministic methods for evaluating near-fault displacement
- Appendix-1_2** Earthquake surface rupture (fault displacement) assessment using dynamic rupture models: Case study of the 1999 Chi-chi Taiwan earthquake
- Appendix-1_3** Study on the evaluation method for fault displacement based on characterized source model
- Appendix-1_4** Stress drop inferred from dynamic rupture simulations consistent with Moment-Rupture area empirical scaling models: Effects of weak shallow zone
- Appendix-1_5** Study on the Evaluation Method for Fault Displacement: Probabilistic Approach Based on Japanese Earthquake Rupture Data -Principal fault displacements-
- Appendix-1_6** Study on the Evaluation Method for Fault Displacement: Probabilistic Approach Based on Japanese Earthquake Rupture Data -Distributed fault displacements-
- Appendix-1_7** PERMANENT DISPLACEMENT FROM SURFACE-RUPTURING EARTHQUAKES: INSIGHTS FROM DYNAMIC RUPTURE OF Mw7.6 1999 CHI-CHI EARTHQUAKE
- Appendix-1_8** Study on the evaluation method for fault displacement: Deterministic evaluation approach based three step considerations.
- Appendix-1_9** Study on the Evaluation Method for Fault Displacement: Probabilistic Approach Based on Japanese Earthquake Rupture Data - Principal fault displacements along the fault-
- Appendix-1_10** Investigation of off-fault displacement

Framework of probabilistic and deterministic methods for evaluating near-fault displacement

Inoue, N.¹, Tonagi, M.², Takahama, T.², Matsumoto, Y.², Kitada, N.¹, Dalguer, Luis A.³ and Irikura, K.³

¹Geo-Research Institute (GRI), Osaka, Japan

²Kozo Keikaku Engineering, Inc. (KKE), Tokyo, Japan

³Aichi Institute of Technology (AIT), Toyota, Japan

E-mail contact of main author: naoto@geor.or.jp

1 Introduction

In IAEA Specific Safety Guide (SSG)-9 (INTERNATIONAL ATOMIC ENERGY AGENCY, 2010), section 8.10 describes that probabilistic methods for evaluating fault displacement should be used if no sufficient basis is provided to decide conclusively that the fault is not capable by using the deterministic methodology described in section 8.3-8.7. In addition, International Seismic Safety Centre (ISSC) published it as ANNEX of Safety Reports Series No. 85 (Ground Motion Simulation Based on Fault Rupture Modelling for Seismic Hazard Assessment in Site Evaluation for Nuclear Installations: IAEA, 2015) to realize seismic hazard for Nuclear Installations described in SSG-9 and shows the utility of the deterministic and probabilistic evaluation methods for fault displacement in the annex of the safety report. In the SSG-9, two types of fault displacement are introduced: primary fault and secondary fault displacements. In Japan, New Regulatory Requirements (Nuclear Regulation Authority, NRA) require that important nuclear facilities shall be established on ground where fault displacement will not arise when earthquakes occur in the future. In other words, nuclear facilities important to seismic safety have been prohibited from constructing on the ground with occurrence of fault displacement. Therefore, it is important to obtain the-state-of-art knowledge on fault displacement. Under these situations, we need to develop the evaluation methods for fault displacement of primary and secondary faults. We are studying deterministic and probabilistic evaluating methods to evaluate the fault displacements

based on tentative analyses of observed records such as surface earthquake faults and near-fault strong ground motions from inland crustal earthquake accompanied by fault displacements.

2 Deterministic Evaluation Approach

We attempt to estimate fault displacements using slip distributions on source faults dynamically evaluated based on a characterized source model explaining observed near-fault broad band ground motions. First, the characterized source models are estimated with forward modeling using empirical Green's function method and theoretical method (IAEA, 2015). Second, slip distributions on source faults are dynamically evaluated based on the characterized source models. The validity of dynamically constructed slip distributions are examined by comparison of observed waveforms and synthetic waveforms estimated by dynamic simulation. Referring the dynamically constructed slip distributions, we study an evaluation method for surface fault displacement using finite element method and hybrid method, which combines particle method and distinct element method. For an example, we show the result tentatively developed for the 1999 Chi-Chi earthquake.

3 Probabilistic Evaluation Approach

In the probabilistic evaluation approach, Probabilistic Fault Displacement Hazard Analysis (PFDHA), there are two types of fault displacement related to the earthquake fault: principal fault displacement and distributed fault displacement. As mentioned above, distributed fault displacement should be evaluated in important facilities, such as Nuclear Installations. Youngs et al. (2003) defined the distributed fault as fault displacement on other faults or shears, or fractures in the vicinity of the principal rupture in response to the principal faulting. Other researchers treated the data of distributed fault around principal fault and modeled according to their definitions (e.g. Petersen et al., 2011; Takao et al., 2013, 2014). Their distributed fault displacement data exclude some kind of displacement, such as triggered displacement, landslide, from secondary fault displacement described in the

SSG-9. We compiled fault displacement in and around Japan and constructed the slip-distance relationship depending on fault types.

4 Concluding Remarks

In the current status, the results of the numerical simulation show the surface stress change strongly depends on the geometry of the fault and the physical property of surface materials. In the result of the PFDHA, slip-distance relationship of distributed fault displacement (reverse fault) on the foot-wall indicated difference trend compared with that on hanging-wall, although the fault displacement data in PFDHA are sparse because we arrange fault displacement data into each mechanism. We will integrate the both results to better understand the distributed fault displacement in the future.

Acknowledgment: This research was part of the 2014-2015 research project ‘Development of evaluating method for fault displacement’ by the Secretariat of Nuclear Regulation Authority (S/NRA), Japan.

- [1] INTERNATIONAL ATOMIC ENERGY AGENCY (2010) Seismic Hazards in Site Evaluation for Nuclear Installations, IAEA Safety Standards Series, No. SSG-9, Vienna: INTERNATIONAL ATOMIC ENERGY AGENCY.
- [2] INTERNATIONAL ATOMIC ENERGY AGENCY (2015) Ground Motion Simulation Based on Fault Rupture Modelling for Seismic Hazard Assessment in Site Evaluation for Nuclear Installations, IAEA Safety Reports Series, No. 85, Vienna: INTERNATIONAL ATOMIC ENERGY AGENCY.
- [3] Youngs, Robert R., Arabasz, Walter J., Anderson, R. Ernest, Ramelli, Alan R., Ake, Jon P., Slemmons, David B., McCalpin, James P., Doser, Diane I., Fridrich, Christopher J., Swan, Frank H., Rogers, Albert M., Yount, James C., Anderson, Laurence W., Smith, Kenneth D., Bruhn, Ronald L., Knuepfer, Peter L. K., Smith, Robert B., dePolo, Craig M., O’Leary, Dennis W., Coppersmith, Kevin J., Pezzopane, Silvio K., Schwartz, David P., Whitney, John W., Olig, Susan S., and Toro, Gabriel R. (2003)

A Methodology for Probabilistic Fault Displacement Hazard Analysis (PFDHA), *Earthquake Spectra*, Vol. 19, No. 1, pp. 191-219.

- [4] Petersen, Mark D., Dawson, Timothy E., Chen, Rui, Cao, Tianqing, Wills, David P.; Frankel Arthur D. Petersen Mark D., Christopher J.; Schwartz, Dawson, Timothy E., Chen, Rui, Cao, Tianqing, Wills, Christopher J., Schwartz, David P., and Frankel, Arthur D. (2011) Fault displacement hazard for strike-slip faults, *Bulletin of the Seismological Society of America*, Vol. 101, No. 2, pp. 805-825.
- [5] Takao, Makoto, Tsuchiyama, Jiro, Annaka, Tadashi, and Kurita, Tetsushi (2013) Application of Probabilistic Fault Displacement Hazard Analysis in Japan, *Journal of Japan Association for Earthquake Engineering*, Vol. 13, No. 1, pp. 17-32.
- [6] Takao, Makoto, Ueta, Keiichi, Annaka, Tadashi, Kurita, Tetsushi, Nakase, Hitoshi, Kyoya, Takashi, and Kato, Junji (2014) Reliability Improvement of Probabilistic Fault Displacement Hazard Analysis, *Journal of Japan Association for Earthquake Engineering*, Vol. 14, No. 2, pp. 216-236.

Earthquake surface rupture (fault displacement) assessment using dynamic rupture models: Case study of the 1999 Chi-chi Taiwan earthquake

By Luis A. Dalguer¹, Kojiro Irikura², Hao Wu² and KKE Team³

¹swissnuclear, Aarauerstrasse 55, 4601 Olten, Switzerland

²Aichi Institute of Technology, Japan

³KOZO KEIKAKU ENGINEERING Inc, Japan

Large fault displacements resulted from surface-rupturing faulting have been observed during the 1999 Chi-Chi, Taiwan, earthquake, reaching amplitudes over 15 m. This observation provides excellent opportunity to investigate the causative features of fault displacements of such as large events. In this paper we evaluate the effect of fault mechanism, fault geometry, buried rupture and weak shallow layer (WSL) zone on the surface rupturing. Rupture in the WSL zone is expected to operate with enhanced energy absorption mechanism. The problem is tackled by using spontaneous dynamic rupture simulations of asperity models that break the free-surface. The asperities represent the so-called Strong Motion Generation Areas (SMGA), as defined by Miyake et al (2003) and Irikura and Miyake (2011). The characterized source model consists of several SMGAs/Asperities with high stress drops and the background area with low stress drop. The WSL is assumed to have 2km depth and parameterized with zero or negative stress drop. After simulating the ground motion and fault displacement of the Chi-chi earthquake, we vary the characteristics of the SWL, geometry of the dipping fault, buried rupture and fault mechanism. Our simulations show that the asperities are the main driver elements to break the shallow layer and free-surface. But the WSL characteristics define the amplitude of the fault displacement. Characterizing the WSL in term of stress drop, we found that the WSL with zero stress drop produces larger slip and peak slip velocities than the one with negative stress drop. Zero stress drop on the shallow zone may over-predicts ground motion and permanent displacement, leading to unrealistic scenarios. Suggesting that the WSL plays an important role on the prediction of final slip and fault displacement. Buried rupture inhibits the extension of the fault rupture along strike. In our case study, if rupture stop at 2.0km depth (i.e. it does not break the shallow layer) the rupture along strike stops earlier. However, at 1km depth, the rupture successfully extends along the whole fault area. This suggests that when rupture approaches to the free-surface, the chance to the rupture become larger along strike increases significantly. A reverse rupture with lower dip angle is more capable to break the free-surface than fault with large dip angle. In our case study, we show that a vertical dipping fault is un-capable to break the free-surface, consequently rupture does not extend along strike. A vertical strike slip fault with the same parameterization as the reverse fault does not break the free-surface and neither rupture extend further along strike. Therefore, a strike slip fault ruptures less area than the vertical dipping fault, suggesting that dipping faults are more capable to brake larger area and producing larger fault displacements than strike slip faults.

Title:

Study on the evaluation method for fault displacement based on characterized source model

Author:

M. TONAGI¹⁾, T. TAKAHAMA¹⁾, Y. MATSUMOTO¹⁾, N. INOUE²⁾,
K. IRIKURA³⁾, LUIS ANGEL DALGUER³⁾

1) Kozo Keikaku Engineering, 2) Geo-Research Institute, 3) Aichi Institute of Technology

Abstract:

In IAEA Specific Safety Guide (SSG) 9 describes that probabilistic methods for evaluating fault displacement should be used if no sufficient basis is provided to decide conclusively that the fault is not capable by using the deterministic methodology. In addition, International Seismic Safety Centre compiles as ANNEX to realize seismic hazard for nuclear facilities described in SSG-9 and shows the utility of the deterministic and probabilistic evaluation methods for fault displacement.

In Japan, it is required that important nuclear facilities should be established on ground where fault displacement will not arise when earthquakes occur in the future.

Under these situations, based on requirements, we need develop evaluation methods for fault displacement to enhance safety in nuclear facilities. We are studying deterministic and probabilistic methods with tentative analyses using observed records such as surface fault displacement and near-fault strong ground motions of inland crustal earthquake which fault displacements arose. In this study, we introduce the concept of evaluation methods for fault displacement. After that, we show parts of tentative analysis results for deterministic method as follows:

(1) For the 1999 Chi-Chi earthquake, referring slip distribution estimated by waveform inversion, we construct a characterized source model (Miyake et al., 2003, BSSA) which can explain observed near-fault broad band strong ground motions.

(2) Referring a characterized source model constructed in (1), we study an evaluation method for surface fault displacement using hybrid method, which combines particle method and distinct element method.

At last, we suggest one of the deterministic method to evaluate fault displacement based on characterized source model.

This research was part of the 2015 research project ‘Development of evaluating method for fault displacement’ by the Secretariat of Nuclear Regulation Authority (S/NRA), Japan.

Title:

Stress drop inferred from dynamic rupture simulations consistent with Moment-Rupture area empirical scaling models: Effects of weak shallow zone

Author:

LUIS ANGEL DALGUER^{1),3)}, HIROE MIYAKE²⁾, KOJIRO IRIKURA¹⁾, HAO WO¹⁾

1)Aichi Institute of Technology, 2)University of Toyo, 3)Swissnuclear

Abstract:

Empirical scaling models of seismic moment and rupture area provide constraints to parameterize source parameters, such as stress drop, for numerical simulations of ground motion. There are several scaling models published in the literature. The effect of the finite width seismogenic zone and the free-surface have been attributed to cause the breaking of the well know self-similar scaling (e.g. Dalguer et al, 2008) given origin to the so called L and W models for large faults. These models imply the existence of three-stage scaling relationship between seismic moment and rupture area (e.g. Irikura and Miyake, 2011). In this paper we extend the work done by Dalguer et al 2008, in which these authors calibrated fault models that match the observations showing that the average stress drop is independent of earthquake size for buried earthquakes, but scale dependent for surface-rupturing earthquakes. Here we have developed additional sets of dynamic rupture models for vertical strike slip faults to evaluate the effect of the weak shallow layer (WSL) zone for the calibration of stress drop. Rupture in the WSL zone is expected to operate with enhanced energy absorption mechanism. The set of dynamic models consists of fault models with width 20km and fault length $L=20\text{km}, 40\text{km}, 60\text{km}, 80\text{km}, 100\text{km}, 120\text{km}, 200\text{km}, 300\text{km}$ and 400km and average stress drop values of $2.0\text{MPa}, 2.5\text{MPa}, 3.0\text{MPa}, 3.5\text{MPa}, 5.0\text{MPa}$ and 7.5MPa . For models that break the free-surface, the WSL zone is modeled assuming a 2km width with stress drop 0.0MPa or -2.0MPa . Our results show that depending on the characterization of the WSL zone, the average stress drop at the seismogenic zone that fit the empirical models changes. If WSL zone is not considered, that is, stress drop at SL zone is the same as the seismogenic zone, average stress drop is about 20% smaller than models with WSL zone. By introducing more energy absorption at the SL zone, that could be the case of large mature faults, the average stress drop in the seismogenic zone increases. Suggesting that large earthquakes need higher stress drop to break the fault than buried and moderate earthquakes. Therefore, the value of the average stress drop for large events that break the free-surface depend on the definition of the WSL. Suggesting that the WSL plays an important role on the prediction of final slip and fault displacement.

Title:

Study on the Evaluation Method for Fault Displacement: Probabilistic Approach Based on Japanese Earthquake Rupture Data - Principal fault displacements -

Author:

N.KITADA¹⁾, N. INOUE¹⁾, M. TONAGI²⁾

1) Geo-Research Institute, 2) Kozo Keikaku Engineering

Abstract:

The purpose of Probabilistic Fault Displacement Hazard Analysis (PFDHA) is estimate fault displacement values and its extent of the impact. There are two types of fault displacement related to the earthquake fault: principal fault displacement and distributed fault displacement. Distributed fault displacement should be evaluated in important facilities, such as Nuclear Installations. PFDHA estimates principal fault and distributed fault displacement. For estimation, PFDHA uses distance-displacement functions, which are constructed from field measurement data. We constructed slip distance relation of principal fault displacement based on Japanese strike and reverse slip earthquakes in order to apply to Japan area that of subduction field. However, observed displacement data are sparse, especially reverse faults. Takao et al. (2013) tried to estimate the relation using all type fault systems (reverse fault and strike slip fault). After Takao et al. (2013), several inland earthquakes were occurred in Japan, so in this time, we try to estimate distance-displacement functions each strike slip fault type and reverse fault type especially add new fault displacement data set.

To normalized slip function data, several criteria were provided by several researchers. We normalized principal fault displacement data based on several methods and compared slip-distance functions. The normalized by total length of Japanese reverse fault data did not show particular trend slip distance relation. In the case of segmented data, the slip-distance relationship indicated similar trend as strike slip faults. We will also discuss the relation between principal fault displacement distributions with source fault character. According to slip distribution function (Petersen et al., 2011), strike slip fault type shows the ratio of normalized displacement are decreased toward to the edge of fault. However, the data set of Japanese strike slip fault data not so decrease in the end of the fault. This result indicates that the fault displacement is difficult to appear at the edge of the fault displacement in Japan.

This research was part of the 2014-2015 research project 'Development of evaluating method for fault displacement' by the Secretariat of Nuclear Regulation Authority (NRA), Japan.

Title:

Study on the Evaluation Method for Fault Displacement: Probabilistic Approach Based on Japanese Earthquake Rupture Data - Distributed fault displacements -

Author:

N. INOUE¹⁾, N. KITADA¹⁾, M. TONAGI²⁾

1) Geo-Research Institute, 2) Kozo Keikaku Engineering

Abstract:

Distributed fault displacements in Probabilistic Fault Displacement Analysis (PFDHA) have an important role in evaluation of important facilities such as Nuclear Installations. In Japan, the Nuclear Installations should be constructed where there is no possibility that the displacement by the earthquake on the active faults occurs. Youngs et al. (2003) defined the distributed fault as displacement on other faults or shears, or fractures in the vicinity of the principal rupture in response to the principal faulting. Other researchers treated the data of distribution fault around principal fault and modeled according to their definitions (e.g. Petersen et al., 2011; Takao et al., 2013).

We organized Japanese fault displacements data and constructed the slip-distance relationship depending on fault types. In the case of reverse fault, slip-distance relationship on the foot-wall indicated difference trend compared with that on hanging-wall. The process zone or damaged zone have been studied as weak structure around principal faults. The density or number is rapidly decrease away from the principal faults. We contrasted the trend of these zones with that of distributed slip-distance distributions.

The subsurface FEM simulation have been carried out to investigate the distribution of stress around principal faults. The results indicated similar trend compared with the distribution of field observations. This research was part of the 2014-2015 research project 'Development of evaluating method for fault displacement' by the Secretariat of Nuclear Regulation Authority (S/NRA), Japan.



PERMANENT DISPLACEMENT FROM SURFACE-RUPTURING EARTHQUAKES: INSIGHTS FROM DYNAMIC RUPTURE OF Mw7.6 1999 CHI-CHI EARTHQUAKE

L.A. Dalguer⁽¹⁾, K. Irikura⁽²⁾, H. Wu⁽³⁾

⁽¹⁾ Structural Engineer and Seismologist, Swissnuclear, Switzerland, luis.dalguer@swissnuclear.ch

⁽²⁾ Professor, Aichi Institute of Technology, Japan, kojiroirikura@gmail.com

⁽³⁾ Post-doctoral researcher, Aichi Institute of Technology, Japan, haowuseis@gmail.com

Abstract

Large permanent displacements, sometimes named “fling”, resulted from surface-rupturing faulting have been observed in some earthquakes, such as the 1999 Kocaeli, 1999 Chi-Chi, 2002 Denali, reaching amplitudes over 8 m. This type of near-source ground motion is different from ordinary ground motion often evaluated by engineers and seismologist, for example to derive traditional ground motion prediction equations or to conduct seismic hazard studies. These permanent displacements are formed from coherent long period velocity pulses caused mainly by the offset of the ground surface when fault-rupture extends to the earth surface. To further investigate this type of ground motion, we developed dynamic rupture simulations of the Mw7.6 1999 Chi-Chi, Taiwan earthquake using asperity models in which the shallow layer (SL) of the first 2km depth is assumed to operate during rupture with enhanced energy absorption mechanism, as such it is parameterized with negative stress drop. Our physics-based dynamic rupture models show that the velocity ground motion causing permanent displacement near the source is dominated by the energy carried by the slip velocity pulse at the shallow layer fault of the first 2km depth, though this shallow zone is characterized with negative or zero stress drop. The asperities are the main driver elements to break the shallow layer and free-surface, but if surface rupture is not allowed, the rupture is inhibited to extend along strike, consequently the velocity pulse causing permanent displacement is reduced significantly. This study suggests that the slip velocities at the shallow fault zone, in which zero or negative stress drop operates, are the main source causing strong velocity pulses causing permanent displacement near the source. Therefore, when using simplified models, such as kinematic models, to study near source ground motion of surface-rupturing earthquakes, these slip velocity functions at the shallow zone have to be carefully considered.

Keywords: Permanent displacement, surface rupture, dynamic rupture simulation, slip velocity function, near-source ground motion.



1. Introduction

Permanent ground displacement, named also as “fling” in the earthquake engineering community [e.g., 1, 2, 3], is usually observed from large earthquakes, especially in surface-rupturing events, in which this offset can be significantly large near the fault reaching amplitudes over 1.0 to 10 m, as has been observed in some events such the 1999 Kocaeli [e.g. 4], 1999 Chi-Chi [e.g. 5, 6], 2002 Denali [e.g. 7], 2008 Wenchuan [e.g. 8], 2011 Tohoku [e.g. 9]. These permanent displacements are dynamically formed from coherent long period velocity pulses (known as “fling-pulse”) in the direction of the fault slip and it is significantly amplified by the offset of the ground surface when fault-rupture extends to the earth surface. These fling-pulses are different from those caused by forward directivity [e.g. 10], in which the velocity pulse is enhanced in the direction normal to the fault slip and does not produce amplified permanent displacement. Though the fling-pulse and the corresponding permanent displacement is understood in general to be an effect of the permanent tectonic deformation caused by a rupturing fault, little attention has been down to evaluate the source where waves are radiating to produce such pulses, that is, the slip velocity function causing fling-pulses. In this paper we focus on the shallow zone of the rupturing-fault. For that purpose, we develop a dynamic rupture simulation of the Mw7.6 1999 Chi-Chi Taiwan earthquake. The fault is characterized with simple asperities models to define the fault rupture to investigate the slip velocity function at the shallow layer (SL). The SL of the first 2km depth is assumed to operate during rupture with enhanced energy absorption mechanism, as such it is parameterized with negative stress drop [e.g. 11, 12]. We show that this SL fault zone, even in such conditions defined here, are the main source causing strong velocity pulses causing strong ground motion and permanent displacement near the source. Suggesting that these slip velocity functions at the SL have to be carefully considered when developing models for ground motion prediction.

2. General methodology for asperity model parameterization

The fault is represented by asperity areas named as Strong Motion Generation Areas (SMGA), as defined by Miyake et al [13] and Irikura and Miyake [14], and background areas. The asperities are characterized with high stress drop compared to the background. Within this concept, the methodology and procedure to parameterize this type of fault models are as follow:

- 1) Define rupture area: if there is not a target event in which rupture area is known, it can be derived from an empirical scaling relations [e.g.14,15,16, 17, 18, 19]
- 2) Define asperity area. In this study we use the characteristic slip models proposed by Somerville et al. [16]. These authors analyzed kinematic images from source inversions of past earthquakes and proposed two main statistical properties: i) the average of combined asperity area is 0.22 times the total rupture area; ii) average slip on the combined asperities is 2 times the average slip over all the fault.
- 3) Define stress drop ratio between average stress drop on asperities and background stress drop. Dalguer et al. [11, 20] estimated these ratios calibrating asperity dynamic rupture models constrained with the kinematic characterization of Somerville et al. [16]. The general tendency is that stress-drop ratios are in the range of 0.05 to 0.1 for buried earthquakes and -0.15 to 0.05 for surface-rupturing
- 4) Define average dynamic stress drop: Dalguer et al. [11, 20] calibrated dynamic asperity models that fit the empirical scaling relations. This calibration permits estimating the average stress drops consistent with the empirical scaling model. From these calibration, these authors proposed a variation of average stress drop depending on the ratio L/W , where L and W are respectively the length and width of the fault.
- 5) Define absolute values of stress drop on asperity areas. If available a kinematic source slip distribution, the stress drop distribution from the kinematic model can be estimated solving the elastodynamic equations [e.g. 21,22] and then define asperity areas following Somerville et al. [16]. Another procedure is following the method of Kamae and Irikura [23] in which the parameters seismic moment and stress drop are quantified by forward modeling using the empirical Green's function method while assuming the asperities at segments with large slips in the fault plane based on the results of waveform inversion. They applied this model to the 1995 Hyogoken-Nambu Earthquake.



- 6) The steps described until 5 serve to define initial values of the stress drop distribution. These values may need refinement by trial and errors to fit the target event, such as slip distribution and moment magnitude.

3. Parameterization of the Shallow Layer (SL)

It is well accepted by the community that the rupture at the SL may operate in a distinctive manner from the rest of the fault. This is due to the formation of incompetent fault gouge, cracking [e.g. 24, 25], presence of thick surface deposits of sediments, fissured rocks and other forms of brittle rock damage that have evolved over many earthquake cycles and may even have formed flower-like zone structures with significant shallow damage that decreases in amplitude and width with depth [e.g. 26, 27, 28, 29, 30]. These shallow weak zones are maybe formed because the normal stress is depth dependent. Therefore, the shallow strength is limited to the weight of the overburden (as in normal faulting environments) that is not able to maintain large shear stresses [e.g., 23] and therefore can easily damage or fracture. This damage zone can be accumulated during the lifetime of a fault, either as the result of dynamic stress change induced by rupture during an earthquake [e.g., 26, 27, 28, 29] or from quasi static deformation during the life of a shear fault [e.g., 31]. The main feature of this shallow depth zone is that it operates during rupture with an enhanced energy absorption mechanism. This makes the frictional properties of the shallow zone be distinct from those at deeper levels [e.g. 32, 33]. This zone can be characterized by velocity strengthening friction. To approximately mimic this mechanism, we impose a negative stress drop at shallow depth. And to account for the fault strength depth dependent in this shallow zone, the relative strength of the fault is reduced when approaching to the free-surface. For the case study in this paper, we define the first 2 km depth as the weak shallow zone. It is worthy to notice that if this shallow depth is not parameterized in an appropriate way, early and unphysical rupture process may take place in this zone.

4. Asperity model for the 1999 Chi-Chi, Taiwan, Earthquake

The Chi-Chi, Taiwan, earthquake (Mw 7.6) of 20 September 1999 originated on a low angle reverse fault with a strike of nearly N5°E and a dip between 25° and 36° [34]. The rupture of the causative fault reached the surface and propagated along about 80 km, starting in the south and extending northward on the Chelongpu fault. Spectacular horizontal displacements up to 9.0 m and vertical offsets of 1.0 to 8.0 m were registered along the surface rupture.

The parameterization of the asperity model follows the methodology procedure described above and is guided by the slip [35] and stress drop [36] distribution derived from the results of source inversion [35]. We also used as guideline the asperity model proposed by Ikeda et al [37]. We assume a fault rupture area of 79km length and 39km width with dip angle of 29°. We use the simple slip weakening friction model in the form given by Andrews [38]. The dynamic rupture and near-source ground motion simulations are developed using the Support Operator Rupture Dynamics code (SOR) from Ely et al., [39]. After trial and error we propose an asperity model with five asperities as shown in Fig. 1 for dynamic rupture simulation that approximately fits the target event in term of slip distribution, rupture duration and moment Magnitude. Fig. 1 shows the stress drop, strength excess and critical slip distance (D_c) distribution. D_c is assumed to be larger at the northern asperities than those at the southern. The largest D_c is at the shallow weak zone with 2km depth. Strength excess at the shallow zone decrease when approaching the free-surface, stress drop is negative in this zone with the largest values at the northern. The back ground stress drop in the rest of the fault is assumed to be zero. Fig 2 shows the asperity fault model placed on the geographic map with the trace of the Chelongpu fault.

The different parameterization between southern and northern was set in order to be consistent with the observed feature that characterized this earthquake. As described by Dalguer et al [40], this earthquake ruptured the southern and northern in a different manner, as reflected in the structural damage pattern distribution. Although the strongest ground motion occurred near the northern part of the trace, structural damage was heavier in the southern part. The difference seems to be in the frequency content of ground motion radiation from the source. Southern radiated higher ground motion capable to damage building, while the northern was stronger at low frequency. In order to reproduce this feature, frictional parameters need to be different in the northern and southern. The northern needs to be characterized by large fracture energy (consequently large D_c) and the shallow zone at the northern with larger energy absorption mechanism than the southern part.

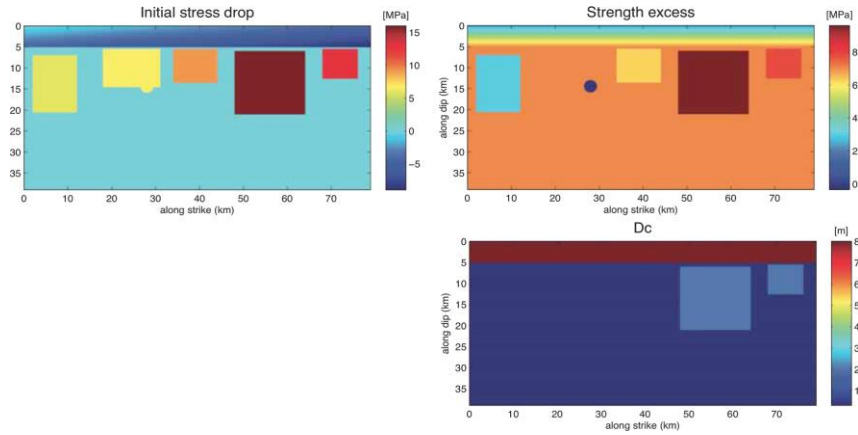


Fig. 1 Proposed asperity source model for this study for dynamic rupture simulation. Left shows stress drop distribution, top right strength excess and bottom right critical slip distance (Dc).

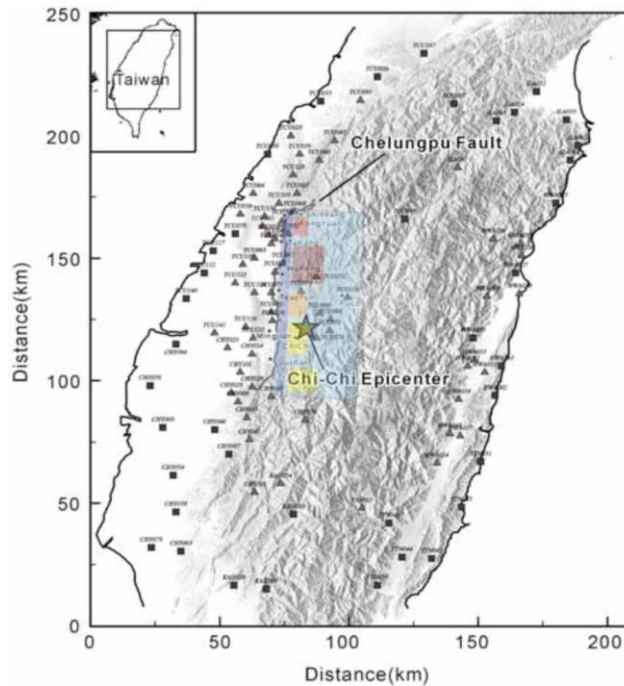


Fig. 2 Location of the proposed asperity source model on the geographic map with the trace of the Chelungpu fault and epicenter of the 1999 Chi-Chi, Taiwan, earthquake.

5. Simulation results

5.1 Source rupture solution

Figure 3 shows the dynamic rupture solution represented by the final slip, peak slip velocity, rupture speed and rupture time distribution along the fault. The simulation produces a moment magnitude of $M_w=7.64$. Slip distribution is consistent with the slip distribution obtained from source inversion with the large slip at the northern asperity. Rupture breaks about 75% of the free-surface that interacts with the ruptured fault, with the largest offset of about 10m at the northern side, that is consistent with the observations. Peak slip velocity (obtained directly from the simulation without filtering) is also dominated by the asperities, suggesting that most of the seismic radiation energy come from the asperities. Notice that at the shallow zone large slip velocities is observed, specially at the northern site. A close looks of the slip velocity function at different points on the fault

is shown in Figure 4. These slip velocity waveforms are low pass filtered with a frequency cut of 3.0Hz (the maximum frequency resolvable in our simulation is 2.0Hz). Even though the shallow zone is dominated by negative stress drop, seismic radiation is maybe considerable from this zone due to the large slip velocity. Rupture speed accelerates at the asperities and slow down when enter into the background. This is clearly observed at contour plot that overlap the slip and peak slip distribution. The rupture speed at the shallow zone is very complex with acceleration and deaccelerations processes. The free-surface play an important role to accelerate the rupture. The rupture reaches the northern part after about 26 seconds.

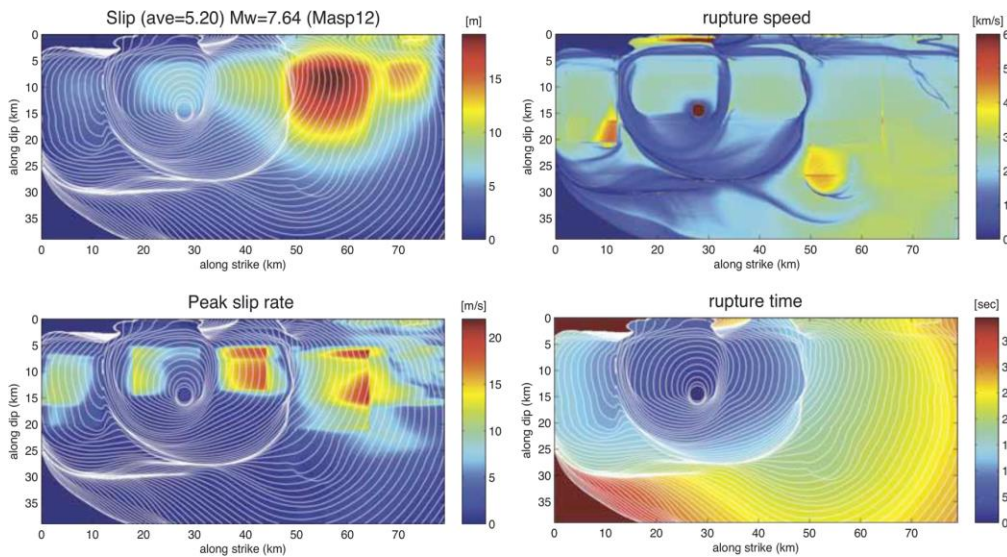


Fig. 3 Dynamic rupture solution represented by the final slip distribution (top left), peak slip velocity (bottom left), rupture speed (top right) and rupture time (bottom right). Contour lines on the slip and peak slip rate images are the rupture time each 0.5 seconds

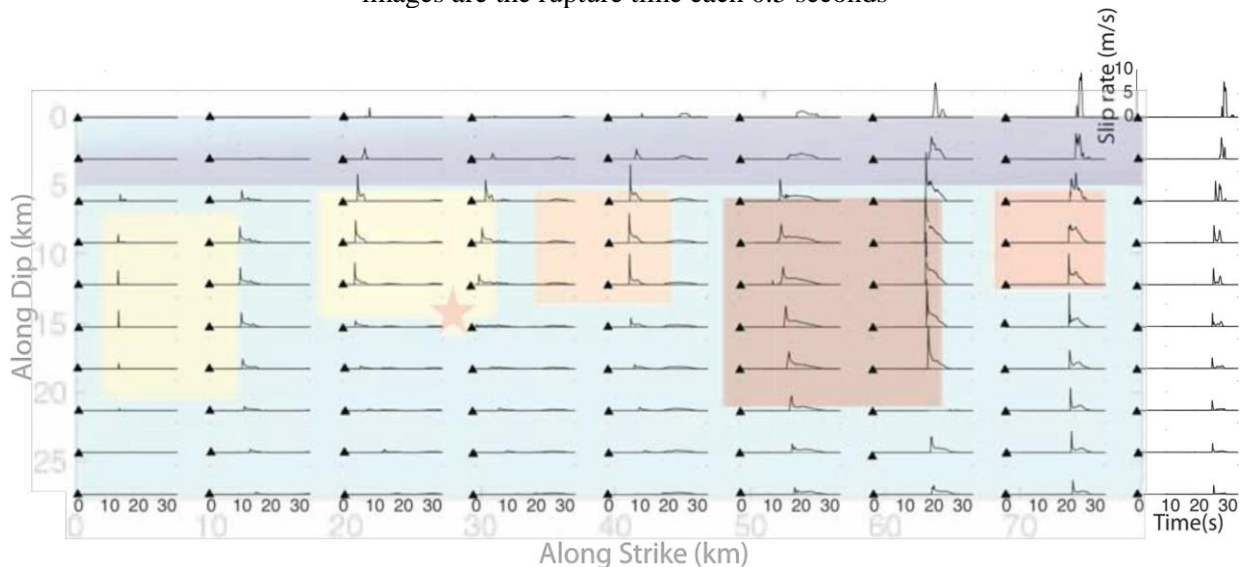


Fig.4. Slip velocity functions resulted from the dynamic rupture simulation at selected points on the fault. These slip velocity waveforms are low pass filtered with a frequency cut of 3.0Hz.

5.2 Fault displacement and ground motion compared with observed data

Figure 5 shows the fault displacement of our preferred model compared with the observed data. Overall the fault displacement along the fault is consistent with the observed data. These results can be improved by tuning the weak shallow zone.

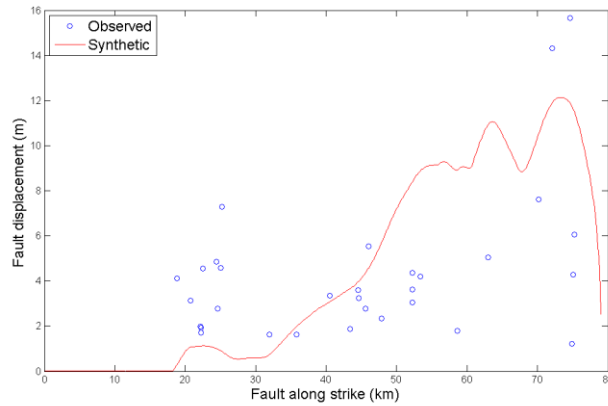


Fig. 5. Fault displacement compared with observed data [41]

The 3 components of velocity and displacement compared with observed data [42] at some stations with permanent displacement are shown in Fig. 6. Seismograms passed a low pass filter with frequency cut off of 0.5Hz. In all the figures, left column are velocity and right column displacement of three components (EW, NS and UD). In general synthetic follow the general pattern of observation. The velocity ground motion is a clear long period pulse that exhibit in the three components.

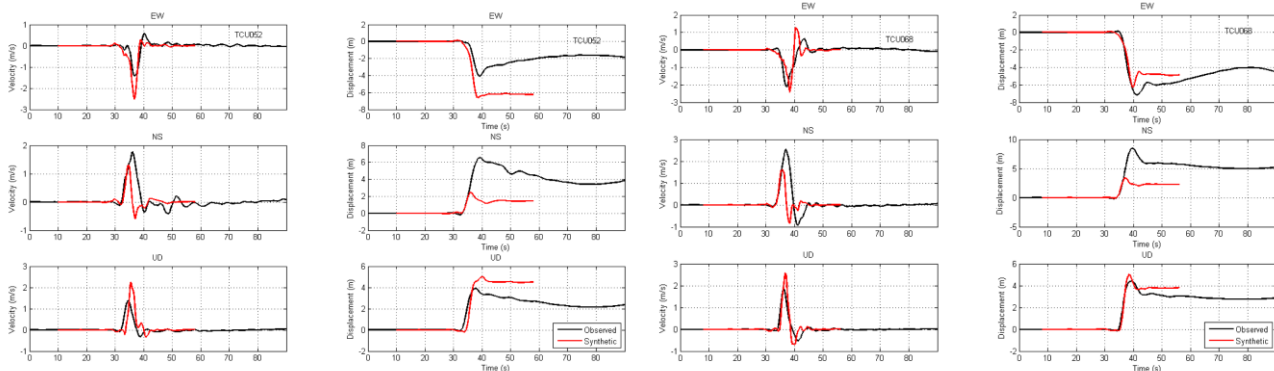


Fig. 6 Comparison with observed data of displacement and velocity ground motion at some selected station that with permanent displacement

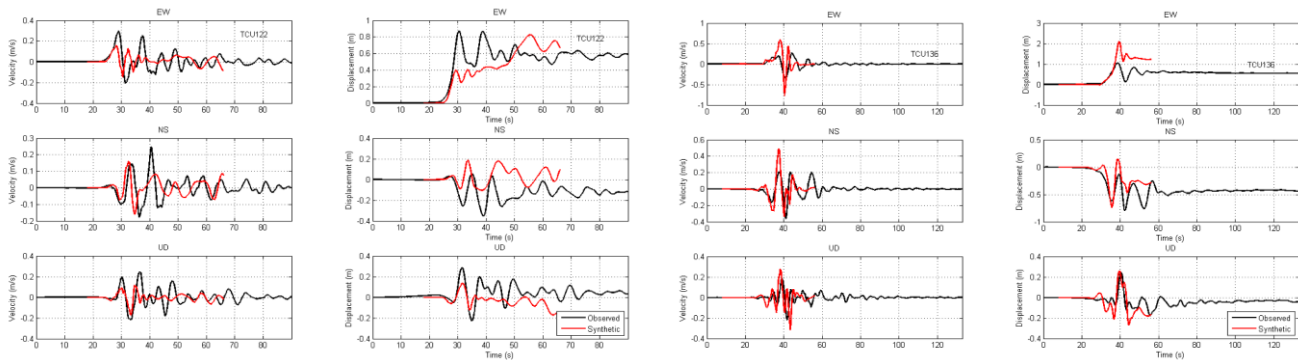


Fig. 6 (continuation) Comparison with observed data of displacement and velocity ground motion at some selected station that with permanent displacement

5.3 Effects of zero stress drop at the shallow zone

We evaluate the effect of zero stress drop at the shallow zone. The asperity and background are the same as the preferred model. Zero stress drop implies that the frictional strength drops to the level of the initial stress, that is contrary to our preferred model in which frictional strength behave with strength hardening during rupture.

Fig. 7 shows a comparison of the slip and peak slip velocity between these two models. Though peak slip velocity is similar at the seismogenic zone, the model with zero stress drop predicts the largest values at the free-surface of the northern site. The slip distribution of the model with zero stress drop is higher over all the fault than the model with negative stress drop. The largest values are predicted at the free-surface and the moment magnitude is $M_w=7.7$. It suggests that zero stress drop significantly enhance the size of the earthquake. Permanent displacement also increases to very high values as shown in Figure 8. These figure shows the permanent horizontal displacement for the two models. Both models show the rotation at the northern part of the horizontal displacement, as earlier mentioned. As described before, this rotation of the ground motion is due to the rupture directivity along the strike of dipping faults that break the free-surface. The rotation increases with the propagation distance due to the interaction of the rupture propagation with the free-surface. As a consequence, the amplitude of fault parallel component significantly increases to values comparable to the fault normal component

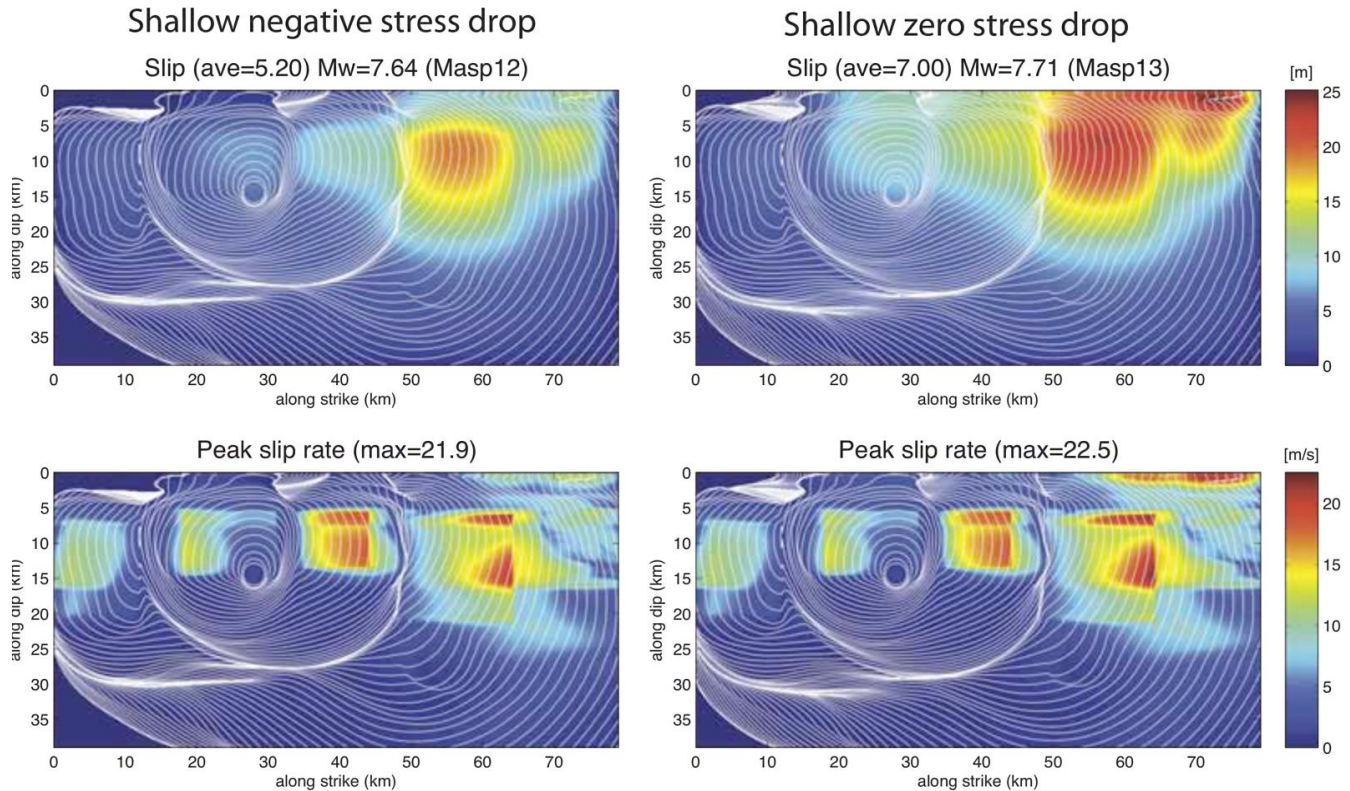


Fig.7 Dynamic rupture solution represented by the final slip distribution (top) and peak slip velocity (bottom) for the asperity models with negative stress drop at the shallow zone (left) and with zero stress drop at the shallow zone (right). Contour lines on the slip and peak slip rate images are the rupture time each 0.5 seconds.

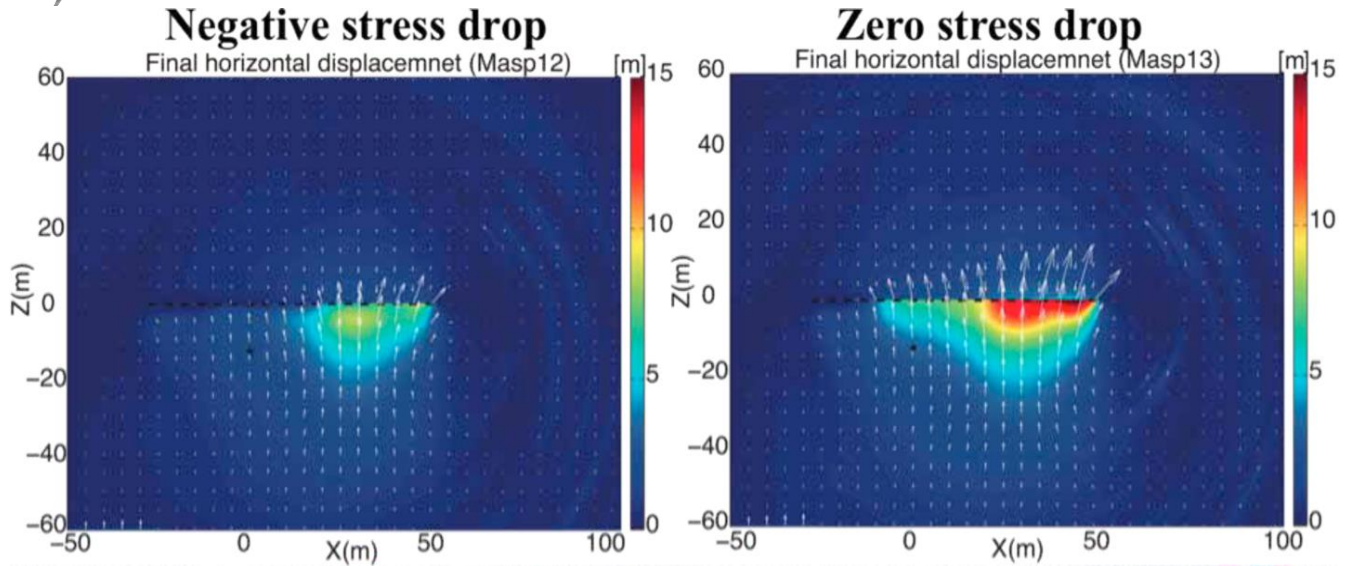


Fig. 8 Final horizontal displacement for the asperity models with negative stress drop at the shallow zone (left) and with zero stress drop at the shallow zone (right). Arrows represent the direction of the displacement vector. Dashed black line is the trace of the fault intersecting the free-surface. Black star is the epicenter. Right side is the northern

5.3 Effects of buried rupture depth

Here we want to evaluate the effect depth of a buried rupture. For this purpose we forced our rupture model to suddenly stop at 1.0km and 2.0km from the free-surface, i.e., no surface rupturing. To do it we assumed that the frictional strength in this zone is infinite. Figure 9 shows the slip distribution for these two models. The model with 1km buried depth successfully propagates over almost all the allowed rupture area, breaking all the asperities. However, the rupture model with 2km depth stops after braking the first two asperities, resulting in a small event of Magnitude $M_w=6.9$. This suggests that when the shallow zone breaks, rupture further extends along strike.

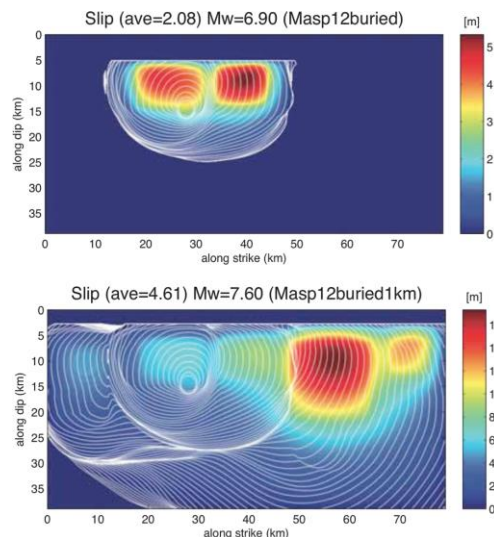


Fig. 9 Final slip distribution from asperity models with fault buried 2km depth (top) and buried 1km depth (bottom). Contour lines on the slip images are the rupture time each 0.5 seconds.



6. Conclusions

We use spontaneous dynamic rupture models to investigate the shallow zone effects on surface rupturing earthquakes of reverse faults and the corresponding permanent displacement. The 1999 Chi-Chi, Taiwan earthquake is used as a case study. The problem is tackled using asperity models. The asperities parameterization for dynamic rupture simulations has its basis on the asperity model characterization of Dalguer et al [11, 20], Somerville et al [16] and Kamae and Irikura [23]. As a case study we use the 1990 Mw 7.6 Chi-Chi, Taiwan, Earthquake. The main conclusions of our investigation for a reverse fault rupture are as follow:

- The asperities are the main driver elements to break the shallow layer and free-surface
- The shallow layer with zero stress drop produces larger slip and peak slip velocities than the one with negative stress drop. Zero stress drop on the shallow zone may over-predict ground motion and permanent displacement, leading to unrealistic scenarios.
- The rupture propagation directivity along the strike for reverse faults that break the freesurface produces horizontal rotation of the ground motion and permanent displacement. This phenomenon results in an increasing of the fault parallel component, reaching to significant values comparable to the fault normal component at long propagation distance of the rupture.
- Buried rupture inhibits the extension of the fault rupture along strike, and consequently the permanent fault displacement. In our case study, if rupture stop at 2.0km depth (i.e. it does not break the shallow layer) the rupture along strike stops earlier. However, at 1km depth, the rupture successfully extends along the whole fault area. This suggests that when rupture approaches to the free surface, the chance to the rupture become larger along strike significantly increases.
- With this study we show that the shallow layer representation in the earthquake modeling play an important role on fault displacement and near source ground motion generation.

7. References

- [1] Abrahamson NA (2002): Velocity pulses in near-fault ground motions, in *Proceedings of the UC Berkeley—CUREE Symposium in Honor of Ray Clough and Joseph Penzien*: Berkeley, California, UC Berkeley, Consortium of Universities for Research in Earthquake Engineering, 9–11 May 2002, 40–41.
- [2] Burks LS, Baker JW (2014): Fling in near-fault ground motions and its effect on structural collapse capacity, in *Tenth U.S. National Conference on Earthquake Engineering, Frontiers of Earthquake Engineering*, Anchorage, Alaska, 21–25 July 2014.
- [3] Kamae R, Abrahamson N, Graves R (2014) : Adding Fling Effects to Processed Ground-Motion Time Histories. *Bull. Seism. Soc. Am.*, Vol. 104, No. 4, pp. 1914–1929, August 2014, doi: 10.1785/0120130272.
- [4] Akkar S, Gülkan P (2002): A Critical Examination of Near-Field Accelerograms from the Sea of Marmara Region Earthquakes, *Bull. Seism. Soc. Am.* **92**, 1, pp. 428–447.
- [5] Shin TC, Teng TL (2001): An overview of the 1999 Chi-Chi, Taiwan, earthquake, *Bull. Seism. Soc. Am.* **91**, 895–913.
- [6] Dalguer LA, Irikura K, Riera J, Chiu HC (2001) : The Importance of the Dynamic Source Effects on Strong Ground Motion During the 1999 Chi-Chi (Taiwan) Earthquake: Brief Interpretation of the Damage Distribution on Buildings. *Bull. Seismol. Soc. Am.*, 95, 1112-1127.
- [7] Dreger D, Hurtado G, Chopra A, Larsen S (2011): Near-Field Across-Fault Seismic Ground Motions, *Bull. Seism. Soc. Am.*, Vol. 101, No. 1, pp. 202–221, February 2011, doi: 10.1785/0120090271
- [8] Lu M, Jun Li X, Wen An X, Zhao J.X (2010): A Preliminary Study on the Near-Source Strong-Motion Characteristics of the Great 2008 Wenchuan Earthquake in China, *Bull. Seism. Soc. Am.*, Vol. 100, No. 5B, pp. 2491–2507, November 2010, doi: 10.1785/0120090132.
- [9] Galvez P, Dalguer LA, Ampuero JP, Giardini D (2016): Rupture reactivation during the 2011 Mw 9.0 Tohoku earthquake: Dynamic rupture and ground motion simulations, *Bull. Seismol. Soc. Am.*, Vol. 106, No. 3, pp. –, June 2016, doi: 10.1785/0120150153.
- [10] Somerville PG, Smith NF, Graves RW, Abrahamson NA (1997): Modification of empirical strong ground motion attenuation relations to include the amplitude and duration effects of rupture directivity, *Seism. Res. Lett.* **68**, 199–222.



- [11] Dalguer LA, Miyake H, Day SM, Irikura K (2008): Surface Rupturing and Buried Dynamic Rupture Models Calibrated with Statistical Observations of Past Earthquakes. *Bull. Seismol. Soc. Am.* 98, 1147-1161, doi: 10.1785/0120070134.
- [12] Pitarka A, Dalguer LA, Day SM, Somerville P, Dan K (2009): Numerical study of ground motion differences between buried and surface-rupturing earthquakes, *Bull. Seism. Soc. Am.*, Vol. 99, No. 3, pp. 1521–1537, June 2009, doi: 10.1785/0120080193.
- [13] Miyake H, Iwata T, Irikura K (2003): Source characterization for broadband ground-motion simulation: kinematic heterogeneous source model and strong motion generation area, *Bull. Seismol. Soc. Am.* 93, 2531–2545.
- [14] Irikura K, Miyake H (2011): Recipe for predicting strong ground motion from crustal earthquake scenarios, *Pure Appl. Geophys.*, 168, 85-104, doi:10.1007/s00024-010-0150-9.
- [15] Wells DL, Coppersmith KL (1994): New empirical relationships among magnitude, rupture width, rupture area, and surface displacement, *Bull. Seismol. Soc. Am.* 84, 974–1002.
- [16] Somerville P, Irikura K, Graves R, Sawada S, Wald D, Abrahamson N, Iwasaki Y, Kagawa T, Smith N, Kowada A (1999): Characterizing crustal earthquake slip models for the prediction of strong ground motion, *Seism. Res. Lett.* 70, 59–80.
- [17] Hanks TC, Bakun WH (2002): A bilinear source-scaling model for M-log A observations of continental earthquakes, *Bull. Seismol. Soc. Am.* 92, 1841–1846.
- [18] Miyakoshi K (2002): Source characterization for heterogeneous source model, *Chikyū Mon. Extra* 37, 42–47 (in Japanese).
- [19] Murotani S, Matsushima S, Azuma T, Irikura K, Kitagawa S (2015): Scaling Relations of Source Parameters of Earthquakes Occurring on Inland Crustal Mega-Fault Systems, *Pure Appl. Geophys.* 172, 1371–1381; DOI 10.1007/s00024-014-1010-9.
- [20] Dalguer LA, Miyake H, Irikura K (2004) : Characterization of dynamic asperity source models for simulating strong ground motion, *Proceedings of the 13th World Conference on Earthquake Engineering (13WCEE)*, Vancouver, B.C., Canada, August 1-6, 2004, Paper No. 3286.
- [21] Dalguer LA, Irikura K, Zhang W, Riera JD (2002): Distribution of Dynamic and Static Stress Changes during 2000 Tottori (Japan) Earthquake: Brief Interpretation of the Earthquake Sequences; Foreshocks, Mainshock and Aftershocks, *Geophys. Res. Lett.*, 29(16), 1758, doi:10.1029/2001GL014333.
- [22] Zhang W, Iwata T, Irikura K, Sekiguchi H, Bouchon (2003): Heterogeneous distribution of the dynamic source parameters of the 1999 Chi-Chi, Taiwan, earthquake, *J. Geophys. Res.*, 108, NO. B5, 2232, doi:10.1029/2002JB001889.
- [23] Kamae K, Irikura K (1998): Source model of the 1995 Hyogo-ken Nanbu earthquake and simulation of near-source ground motion, *Bull. Seismol. Soc. Am.*, 88, 2, 400-412.
- [24] Marone C (1998): Laboratory-derived friction laws and their application to seismic faulting, *Ann. Revs. Earth Plan. Sci.* 26, 643–696.
- [25] Marone C, Scholz CH (1988): The depth of seismic faulting and the upper transition from stable to unstable slip regimes, *Geophys. Res. Lett.* 15, 621–624.
- [26] Dalguer LA, Irikura K, Riera J (2003) : Generation of New Cracks Accompanied by the Dynamic Shear Rupture Propagation of the 2000 Tottori (Japan) Earthquake, *Bull. Seismol. Soc. Am.*, 93, 2236-2252.
- [27] Dalguer LA, Irikura K, Riera J (2003) : Simulation of Tensile Crack Generation by 3D Dynamic Shear Rupture Propagation During an Earthquake. *J. Geophys. Res.*, 108(B3), 2144, doi:10.1029/2001JB001738.
- [28] Shi Z, Day SM (2013): Rupture dynamics and ground motion from 3-D rough-fault simulations *J. Geophys. Res.* , 118, doi:10.1002/jgrb.50094.
- [29] Roten D, Olsen KB, Day SM, Cui Y, Fah D (2014): Expected seismic shaking in Los Angeles reduced by San Andreas Fault zone plasticity , *Geophys. Res. Lett.* , 41, doi:10.1002/2014GL059411
- [30] Ben-Zion Y, Peng Z, Lewis MA, McGuire J (2007): High Resolution Imaging of Fault Zone Structures With Seismic Fault Zone Waves, *Scientific Drilling*, Special Issue No. 1, 78-79, doi:10.2204/iodp.sd.s01.23.2007, 2007.



- [31] Vermilye JM, Scholz CH (1998): The process zone: a microstructural view of fault growth, *J. Geophys. Res.* 103, 12,223–12,237.
- [32] Brune JN, Anooshehpour A (1998): A physical model of the effect of a shallow weak layer on strong ground motion for strike-slip ruptures, *Bull. Seismol. Soc. Am.* 88, 1070–1078.
- [33] Day SM, Ely GP (2002): Effect of a shallow weak zone on fault rupture: Numerical simulation of scale-model experiments, *Bull. Seismol. Soc. Am.* 92, 3006–3021.
- [34] Shin TC, Kuo KW, Lee WHK, Teng TL, Tsai YB (2000): A preliminary report on the 1999 Chi-Chi (Taiwan) Earthquake, *Seism. Res. Lett.* 71, 24–30.
- [35] Iwata T, Sekiguchi H, Irikura K (2000): Rupture process of the 1999 Chi-Chi, Taiwan, earthquake and its near-source strong ground motions, *Proc. International Workshop on Annual Commemoration of Chi-Chi earthquake*, Taipei, Taiwan, Vol.1, 36-46, Sep.
- [36] Zhang W, Iwata T, Irikura K, Sekiguchi H, Bouchon M (2003): Heterogeneous distribution of the dynamic source parameters of the 1999 Chi-Chi, Taiwan, earthquake, *J. Geophys. Res.*, 108, NO. B5, 2232, doi:10.1029/2002JB001889.
- [37] Ikeda T, Kamae K, Miwa S, Irikura K (2004): Source modeling and strong ground motion simulation for the 1999 Chi-Chi, Taiwan earthquake, *Proceedings of the 13th World Conference on Earthquake Engineering (13WCEE)*, Vancouver, B.C., Canada, August 1-6, 2004, Paper No. 1289.
- [38] Andrews DJ (1976): Rupture velocity of plane-strain shear cracks, *J. Geophys. Res.*, 81, 5679-5687.
- [39] Ely G, Day SM, Minster JB (2009): A support-operator method for 3D rupture dynamics, *Geophysical Journal International*, 177 1140-1150, DOI: 10.1111/j.1365246X.2009.04117.x.
- [40] Dalguer LA, Irikura K, Riera J, Chiu HC (2001): The Importance of the Dynamic Source Effects on Strong Ground Motion During the 1999 Chi-Chi (Taiwan) Earthquake: Brief Interpretation of the Damage Distribution on Buildings. *Bull. Seismol. Soc. Am.*, 95, 1112-1127.
- [41] Azuma T, Sugiyama Y, Kariya Y, Awata Y, Lee YH, Shih TS, Lu ST, Wu WY (2000): Displacements and segmentation of the surface fault associated with 1999 Chi-Chi, Taiwan, earthquake, *Annual Report on Active Fault and Paleoseismic Researches*, no.EQ/00/2, pp. 221-235.
- [42] Lee WHK, Shin TC, Kuo KW, Chen KC, Wu CF (2001): CWB Free-Field Strong-Motion Data from the 21 September Chi-Chi, Taiwan, Earthquake. *Bull. Seismol. Soc. Am.*, 91(5), pp. 1370–1376,

Study on the evaluation method for fault displacement: Deterministic evaluation approach based three step considerations.

*Tonagi Masao¹, Tsutomu Takahama¹, Yasuhiro Matsumoto¹, Naoto Inoue², Kojiro Irikura³, LUIS ANGEL DALGUER³

1. KOZO KEIKAKU Engineering Inc., 2. Geo-Research Institute, 3. Aichi Institute of Technology

Fault displacement hazards are very important to enhance seismic safety of nuclear installations. In Japan, important nuclear facilities must be installed in the ground where there is no risk of displacement. And also IAEA Specific Safety Guide (SSG) -9 provides guidelines and procedures for assessing the potential for fault displacement (capability) at or near the site for both new and existing nuclear power plants. Under such background, we are investigating the possibility of evaluation by both deterministic evaluation method and probabilistic evaluation method as to whether or not fault displacement occurs on the ground surface when earthquake occurs.

In this paper, we focus on fault displacement and introduce the concept of deterministic evaluation methods for fault displacement.

We are planning to evaluate fault displacement will occur on the ground surface due to earthquake occurrence by the following three steps.

step1) Construct characterized source models. We will construct a characterization source models that can reproduce strong ground motion near the seismic source with a period of 10 seconds or less.

step2) Consider conduct dynamic rupture simulation with each parameter of the characterized source model constructed in step 1 as input. By dynamic rupture simulation, evaluate the permanent displacement appearing on the ground surface due to the displacement of principal fault. (In step 2, consider calculation area that wide area including the principal fault is taken into both the depth direction and the horizontal direction.)

step3) in step3, targeting a very narrow range of the ground surface (ex. few hundred meters to several kilometers), we consideration a very soft and discontinuous nature of the surface, evaluate displacement by numerical analysis method represented in the finite element method, or the like. In this study, we have conducted a combination of the finite element method (FEM) and the particle method (SPH) method for the analysis method.

In accordance with the above flow, we conducted a tentative analysis for the 1999 Chi-Chi earthquake and compared displacement of observation records and analysis result.

This research was part of the 2016 research project ‘Development of evaluating method for fault displacement ‘ by the Secretariat of Nuclear Regulation Authority (S/NRA), Japan.

Keywords: deterministic approaches, characterized source model, dynamic rupture simulation, subsurface rupture simulation

セッション

S-SS07 地表地震断層の調査・分析・災害評価

タイトル Study on the Evaluation Method for Fault Displacement: Probabilistic Approach Based on Japanese Earthquake Rupture Data - Principal fault displacements along the fault-

N. Kitada, N. Inoue and M. Tonagi

(Geo-Research Institute, Kozo Keikaku [Incorporated](#)

)

The purpose of Probabilistic Fault Displacement Hazard Analysis (PFDHA) is estimate fault displacement values and its extent of the impact. There are two types of fault displacement related to the earthquake fault: principal fault displacement and distributed fault displacement. Distributed fault displacement should be evaluated in important facilities, such as Nuclear Installations. PFDHA estimates principal fault and distributed fault displacement. For estimation, PFDHA uses distance-displacement functions, which are constructed from field measurement data. We constructed slip distance relation of principal fault displacement based on Japanese strike and reverse slip earthquakes in order to apply to Japan area that of subduction field. However, observed displacement data are sparse, especially reverse faults. Takao et al. (2013) tried to estimate the relation using all type fault systems (reverse fault and strike slip) so in this time, we try to estimate distance-displacement functions each strike slip fault type and reverse fault type especially add new fault displacement data set.

To normalized slip function data, several criteria were provided by several researchers. We normalized principal fault displacement data based on several methods and compared slip-distance functions. We normalized by maximum displacement rate, normalized by mean displacement rate. The normalized by total length of Japanese reverse fault data did not show particular trend slip distance relation. In the case of segmented data, the slip-distance relationship indicated similar trend as strike slip faults. We will also discuss the relation between principal fault displacement distributions with source fault character. According to slip distribution function (Petersen et al., 2011), strike slip fault type shows the ratio of normalized displacement are decreased toward to the edge of fault. However, the data set of Japanese strike slip fault data not so decrease in the end of the fault. This result indicates that the fault

displacement is difficult to appear at the edge of the fault displacement in Japan.

This research was part of the 2014-2015 research project ‘Development of evaluating method for fault displacement‘ by the Secretariat of Nuclear Regulation Authority (NRA), Japan.

受付番号 : C004317

Investigation of off-fault displacement

*Naoto Inoue¹, Naoko Kitada¹, Yasuhiro Matsumoto², Tsutomu Takahama², Tonagi Masao², LUIS ANGEL DALGUER³, Kojiro Irikura³

1. Geo-Research Institute, 2. KOZO KEIKAKU ENGINEERING Inc., 3. Aichi Institute of Technology

Discontinuous distributed fault displacements occur around the primary surface rupture in the earthquake. Evaluation of off-fault displacement is important for mitigation of fault displacement hazards. There are two types of off-fault displacement in the view point of a prediction problem. The displacement does not occur only on the active fault, but also off the active fault. Petersen et al. (2011) introduced mapping accuracy for the strike-slip fault. We estimated the mapping accuracy of several Japanese earthquakes at distinct fault side, i.e. hanging-wall/foot-wall by measuring distances between active fault traces and primary surface ruptures. Based on estimation of the mapping accuracy of strike-slip fault, narrow bell-shaped displacement profile across the active faults was inferred. On the contrary, wide bell-shaped displacement profile was estimated and the center shifted to the foot-wall side, in the case of the reverse-fault. The other off-fault displacement is the displacement on the secondary faults. This type of displacement of reverse fault focuses on the hanging-wall. These differences are important to estimation of fault displacement hazard.

Acknowledgments: This research was part of the 2014-2016 research project ‘Development of evaluating method for fault displacement’ by the Secretariat of Nuclear Regulation Authority (NRA), Japan. A part of displacement data was used from Kagohara et al. (2007), which was partly supported by the Grant-in-Aid for Scientific Research (no. 17200053) by Ministry of Education, Science, Sports and Culture.

Keywords: fault displacement hazard, secondary fault

Appendix 2

Appendix-2_1 Surface Rupture Simulations and Physics-based Ground Motion Simulations

Report of NRA project “Surface Rupture Simulations and Physics-based Ground Motion Simulations”

Summary

This is a report corresponding to the dynamic rupture simulations of the 2010 Mw 7.0 Darfield (New Zealand) earthquake. The main fault of this earthquake is strike-slip, almost vertical. But the fault system is rather complex, composed by branches and fault segmentations. Here we develop a simplified planar fault model for dynamic rupture simulations. The fault is characterized by asperity models based on the kinematic asperity source model developed by the KKE group. The fault dimensions are assumed to have a length of 60km and a width of 24km. Dip angle is 82 degree. The kinematic fault model proposed by the KKE group is composed of three asperities named as ASP1, ASP2 and ASP3 with a respective average slip 2.5m, 2.5m, and 2m. We have developed a suite of dynamic rupture models for this characterized kinematic asperity source model. The initial stress drop distribution is computed given the distribution of static displacements following Andrews (1980) method. The first step was to follow a trial and error procedure to estimate the stress drop at each asperity, so that the average slip at each asperity be consistent with the ones from kinematic model. In this first step, 7 models without surface rupture has been generated, in which the preferred model (Model 7) predicts an earthquake of Mw 6.98 with average slip for each asperity (ASP1, Asp2 and ASP3), respectively, 2.7, 2.7, and 2m, corresponding to stress drops of 6.0MPa, 8.5MPa, and 7.0MPa. The background stress drop in the seismogenic zone is assumed to be zero, and a weak shallow layer (SL) zone of the first 2km depth is assumed to operate during rupture with enhanced energy absorption mechanism, as such it is parameterized with negative stress drop and large critical slip distance of 8m. In the second step, the SL zone parameterization is varied, while keeping the same parameterization of model 7 at the seismogenic zone, so that surface rupture be approximately consistent with observed fault displacement. For that purpose, 16 additional models have been developed. From them, 5 models break the free surface, in which our preferred model (model 23) produce fault displacement distribution closer to the observed ones, but average slip at the asperities increased to 3.4m, 3.2 and 2.8m, respectively for ASP1, ASP2 and ASP3. This increase in average slip is due to the contribution of surface rupturing. This preferred model has dynamic parameterization at the SL as follow, strength excess (SE) and critical slip distance (Dc) varies linearly from the seismogenic zone to the free surface, respectively from 6MPa to 1MPa for SE and from 0.2m to 2.5m for Dc. Stress drop is zero at the SL zone. Within the framework of the asperity model, we found that negative stress drop is not necessary in the SL, because this strongly inhibit surface rupturing. The ground motion (velocity and displacement) from our preferred model is compared with observed records in the frequency band of 0.0 to 0.5Hz. Overall synthetics seismograms are consistent with observations, however details of the complexity waveforms from observed records are not reproduced because of our simplified model. Ground motion differences between the models that break the free-surface are negligible. The main differences are found on the subsurface displacement. When compared with the preferred buried models (model 7), ground motion differences are only at the very near to the fault. Indicating that the source of main differences is from the SL parameterization and surface rupturing that affect only the near-source.

Introduction

The 2010 Mw 7.0 Darfield (New Zealand) earthquake is one of the best-recorded earthquakes of this magnitude (figure 1 illustrating the location of the event and the faults). This event has one of the richest strong motion data in New Zealand in recent years. Surface-rupturing was observed in several sites along the main fault, suggesting that rupture reached the surface. As shown in Figure 2 from the study reported by Quigley (2012), surface rupture has been observed at west, central and east segments with maximum values of 5.3m at the central segment. The rupture process and near-source ground motion seem also complex. 8 stations recorded peak accelerations larger than 0.5g, and some of them exceeded 1g (e.g., Fry and Benites, 2010). The earthquake was well captured with many local strong motion recordings that allow for detailed evaluation of the spatial and temporal evolution of the rupture and the near-source ground motion (Figure 3). The fault geometry of this earthquake is rather complex (Fig. 1 and 2) composed with about 8 segments. The earthquake has initiated slowly in a branched fault, and then jumped to the main fault and propagates with high rupture speed in a geometrically complex fault with step-over toward the east and branched toward west. Due to limitations of our numerical code for dynamic rupture simulations, in this project we develop a simplified planar fault (Figure 3). Our main goal is to evaluate the surface rupture and near-source ground motion to capture dominated rupture propagation and near ground motion caused by the main fault.

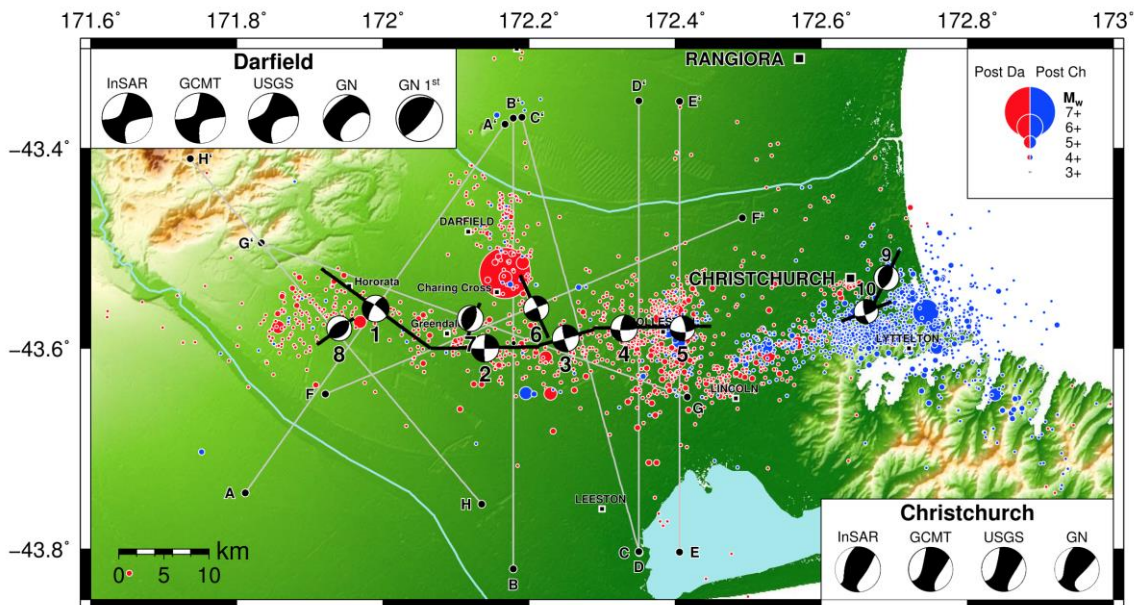


Figure 1. Location of the 8 Darfield fault segments and focal mechanism for the combined 8 Darfield segments. As reference, it is also shown the focal mechanism solution of the 2011 Mw 6.1 Christchurch earthquakes that occurred a couple of months after the Darfield event (Elliot et al.,2012).

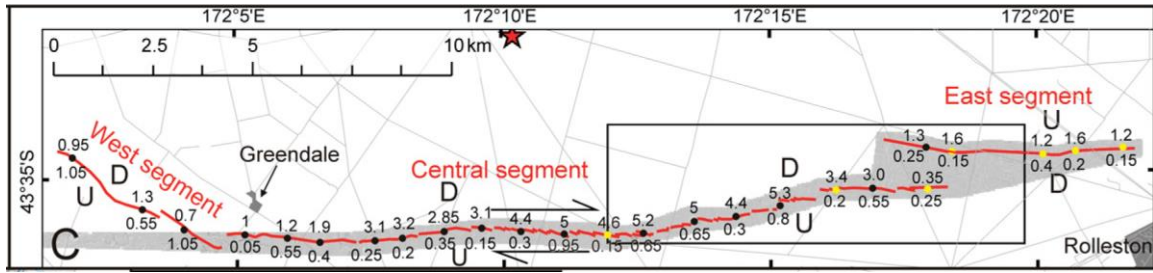


Figure 2. Detail fault trace map of surface rupture (red line). U and D are relative up and down sides. Numbers above the surface rupture line are measured horizontal fault offset, and below are vertical fault offset (after Quigley et al, 2012).

2010Darfield_H28_planer

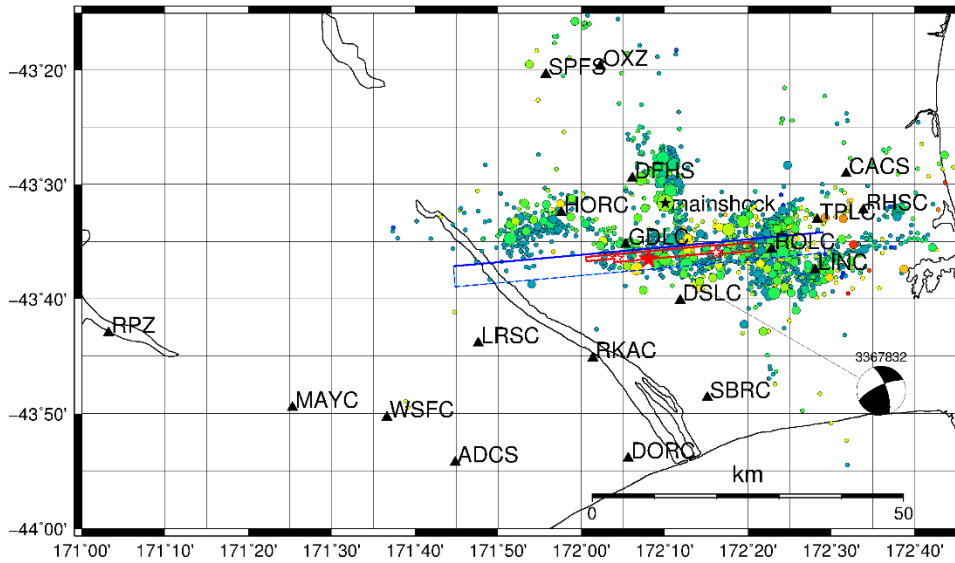


Figure 3. Location of near source stations, aftershock distribution and projection of a simplified planar fault (blue line) with dip angle 82 degree for the dynamic rupture simulation.

Dynamic rupture model

In this project, we develop a simplified dynamic rupture model in a strike slip planar fault with dip angle of 82 degree. Slip weakening friction in the form given by Andrews (1976) is used as constitutive model for dynamic rupture simulation. The parameterization of the stress parameters is based on a kinematic asperity model developed by the KKE group. As shown in Figure 4, the fault dimensions are assumed to have a length of 60km and a width of 24km. The kinematic fault model is composed of three asperities named as ASP1, ASP2 and ASP3 with a respective average slip 2.5m, 2.5m, and 2m (Figure 4)

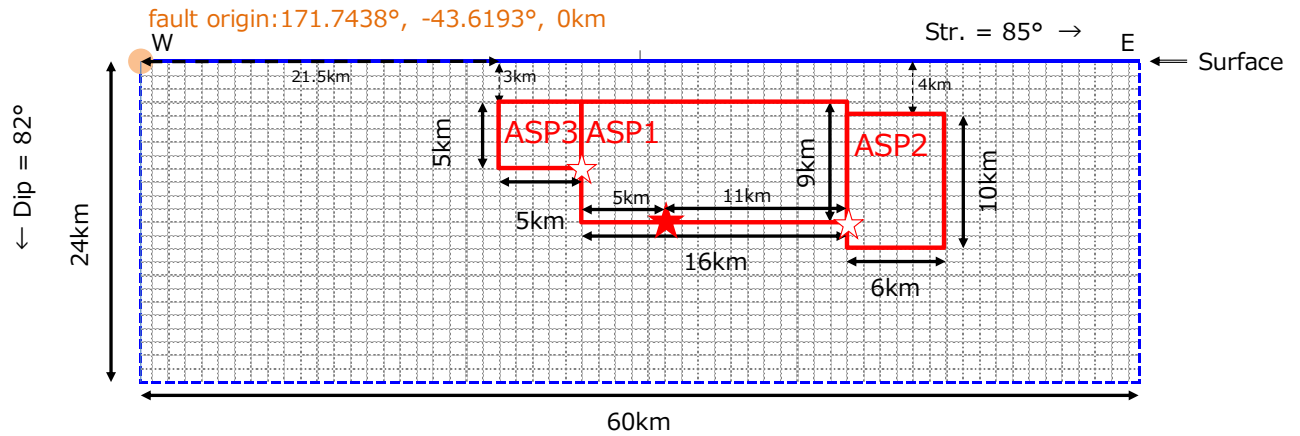


Figure 4. Simplified asperity model in a planar fault proposed by the KKE group.

We use a 1D velocity structure proposed by Guidotti et al.(2011) as illustrated in Figure 5.

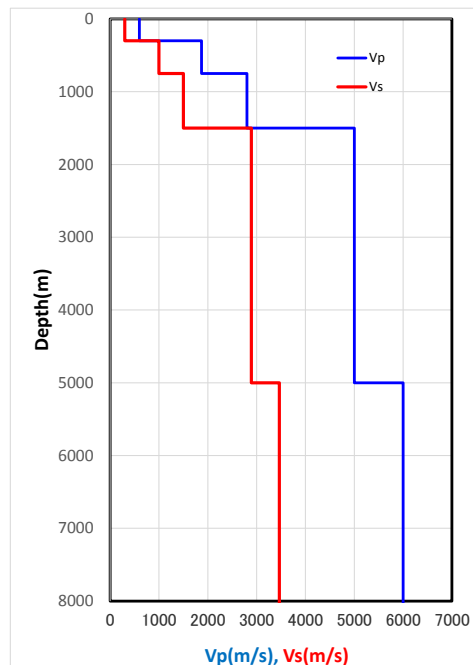


Figure 5. 1D velocity structure (Guidotti et al.,2011) for the dynamic rupture simulation

First step

The first step of the dynamic rupture calculation is to find a model consistent with the kinematic asperity model. The initial stress drop distribution is computed given the distribution of static slip from the kinematic model. For this purpose we use the approach from Andrews (1980) and expanded by Ripperger and Mai (2004). This method follows the concept of a static stiffness function that involves a 2D-Fourier Transform of the slip on the fault. After calculating the initial stress drop distribution, a trial and error procedure is followed to estimate the stress drop at each asperity, so that the average slip at each asperity be consistent with the ones from kinematic model. 7 asperity models without surface rupture have been developed in this first step. The stress drop distribution, strength excess and critical slip distance for the asperity model 7 (preferred model to

date) is shown in Figure 6. The background stress drop in the seismogenic zone is assumed to be zero, and a weak shallow layer (SL) zone of the first 2km depth is assumed to operate during rupture with enhanced energy absorption mechanism, as such it is parameterized with negative stress drop (Figure 6).

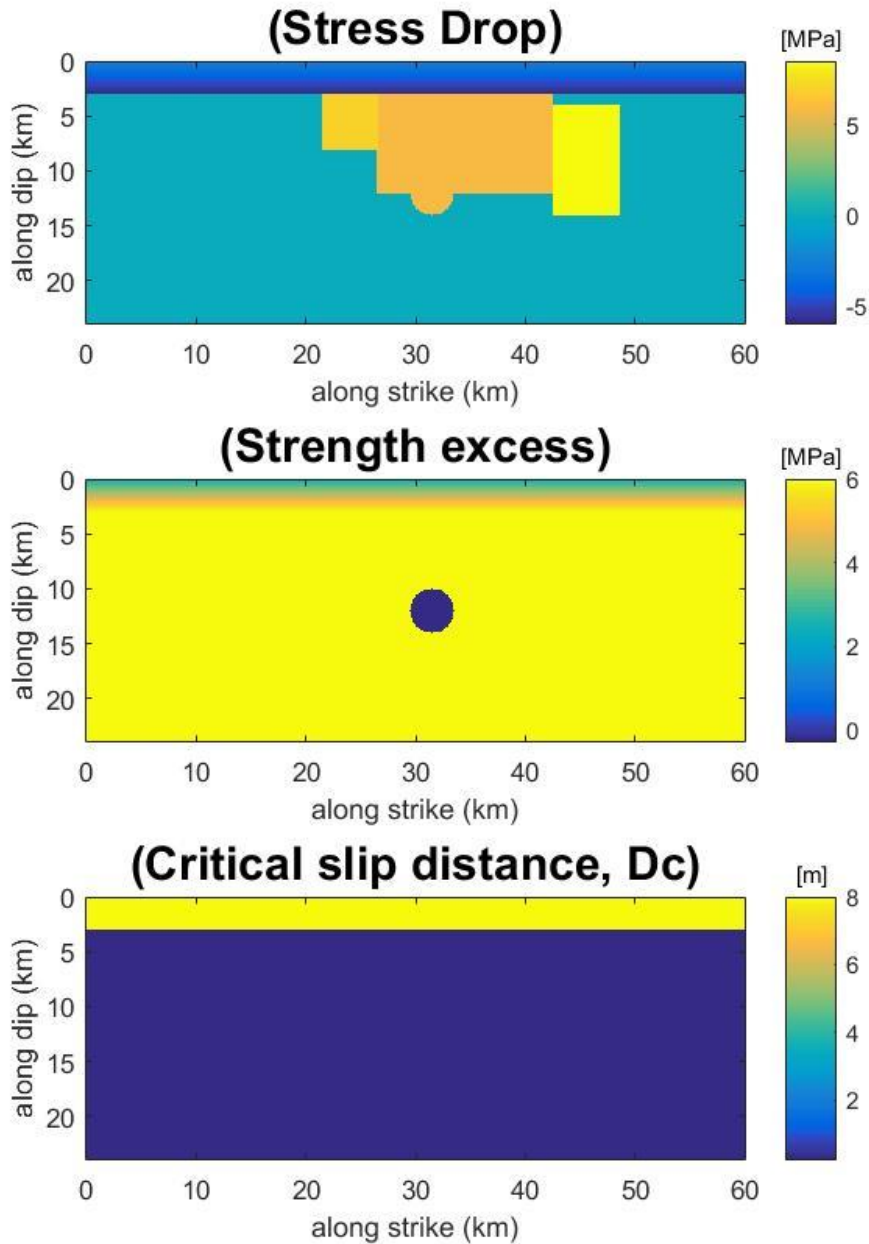


Figure 6. Stress drop, strength excess and critical slip distance distribution for the dynamic rupture simulation of asperity model 7 without surface rupture consistent with the kinematic asperity model.

The asperity model 7 (Figure 6) predicts an earthquake of Mw 6.98 with average slip for each asperity (ASP1, Asp2 and ASP3), respectively, 2.7, 2.7, and 2m, corresponding to stress drops of 6.0MPa, 8.5MPa, and 7.0MPa. Figure 7 shows the dynamic rupture solution of this model, represented by the final slip distribution, rupture time and rupture speed. Rupture time is about 12

seconds and rupture speed is sub-shear. Rupture does not reach the free-surface. The shallow zone needs to be calibrated (second step), so that surface rupture consistent with observations can be simulated. In the second step, new set of simulations are dedicated to evaluate the surface rupture.

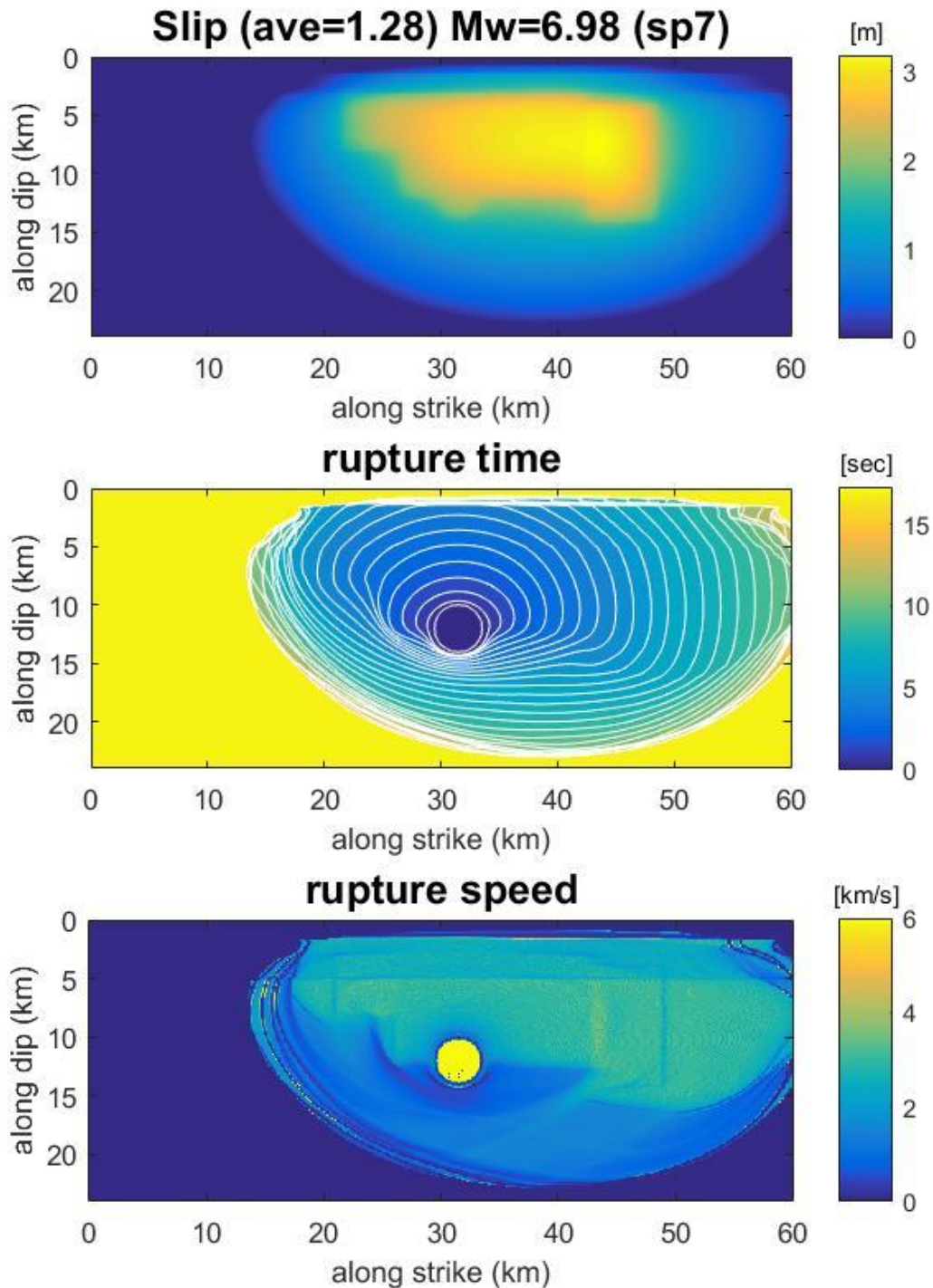


Figure 7. Dynamic rupture solution of asperity model 7, represented by final slip distribution (top), rupture time (middle) and rupture speed (bottom)

Second step

In this second step, the SL zone parameterization is varied, while keeping the same parameterization of model 7 (Figure 6) at the seismogenic zone, so that surface rupture be approximately consistent with observed fault displacement reported by Quigley (2012) and shown in Figure 2. For this purpose, 16 additional models have been developed. From them, 5 models break the free surface. We started varying the stress drop and strength excess at the SL zone while keeping the D_c of 8m. But surface rupture was not successful during this trial. Then we reduced drastically the D_c to lower values between 0.5m to 3m, in which surface rupturing started to be generated. With this trial, we found that larger values of D_c and negative stress drop was not necessary in the SL, because they strongly inhibit surface rupturing. Figure 8 shows a profile of the dynamic parameterization (stress drop, strength excess, critical slip distance) along dip of a section crossing the center of the first asperity (ASP1 from Figure 4) for all the models that break the free-surface (five models presented with solid line) and some models (including model 7) without surface rupturing (dashed line). In this figure 8 (right side) is also presented the along strike average slip profile plotted with dip. This figure shows that the models that break the free-surface enhance considerable the final slip distribution due to surface rupturing. All the surface rupturing models have nearly the same final slip at the seismogenic zone. Notice that Model 20 (no surface rupture) has also the same final slip as the surface rupturing models at the seismogenic zone. This models did not break the free-surface because the presence of negative stress drop at the SL.

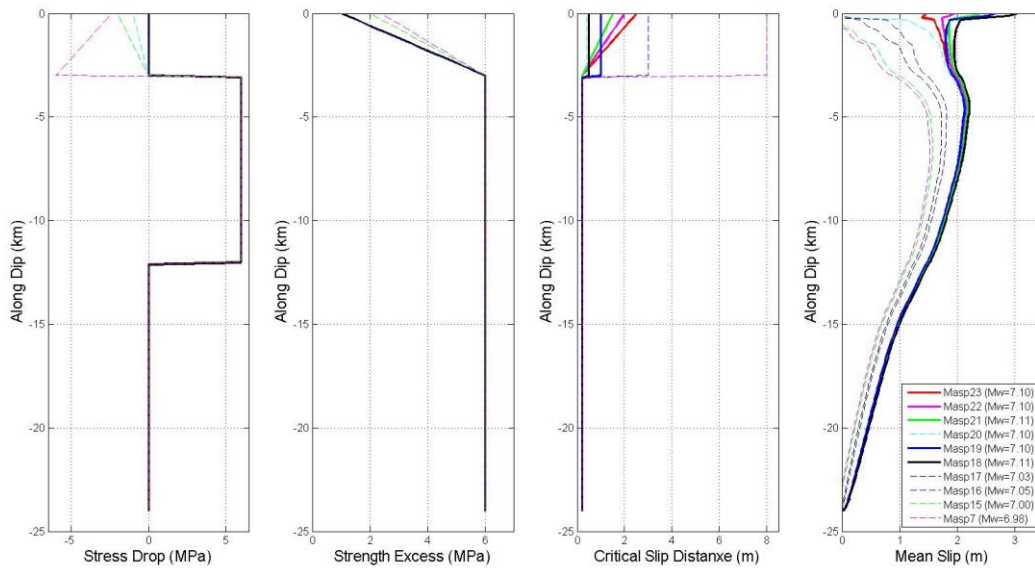


Figure 8. Dynamic parameterization profile (stress drop, strength excess and critical slip distance) along dip crossing the center of asperity 1 (ASP1 in Figure 4) for all models with surface rupturing (solid line) and some models without surface rupturing (dashed line) including Model 7 from Figure 6. Right side of this figures is shows the along strike average final slip of these models.

The rupture propagation (rupture time and rupture speed) in the seismogenic zone is nearly the same for all the models (with and without surface rupturing). This is because the dynamic rupture parameterization at this zone is the same for all the models. This can be seen in Figure 9, in which rupture time along dip and along strike for sections respectively crossing the hypocenter are shown. Along dip, rupture time differ only at the shallow zone due to different parametrization at the SL zone. Along strike the are difference at the west side (left side) due to rupture extension from models that break the free-surface.

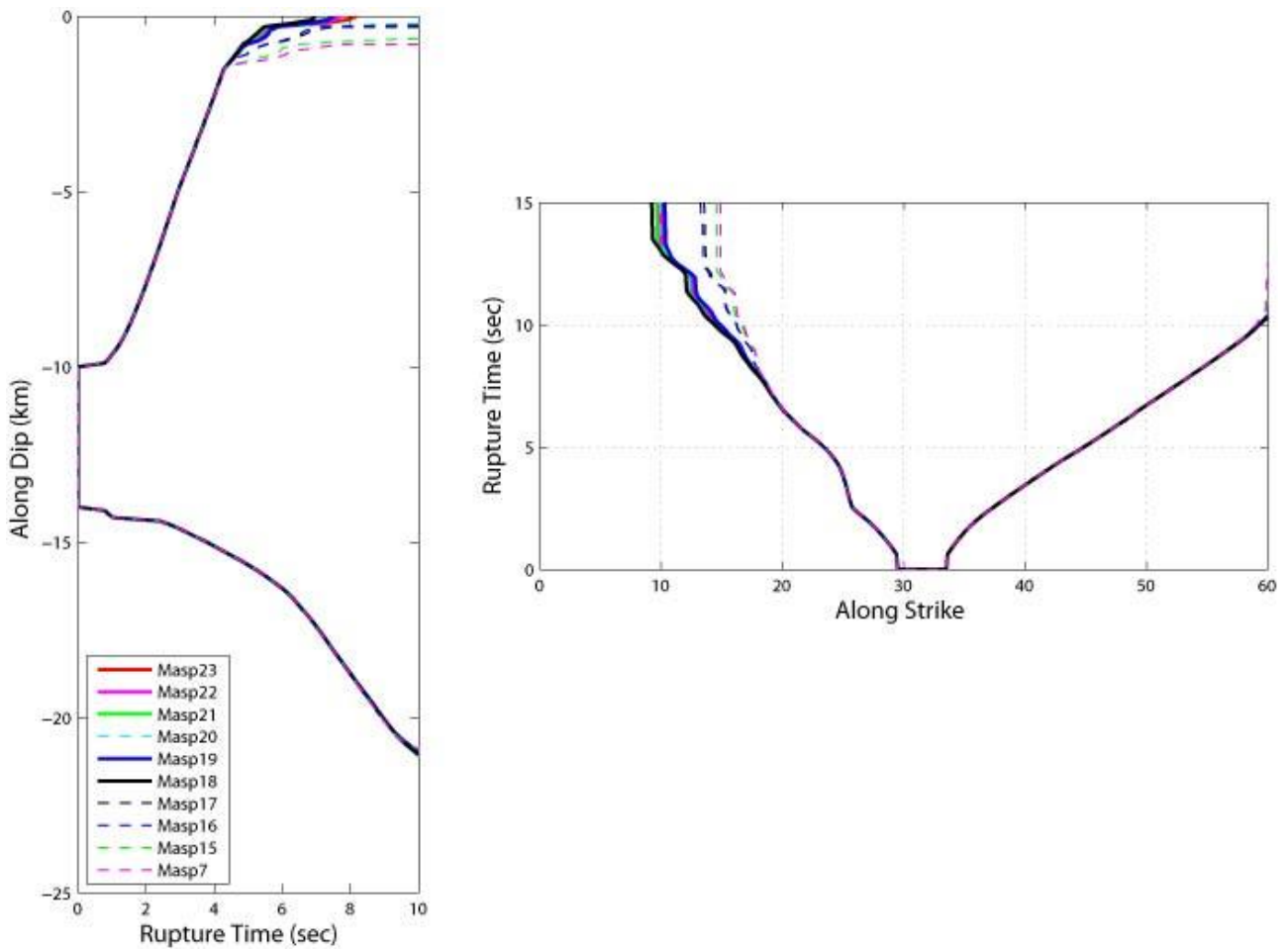


Figure 9. Rupture time along dip (left) and along strike (right) for sections respectively crossing the hypocenter. Solid lines are all models that break the free-surface, and dashed line some models without surface rupturing, including model 7 from Figure 6.

In order to evaluate which of the models with surface rupturing can be considered as best model consisting with observations, we compare the fault offset (fault displacement) distribution along strike with the measured fault offset (Figure 2) reported by Quigley et al (2012). We calculate the final offset from the horizontal and vertical component of fault offset shown in Figure 2 for the west, central and east fault segment as defined by Quigley et al (2012). The location of the measured fault offset has been approximately adapted to our fault model. Figure 10 shows the synthetic fault displacement of all the models with surface rupturing compared with the measured fault offset. Notice that all the models, except model 23, extend the surface rupturing to wider areas compared to the observed ones. Though model 23 does not predict the maximum amplitude, in terms of distribution it is consistent with observations. However, it is important to mention that the observed fault offset (Figure 2) seems that occurs in three fault segments that are not spatially interconnected, that is different to our simplifies dynamic models composed with only one planar fault segment. This simplification in our model is a limitation for better prediction of fault displacement.

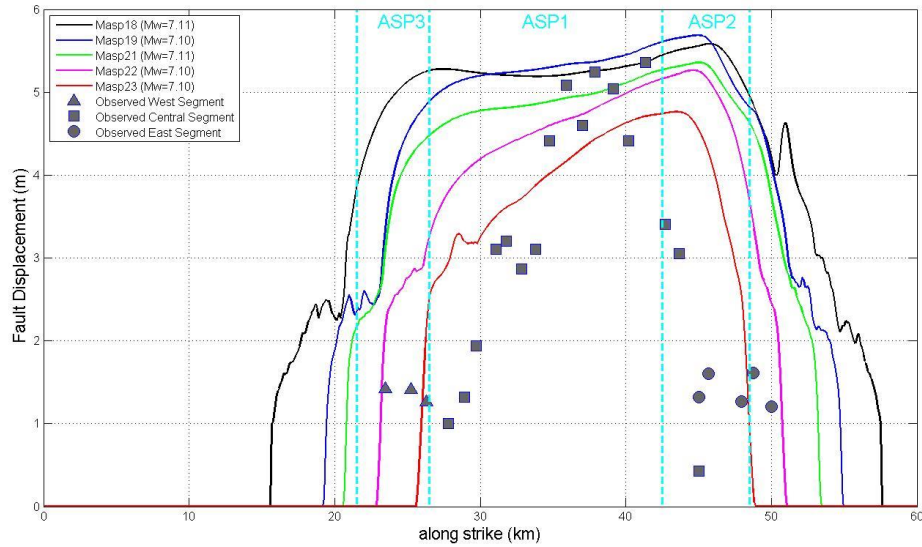


Figure 10. Comparison of synthetic fault displacement (solid lines) from all models that break the free-surface with observed fault offset reported by Quigley et al (2012). Model 23 is considered as the preferred model for being better consistent with the observed spatial distribution.

As mentioned above, our preferred model (model 23) produce fault displacement distribution closer to the observed ones (Figure 10). But compared to model 7, the average slip at the asperities increase to 3.4m, 3.2 and 2.8m, respectively for ASP1, ASP2 and ASP3. This increase in average slip is due to the contribution of surface rupturing. This preferred model has dynamic parameterization at the SL (as shown in Figure 8) of strength excess (SE) and critical slip distance (Dc) varying linearly from the seismogenic zone to the free surface, respectively from 6MPa to 1MPa for SE and from 0.2m to 2.5m for Dc. Stress drop is zero at the SL zone. Figure 11 shows the stress drop, strength excess and critical slip distribution on the fault for model 23. Figure 12 shows the dynamic solution of this preferred model represented by the final slip, rupture time and rupture speed distribution. Notice that rupture propagation (rupture speed and rupture time) are nearly identical to the model 7 (Figure 7) at the seismogenic zone, as well as final slip pattern. The strong differences are at the SL zone. The slip velocity functions, filtered with a low pass filter with frequency cut of 0.5Hz, at different locations are plotted in Figure 13. They are plotted on the top of the final slip distribution. Notice the remarkable slip velocity pulses at surface rupture with amplitudes up to 4.0m/s, while inside the SL zone the slip velocity functions are smooth long period waveforms with lower amplitudes. These pulses at the free-surface generate large permanent displacements at the near-source pulse ground motion, sometimes named “fling”, resulted from surface-rupturing faulting. These have been observed in some earthquakes, such as the 1999 Kocaeli, 1999 Chi-Chi, 2002 Denali. This suggest that the fling-pulses are mainly caused by the abrupt surface rupturing rather than the asperities at the depth or rupture directivity effects. All the models that break the free-surface generate similar slip velocity function at the surface rupture, and at depth are nearly identical. The models with buried rupture also produce similar slip velocity function, but only at the seismogenic zone because of the same stress parameterization. Figure 14 shows these features when comparing slip velocity functions between the buried rupture (model 7) and the surface rupturing models 23 and 18. Though model 23 has been selected as our preferred model because fault displacement in terms of extension along the fault is better consistent with observation, the model 18 is better consistent in term of maximum amplitude of fault displacement. Therefore these two models, and the other surface rupturing models that are in between, can equally be considered good models in terms of ground motion, as will be discussed in the next section

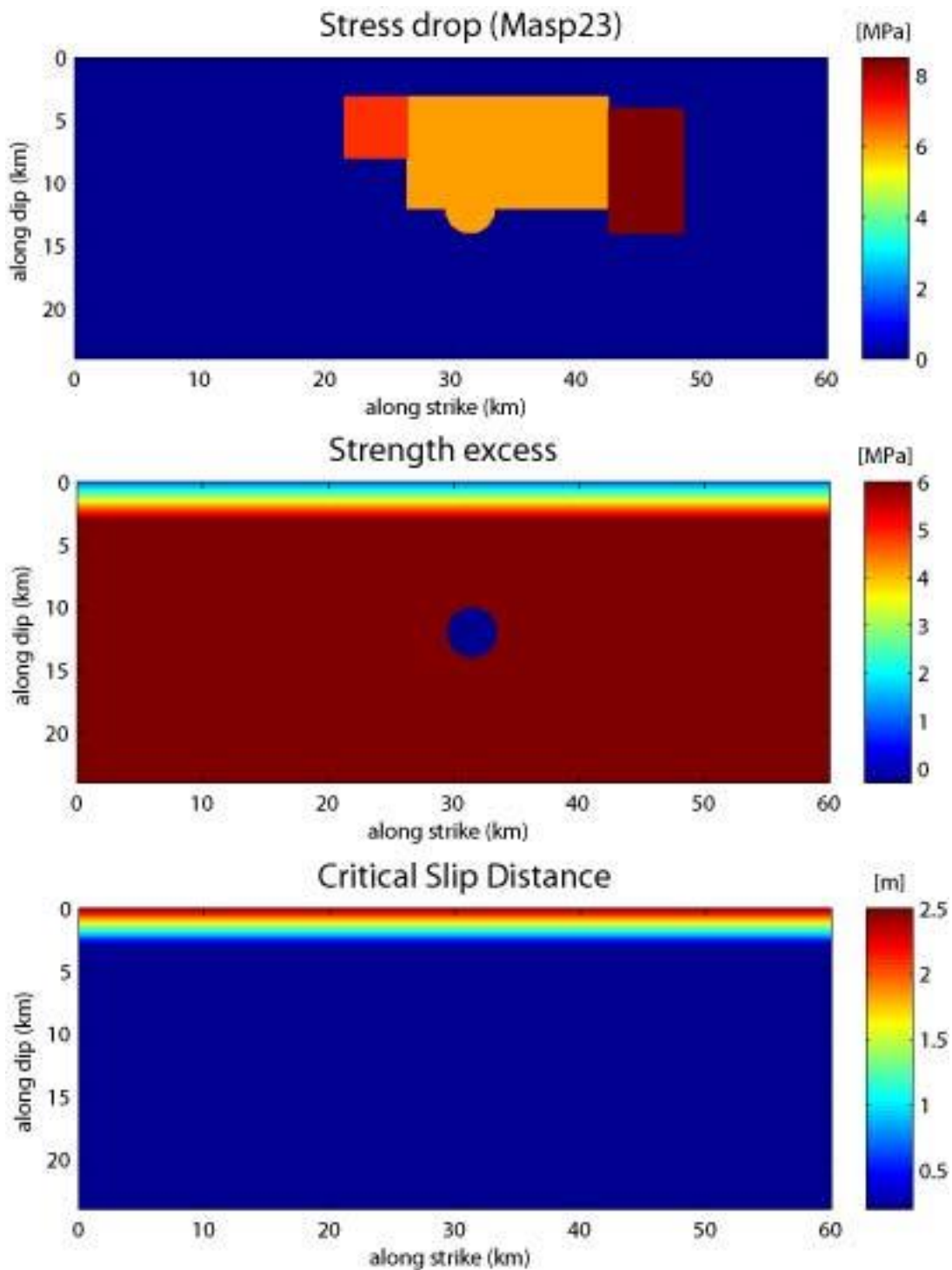


Figure 11. Stress drop, strength excess and critical slip distance distribution for the dynamic rupture simulation of asperity model 23 with surface rupturing better (compared to other models) consistent with the observed fault offset distribution.

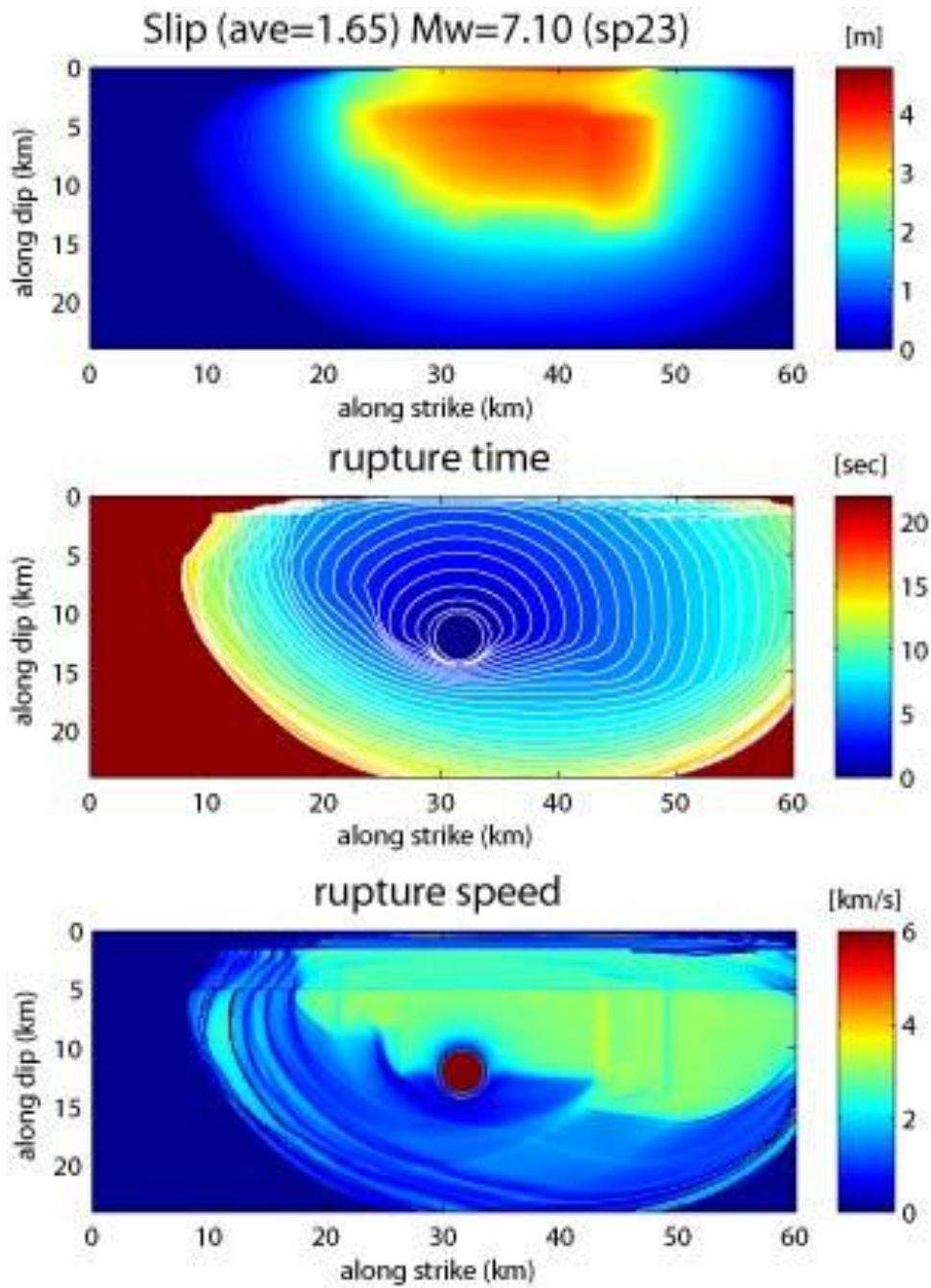


Figure 12. Dynamic rupture solution of asperity model 23, represented by final slip distribution (top), rupture time (middle) and rupture speed (bottom).

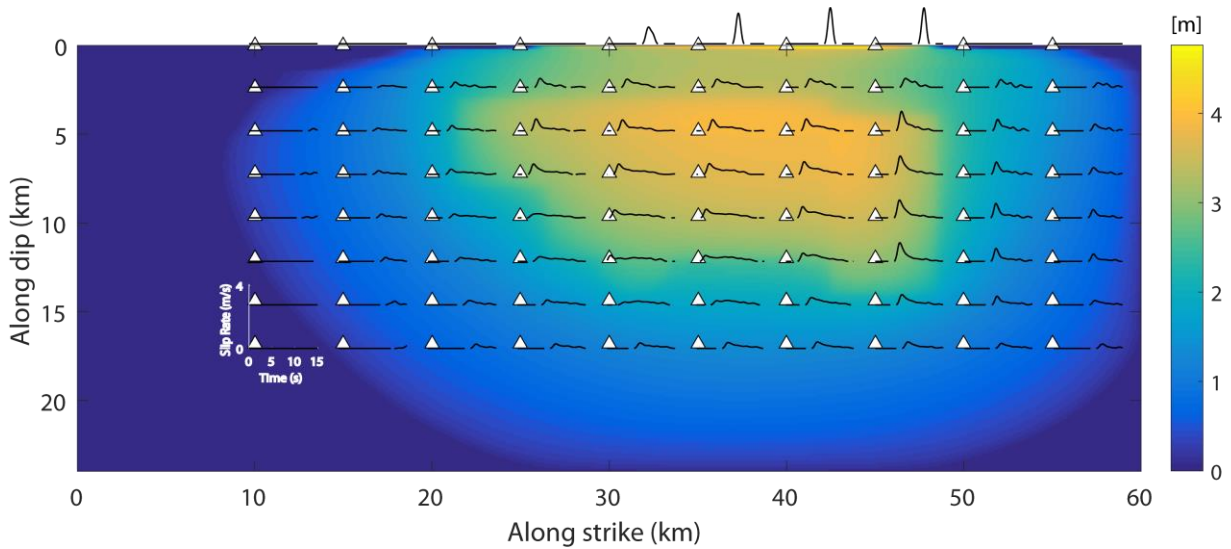


Figure 13. Slip velocity functions distributed at some points on the fault from the model 23. Background correspond to the final slip distribution from the same model.

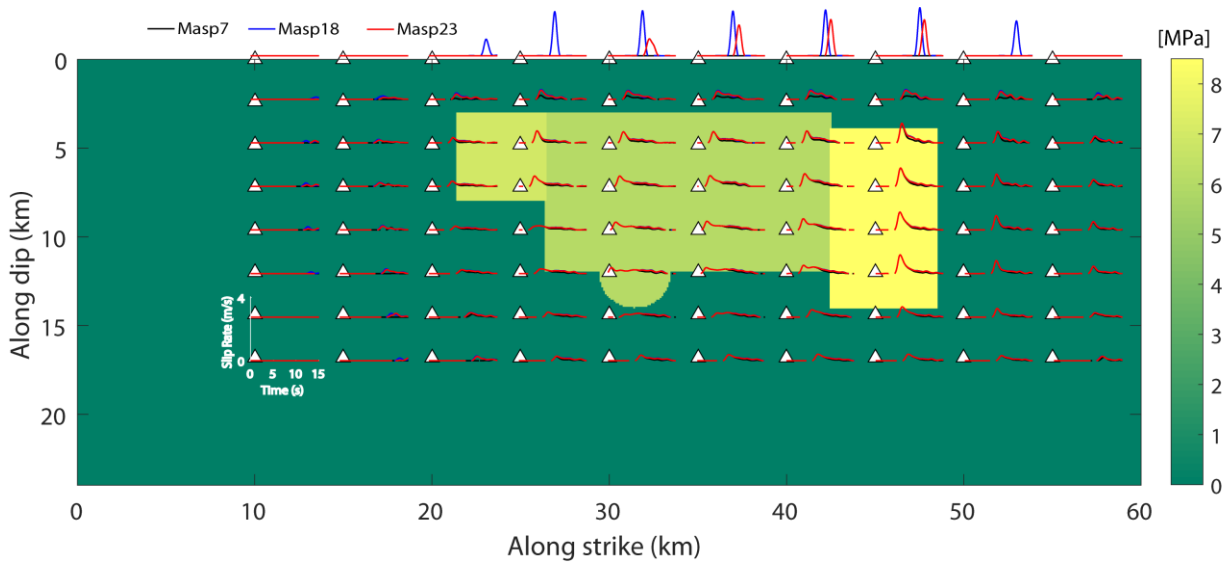


Figure 14. Slip velocity functions distributed at some points on the fault from models 7, 18 and 23. Background correspond to the stress drop distribution of surface rupturing models (18 and 23)

Ground Motion

We have also simulated ground motion at the stations shown in Figure 3. Considering that the source rupture features at the seismogenic zone (on the asperities) are nearly the same between all the models that break the free-surface and buried rupture, as shown in Figure 9 and 14, it is expected that the ground motion differences between these models would be essentially due to the surface rupturing, and it would be reflected at the very near-source ground motion. Therefore selecting the best model in terms of ground motion that best fit the observed records, any of the models that break the free-surface can be considered as good models. In appendix is shown the comparison of the velocity and displacement ground motion between the buried rupture model (Model 7) and surface rupturing models 18 and 23. As shown in these figures, ground motion are nearly identical between the surface rupturing models at all the stations. It suggests that any of our

surface rupturing model can be considered as good in term of ground motion. The differences with the buried rupture is basically at the very-near source, due to the surface rupturing effects.

The comparison of velocity and displacement ground motion with observed records are shown in Figures 15-34 for the 20 stations shown in Figure 3. Comparison is done in the frequency band of 0.0 to 0.5Hz. Overall synthetics seismograms are consistent with observations, however details of the complexity waveforms from observed records are not reproduced because of our simplified model.

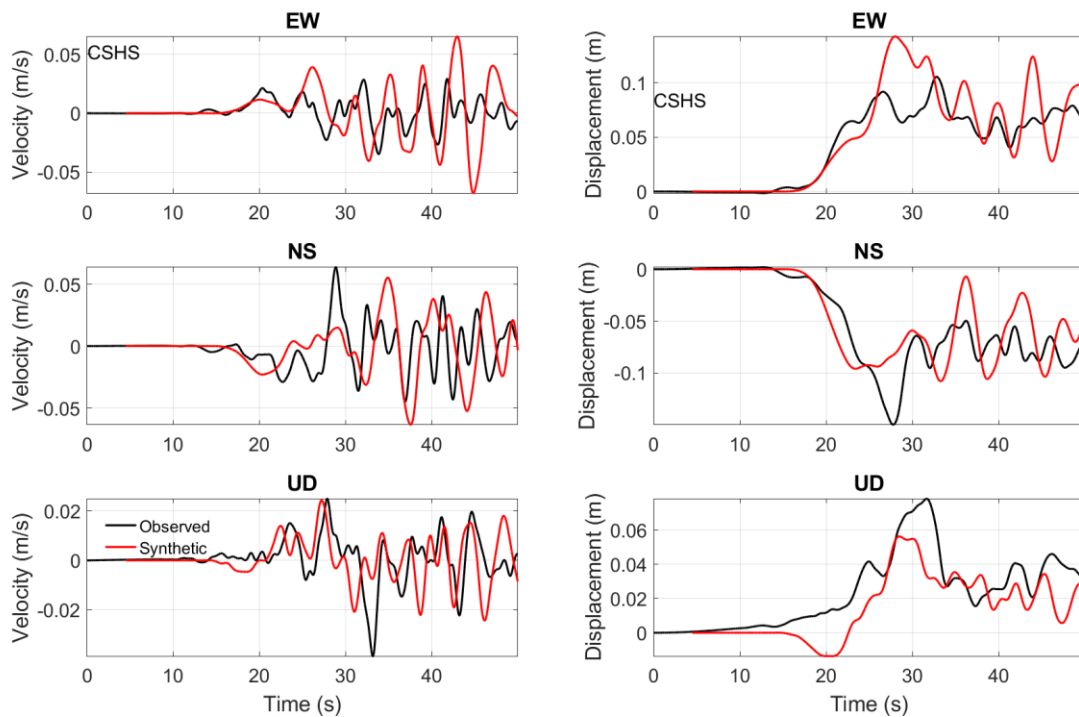


Figure 15. Three components of velocity and displacement ground motion compared with observed records. Station CSHS.

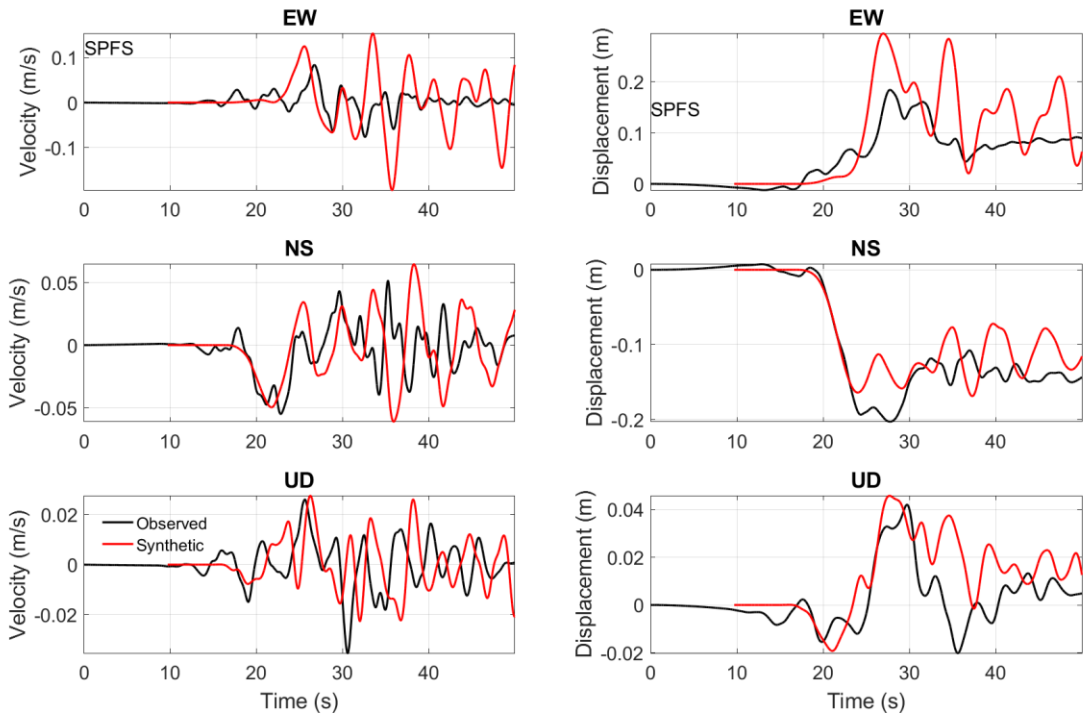


Figure 16. Three components of velocity and displacement ground motion compared with observed records. Station SPFS.

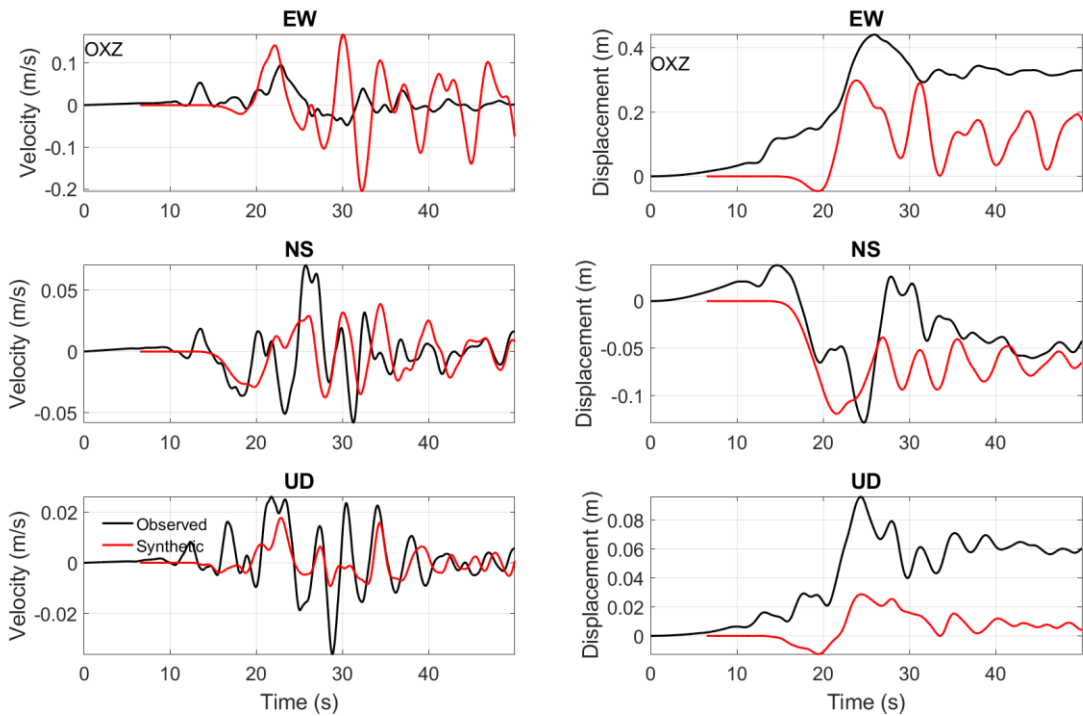


Figure 17. Three components of velocity and displacement ground motion compared with observed records. Station OXZ.

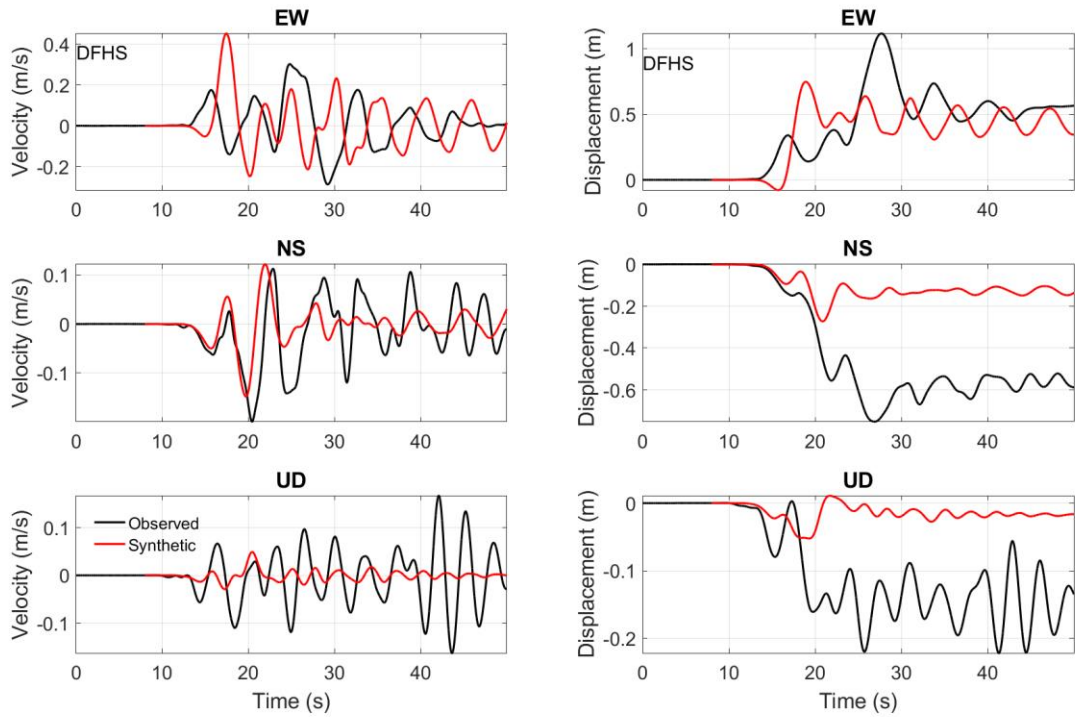


Figure 18. Three components of velocity and displacement ground motion compared with observed records. Station DFHS.

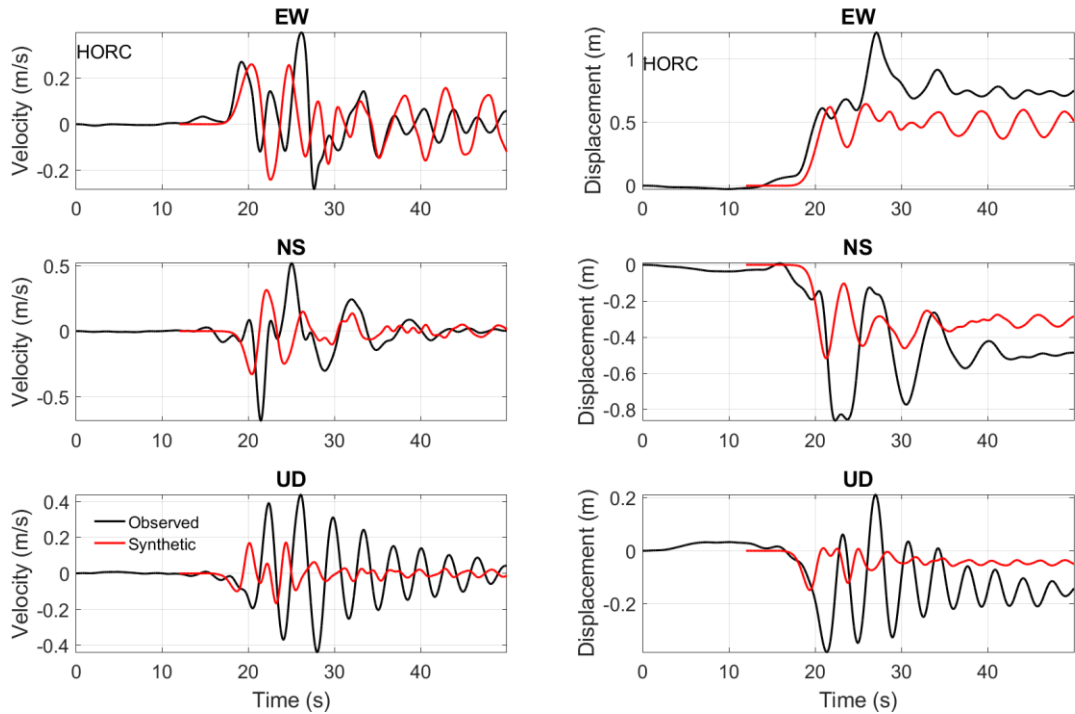


Figure 19. Three components of velocity and displacement ground motion compared with observed records. Station HORC.

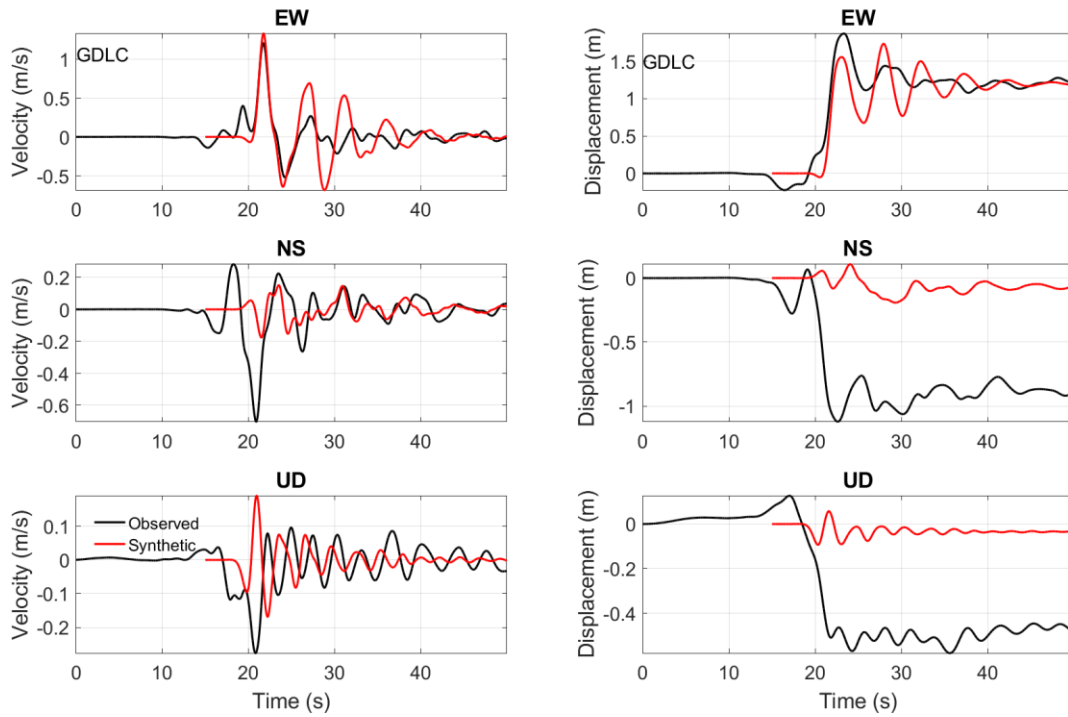


Figure 20. Three components of velocity and displacement ground motion compared with observed records. Station GDLC.

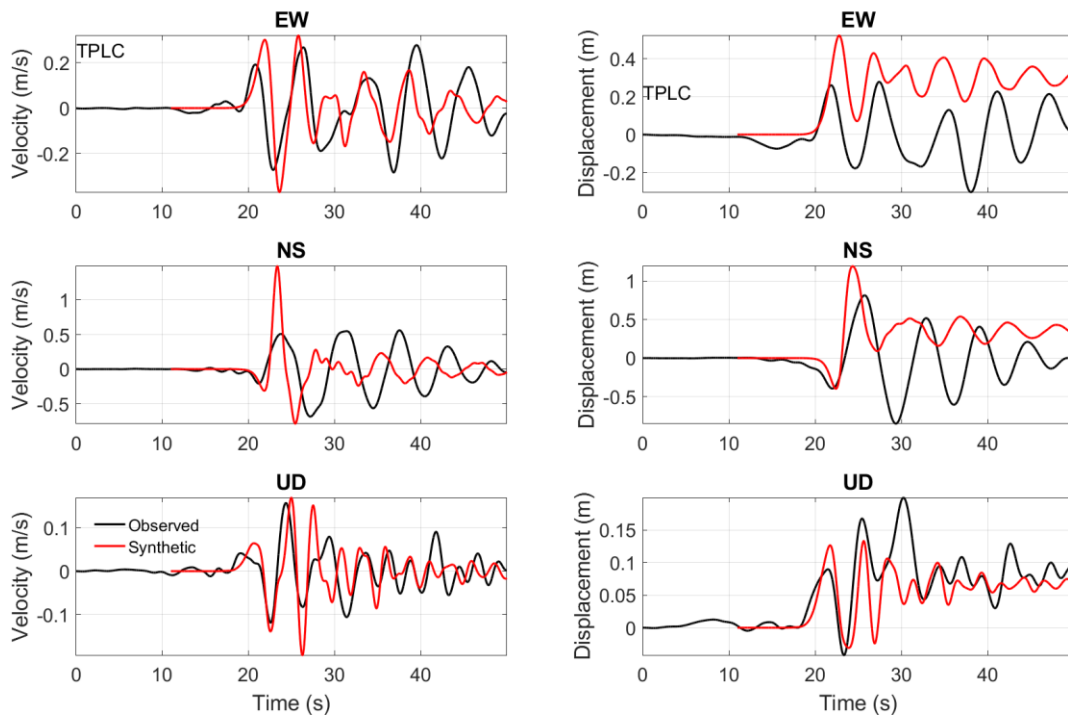


Figure 21. Three components of velocity and displacement ground motion compared with observed records. Station TPLC.

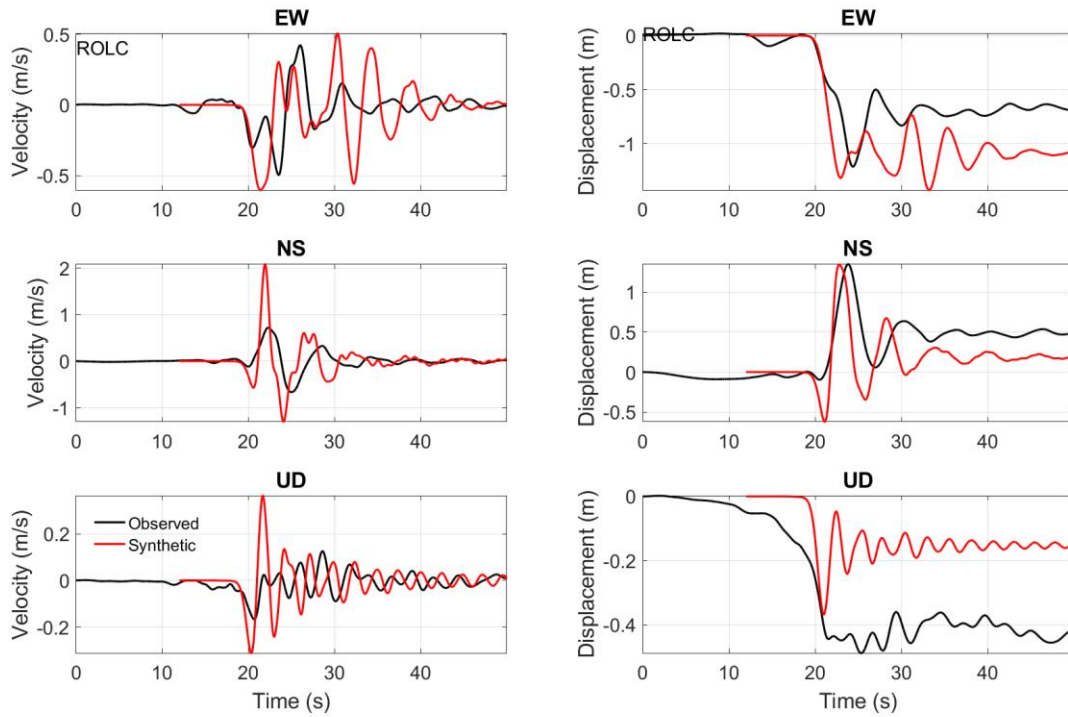


Figure 22. Three components of velocity and displacement ground motion compared with observed records. Station ROLC.

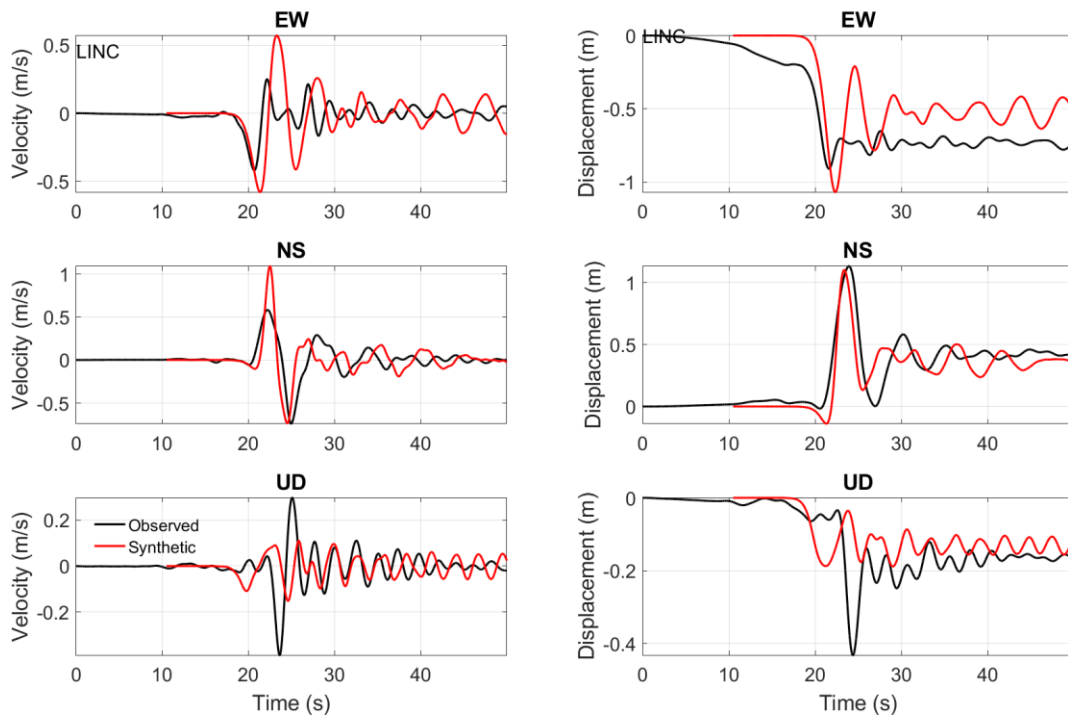


Figure 23. Three components of velocity and displacement ground motion compared with observed records. Station LINC.

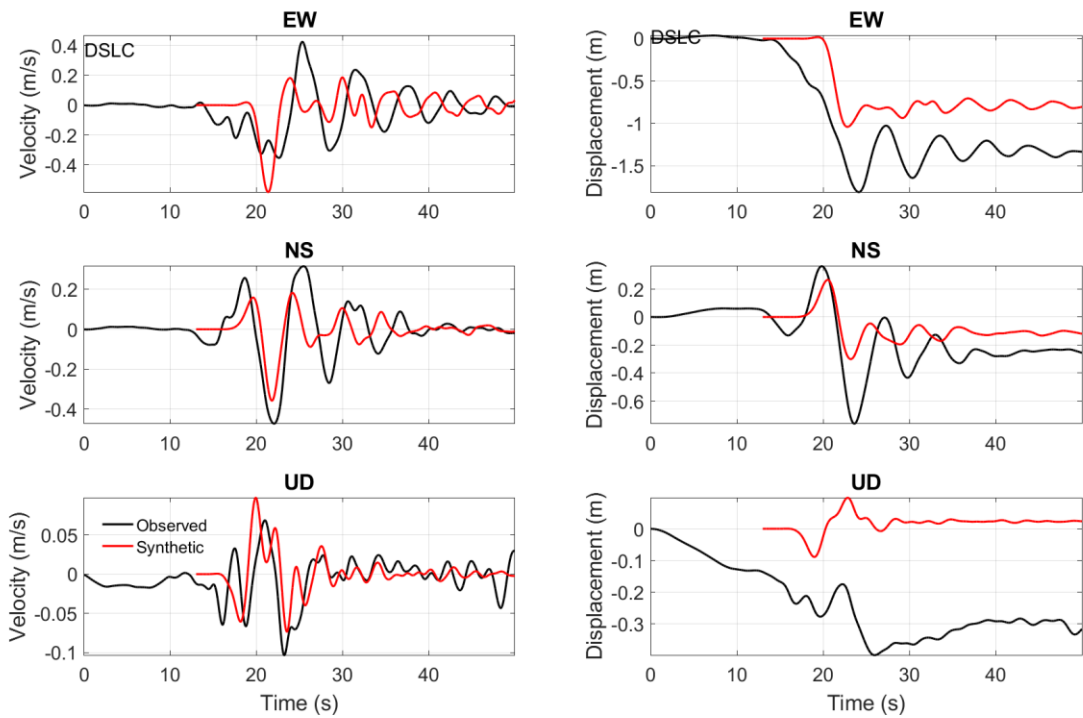


Figure 24. Three components of velocity and displacement ground motion compared with observed records. Station DSLC.

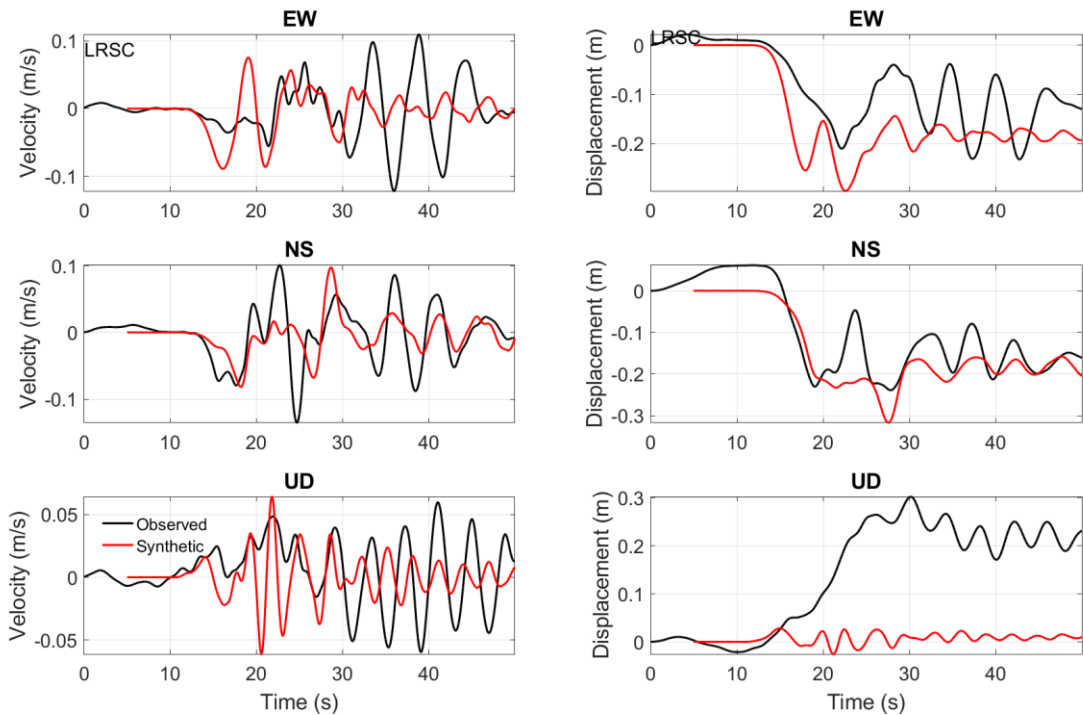


Figure 25. Three components of velocity and displacement ground motion compared with observed records. Station LRSC.

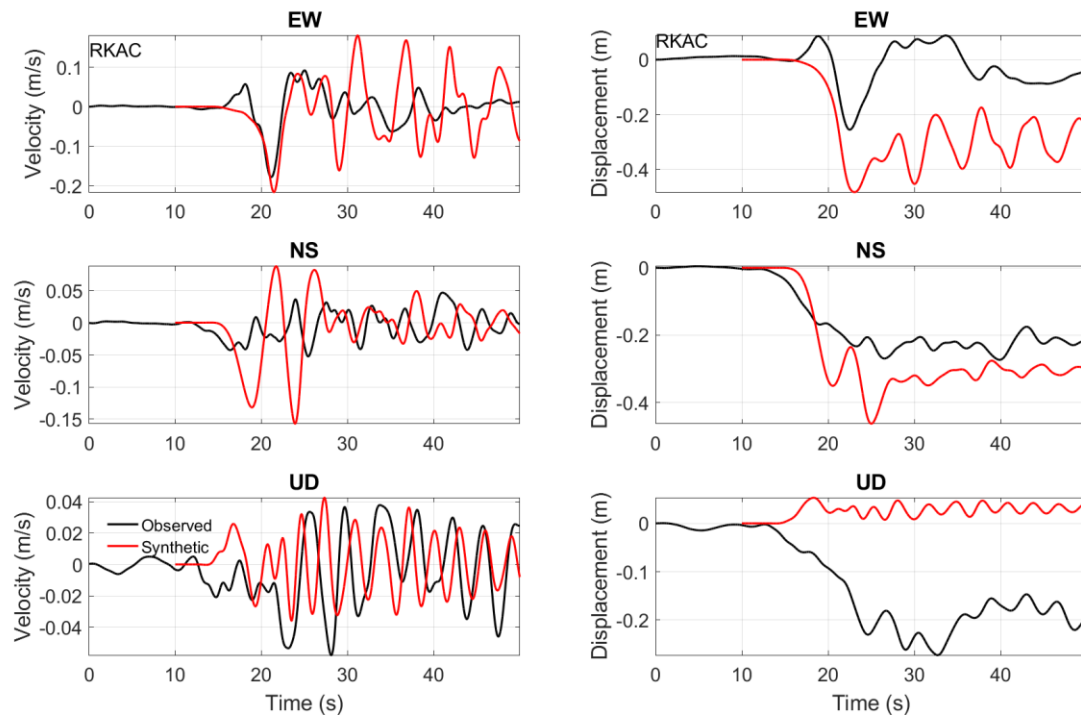


Figure 26. Three components of velocity and displacement ground motion compared with observed records. Station RKAC.

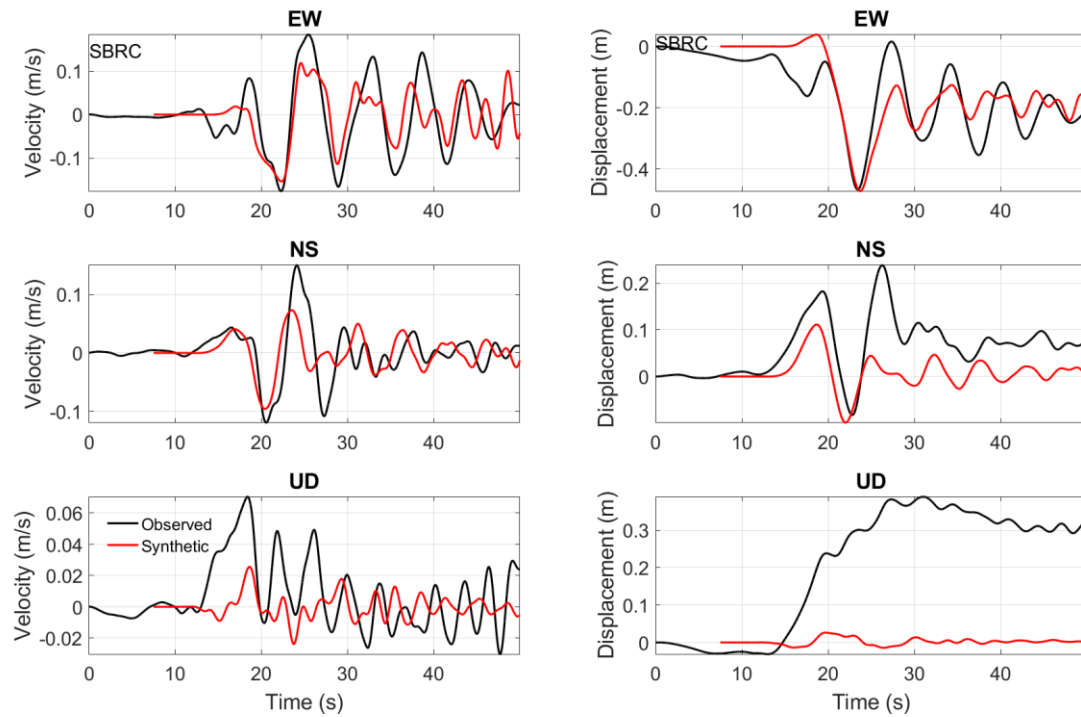


Figure 27. Three components of velocity and displacement ground motion compared with observed records. Station SBRC.

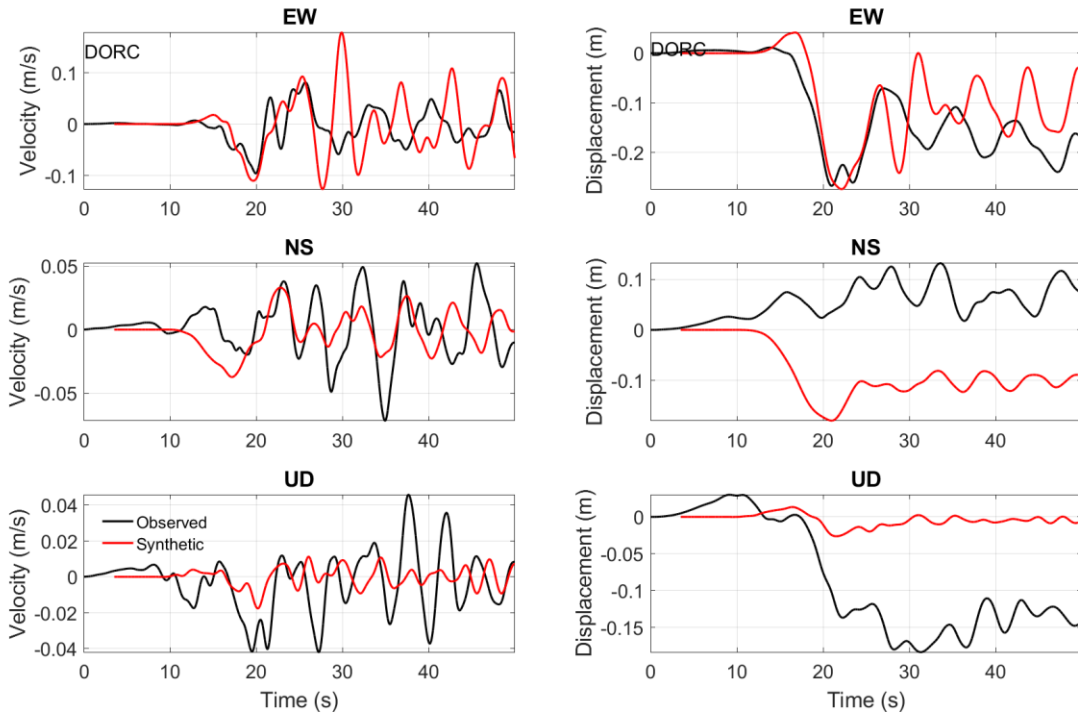


Figure 28. Three components of velocity and displacement ground motion compared with observed records. Station DORC.

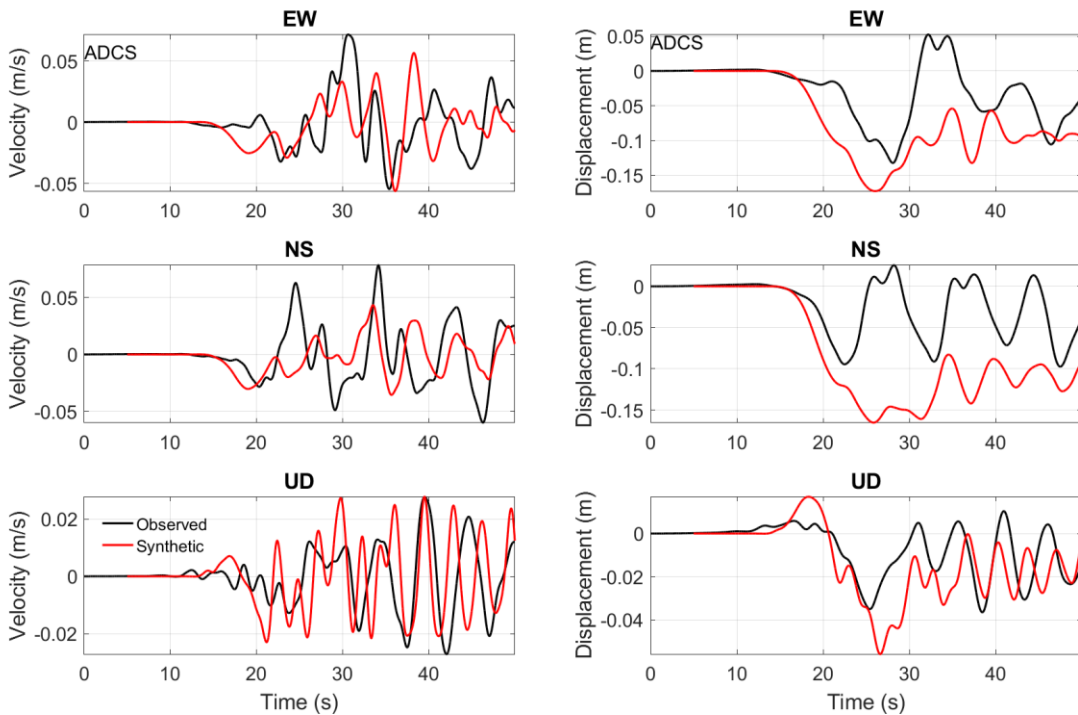


Figure 29. Three components of velocity and displacement ground motion compared with observed records. Station ADCS.

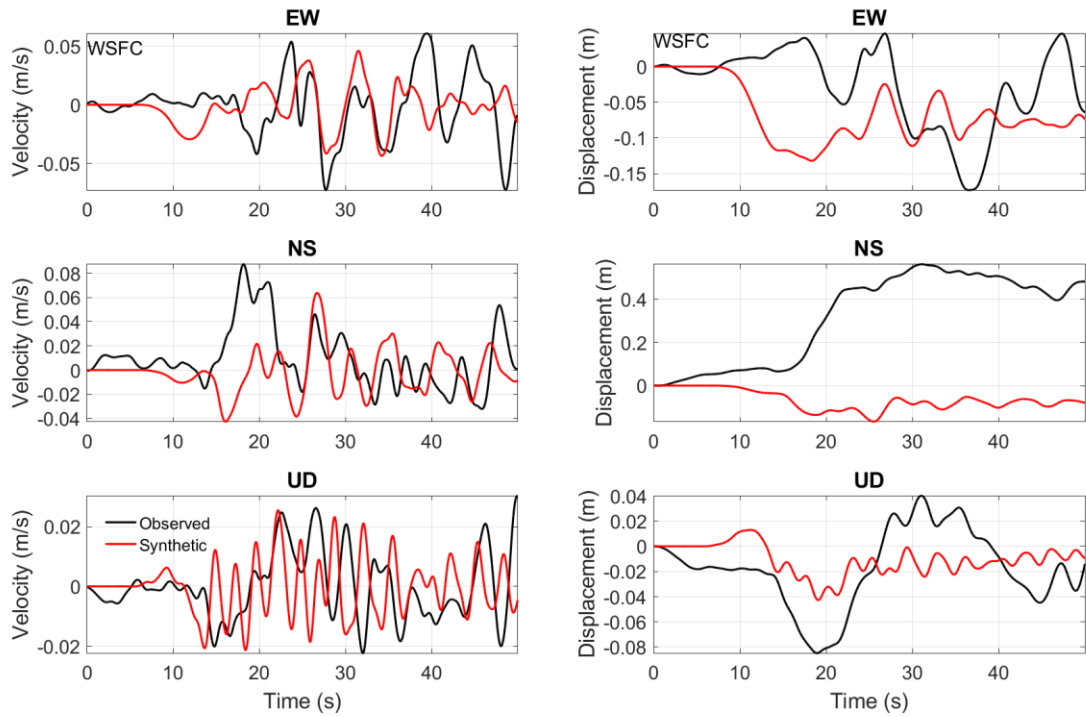


Figure 30. Three components of velocity and displacement ground motion compared with observed records. Station WSFC.

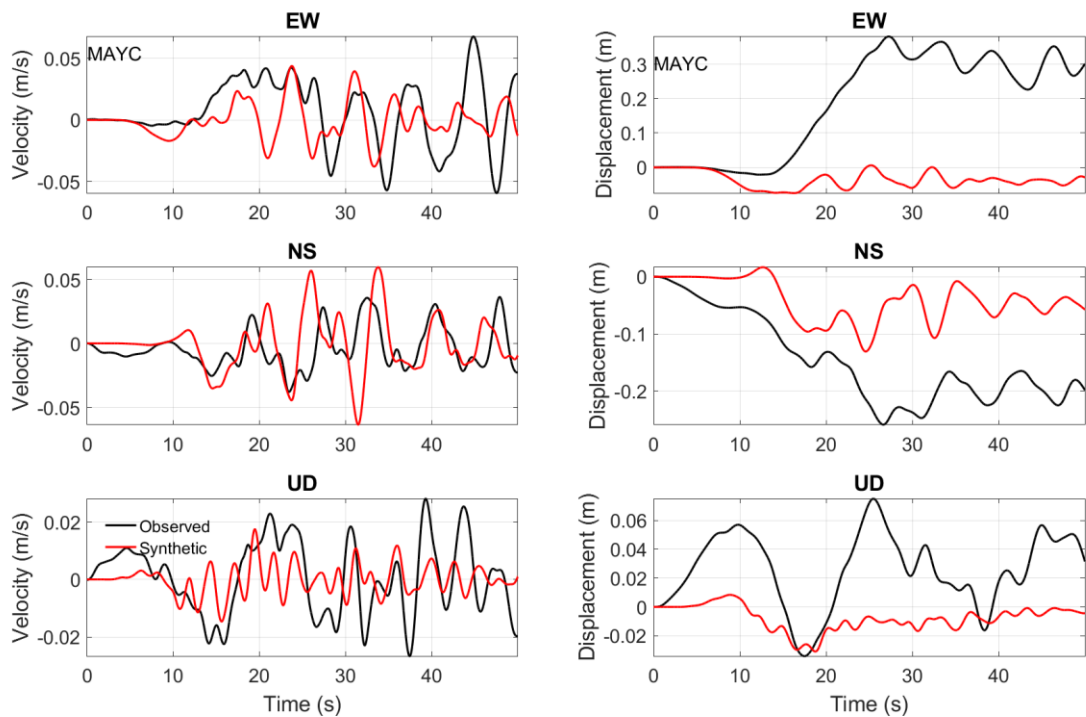


Figure 31. Three components of velocity and displacement ground motion compared with observed records. Station MAYC.

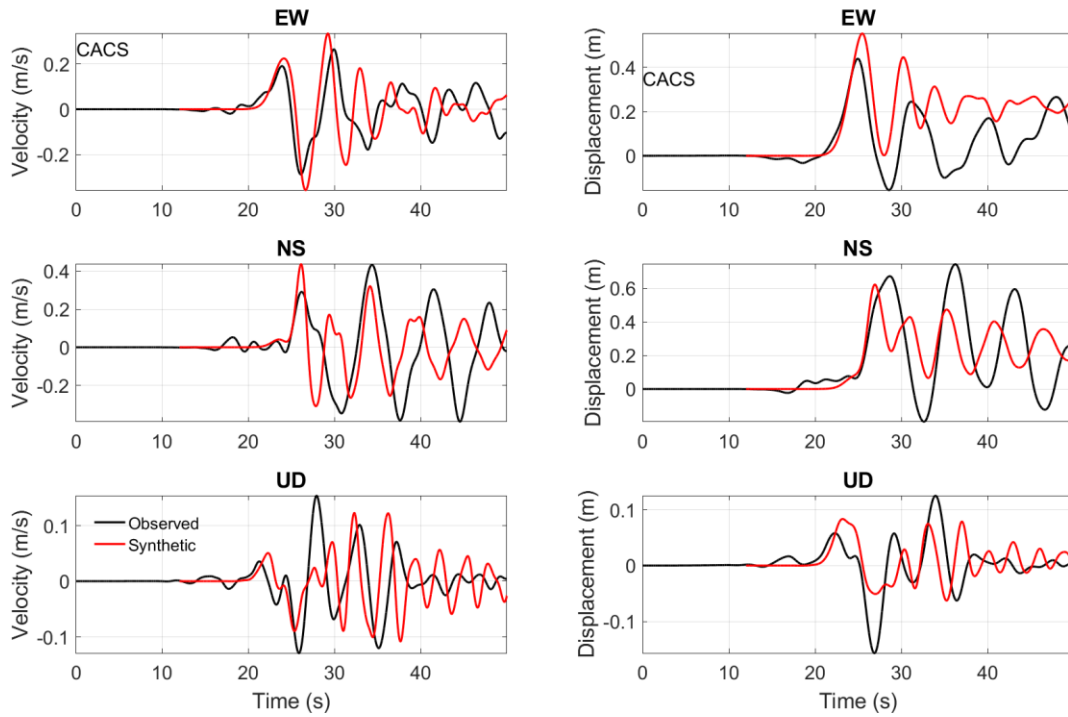


Figure 32. Three components of velocity and displacement ground motion compared with observed records. Station CACS.

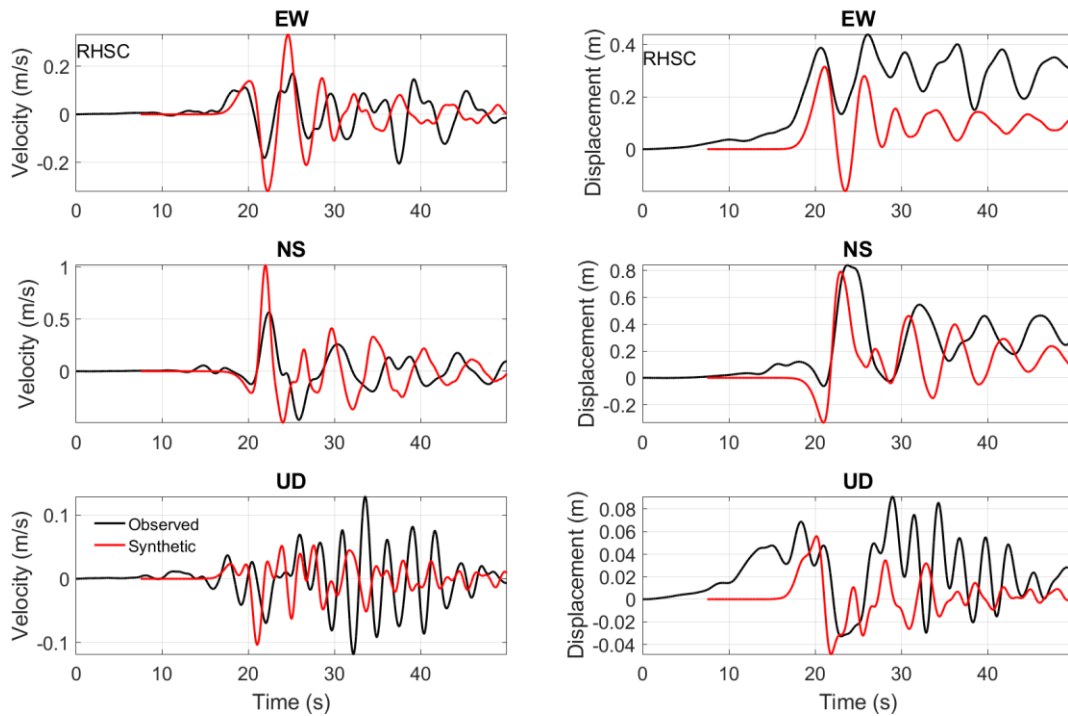


Figure 33. Three components of velocity and displacement ground motion compared with observed records. Station RHSC.

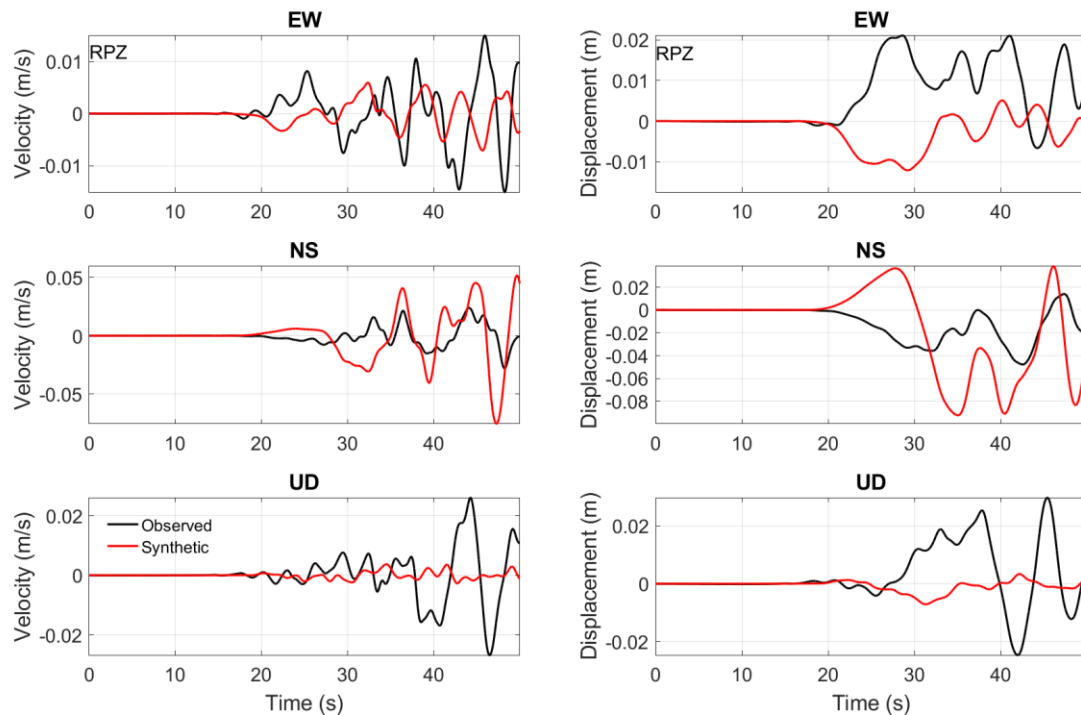


Figure 34. Three components of velocity and displacement ground motion compared with observed records. Station RPZ.

References:

- Andrews, D.J (1976). Rupture velocity of plane-strain shear cracks, *J. Geophys. Res.*, 81, 5679-5687.
- Andrews, D. J. (1980), A stochastic fault model: 1. Static case, *J. Geophys. Res.*,85, 3867–3877.
- Elliott, J.R.; Nissen, E.K.; England, P.C.; Jackson, J.A.; Lamb, S.; Li, Z.; Oehlers, M. and Parson, B. (2012). Slip in the 2010-2011 Canterbury earthquakes, New Zealand, *J. Geophys. Res: Solid Earth*, 117(B3).
- Guidotti, R., Stupazzini, M., Smerzini, C., Paolucci, R. and Ramieri, P., 2011, Numerical Study on the Role of Basin Geometry and Kinematic Seismic Source in 3D Ground Motion Simulation of the 22 February 2011 MW 6.2 Christchurch Earthquake, *Seismological Research Letters*, 82, 767-782.
- Quigley, M; R. Van Dissen, N. Litchfield, P. Villamor, B. Duffy, D. Barrell, K. Furlong, T. Stahl, E. Bilderback and D. Noble (2012). Surface rupture during the 2010 Mw 7.1 Darfi eld (Canterbury) earthquake: Implications for fault rupture dynamics and seismic-hazard analysis, *GEOLOGY*, vol. 40; no. 1; p. 55–58; doi:10.1130/G32528.1
- Ripperger, J., and **P.M. Mai** (2004). Fast computation of static stress changes on 2D faults from final slip distributions, *Geophys. Res. Lett.*, Vol. 31, No. 18, L18610 10.1029/2004GL020594.

Appendix

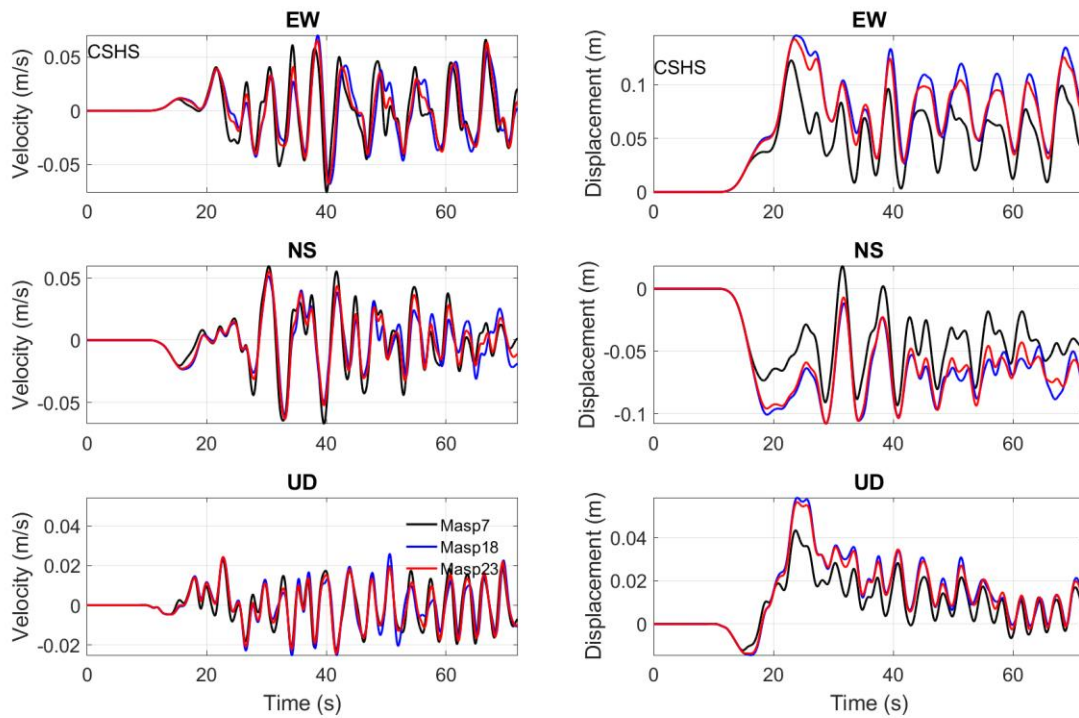


Figure A1. Three components of velocity and displacement ground motion compared between buried model 7 and surface rupturing models 18 and 23. Station CSHS.

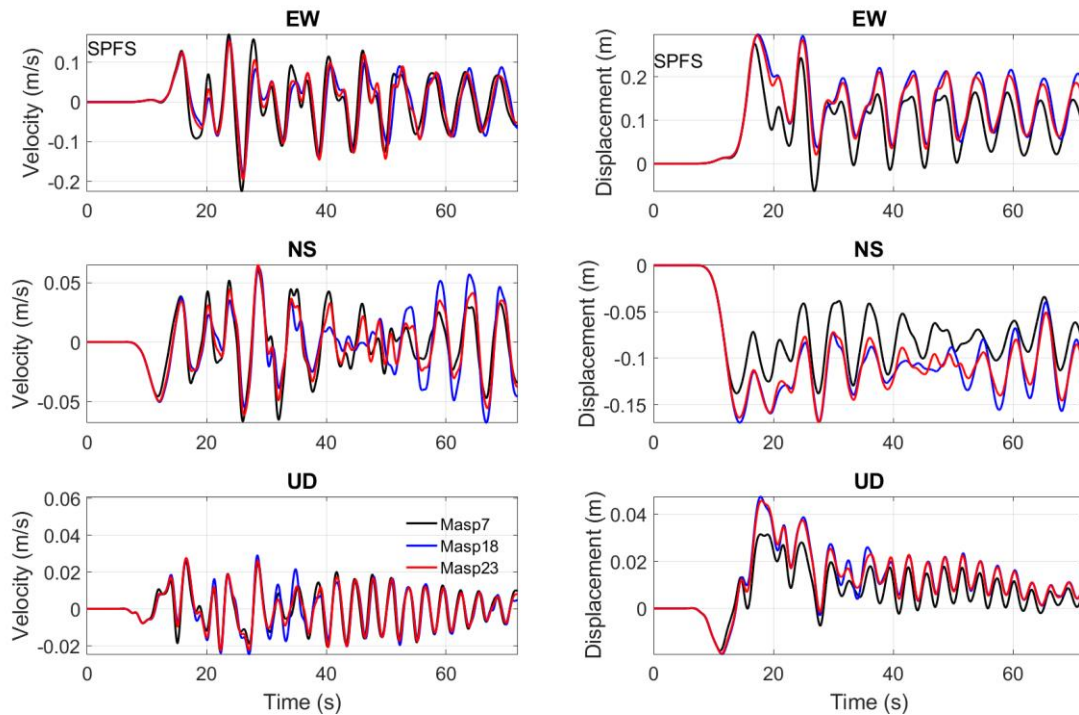


Figure A2. Three components of velocity and displacement ground motion compared between buried model 7 and surface rupturing models 18 and 23. Station SPFS.

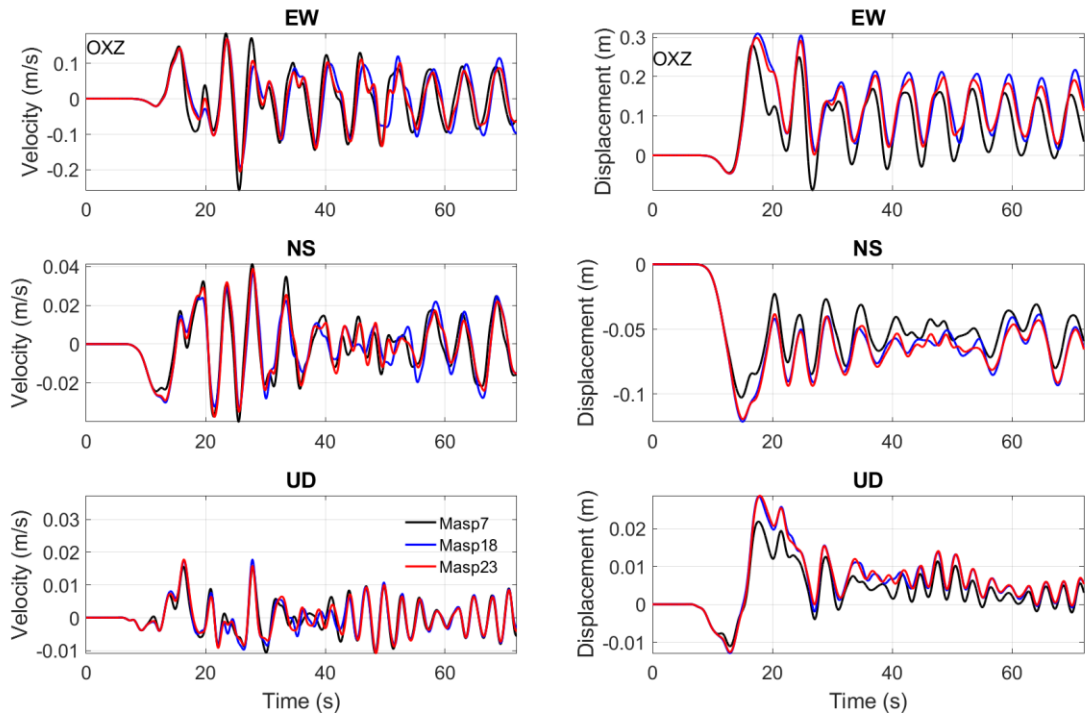


Figure A3. Three components of velocity and displacement ground motion compared between buried model 7 and surface rupturing models 18 and 23. Station OXZ.

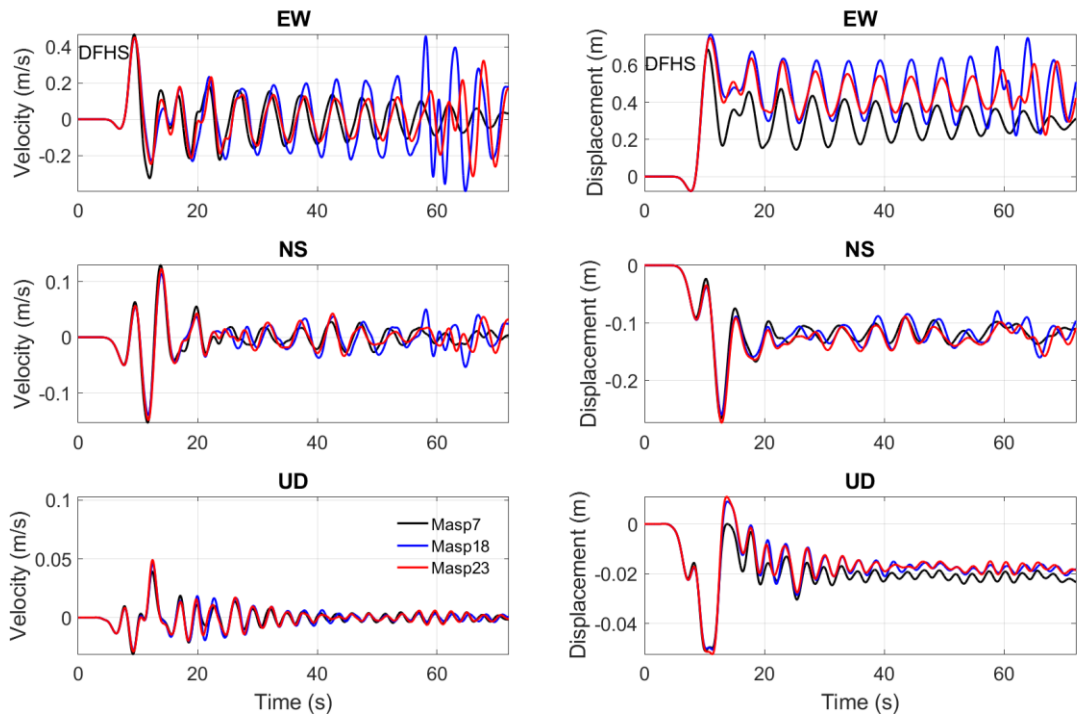


Figure A4. Three components of velocity and displacement ground motion compared between buried model 7 and surface rupturing models 18 and 23. Station DFHS.

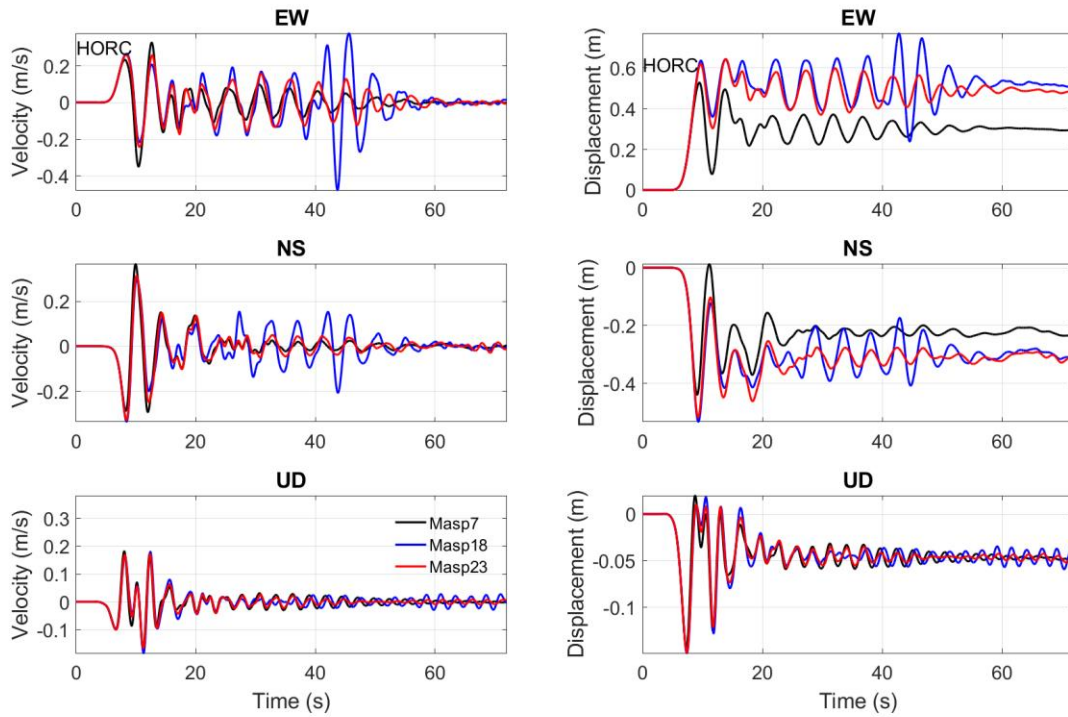


Figure A5. Three components of velocity and displacement ground motion compared between buried model 7 and surface rupturing models 18 and 23. Station HORC.

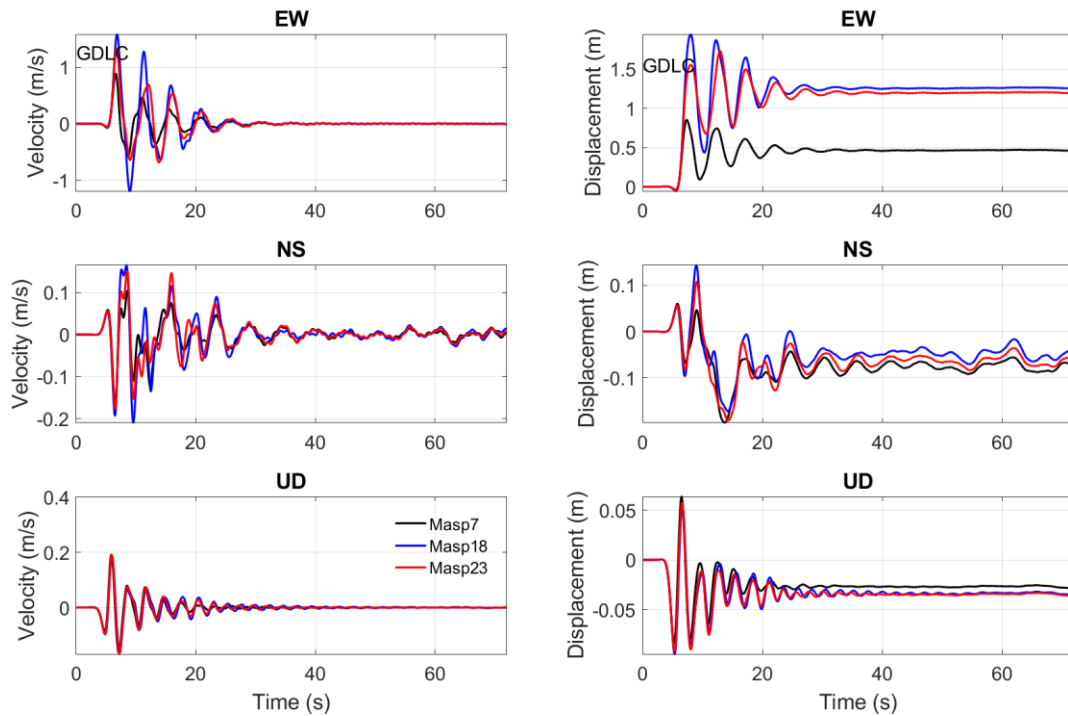


Figure A6. Three components of velocity and displacement ground motion compared between buried model 7 and surface rupturing models 18 and 23. Station GDLC.

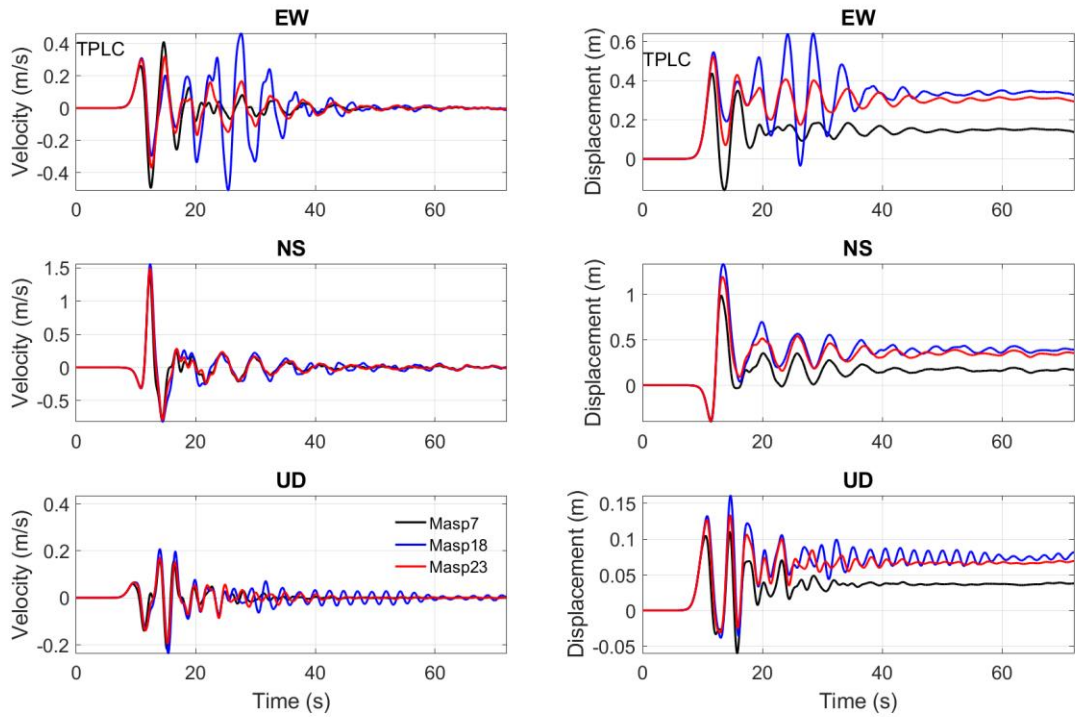


Figure A7. Three components of velocity and displacement ground motion compared between buried model 7 and surface rupturing models 18 and 23. Station TPLC.

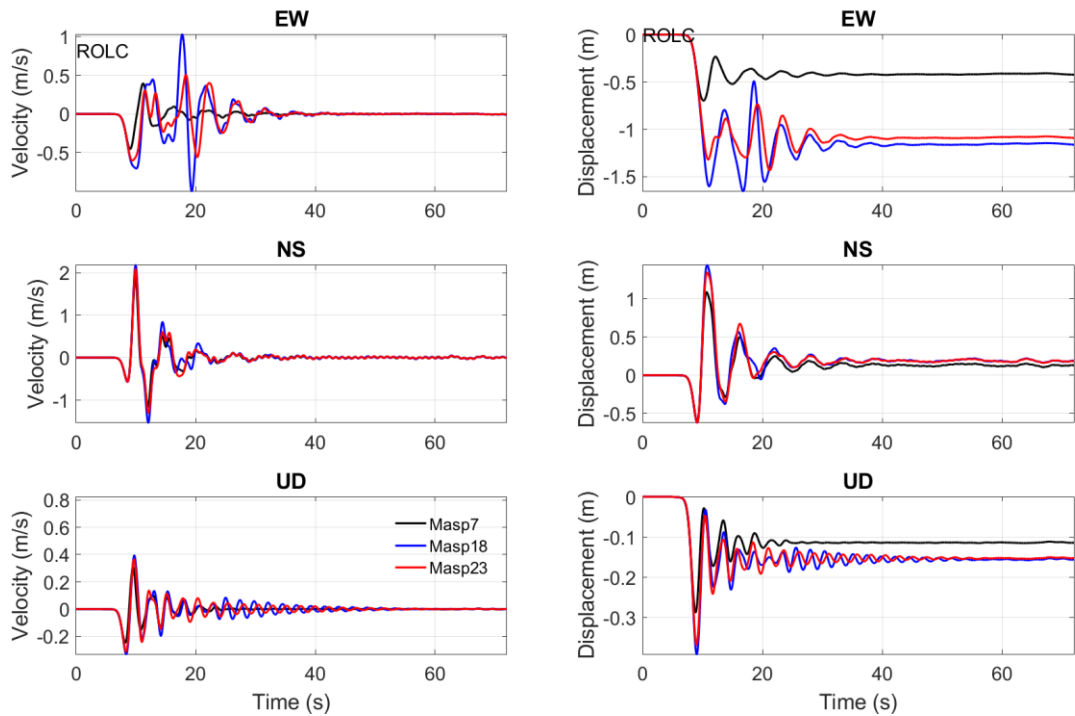


Figure A8. Three components of velocity and displacement ground motion compared between buried model 7 and surface rupturing models 18 and 23. Station ROLC.

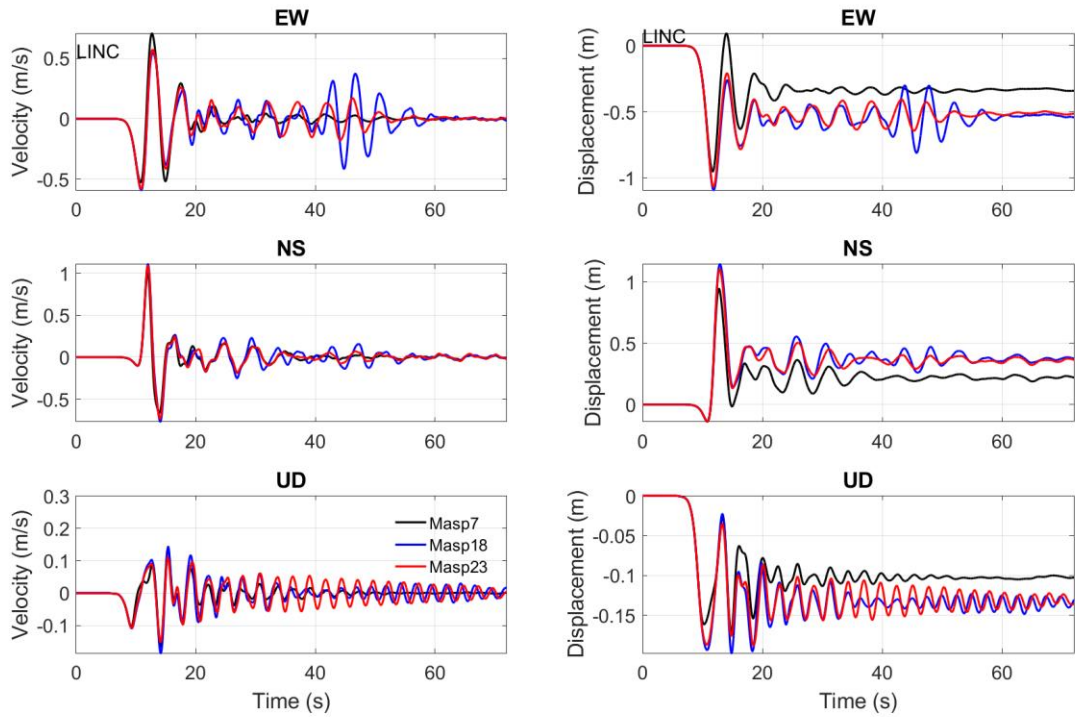


Figure A9. Three components of velocity and displacement ground motion compared between buried model 7 and surface rupturing models 18 and 23. Station LINC.

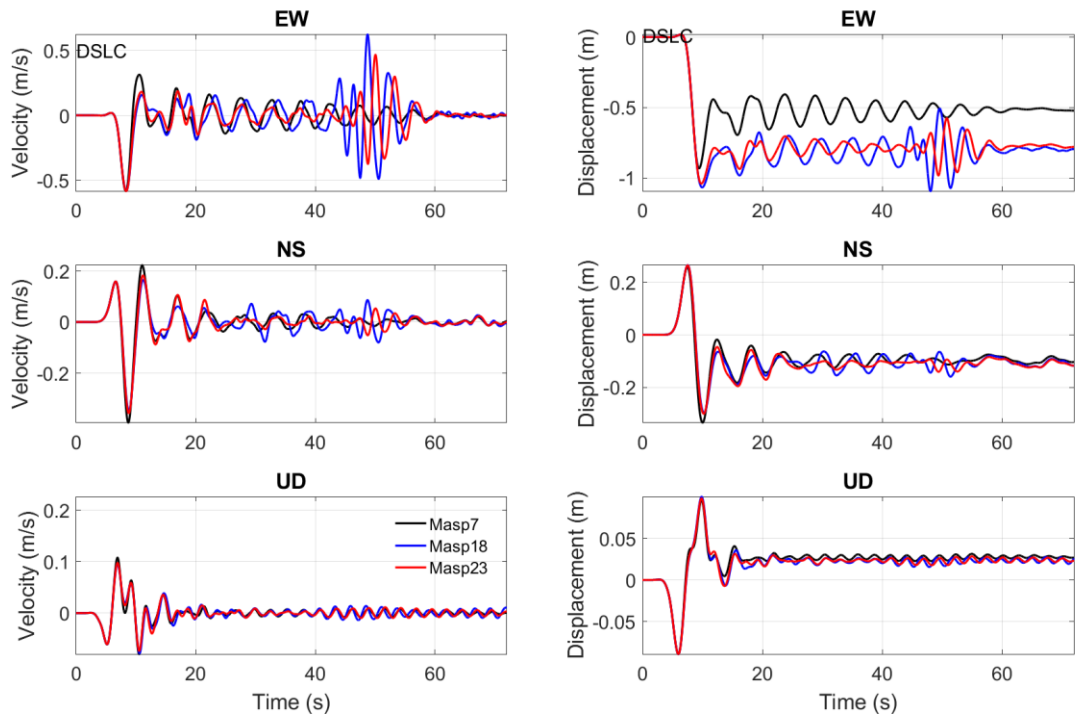


Figure A10. Three components of velocity and displacement ground motion compared between buried model 7 and surface rupturing models 18 and 23. Station DSLC.

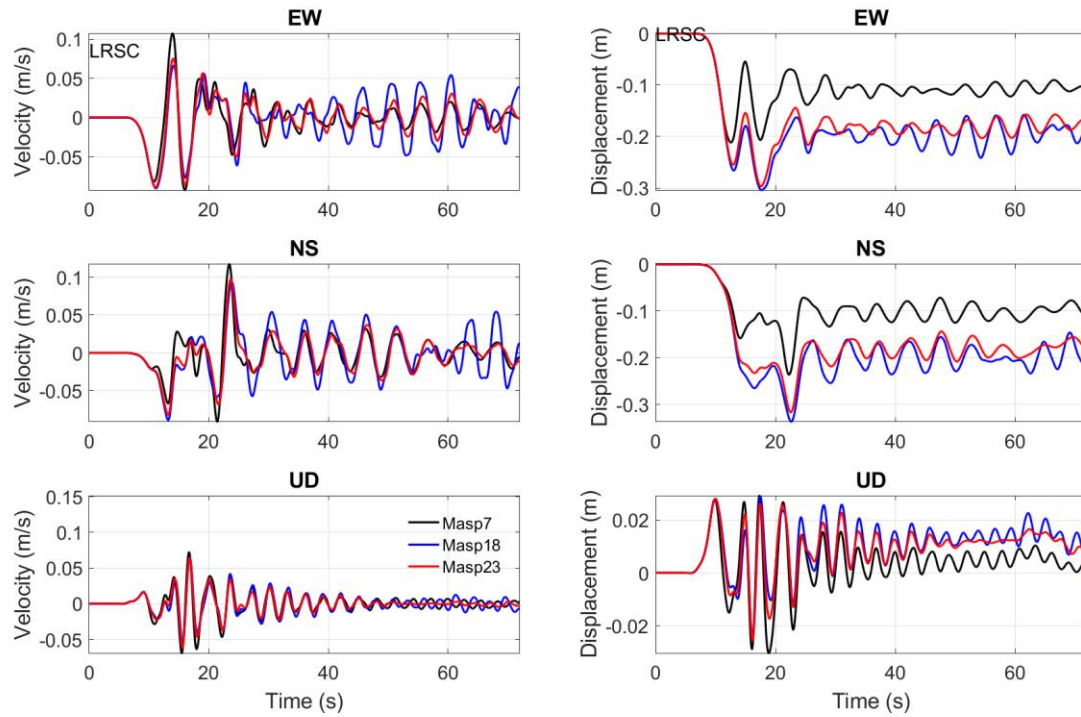


Figure A11. Three components of velocity and displacement ground motion compared between buried model 7 and surface rupturing models 18 and 23. Station LRSC.

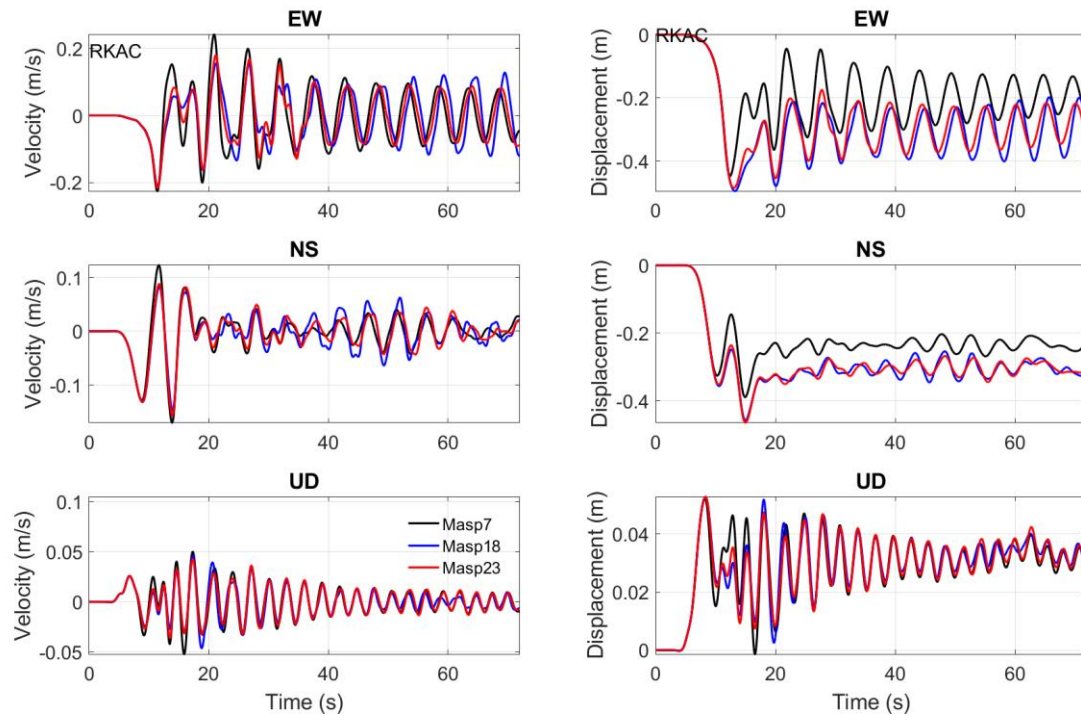


Figure A12. Three components of velocity and displacement ground motion compared between buried model 7 and surface rupturing models 18 and 23. Station RKAC.

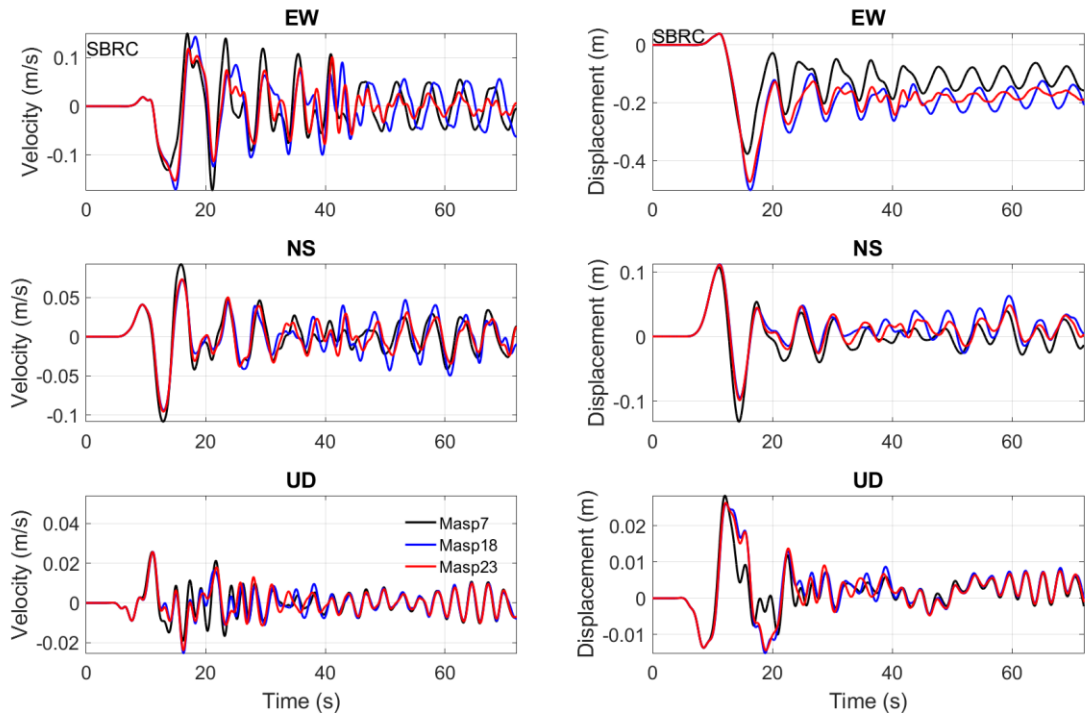


Figure A13. Three components of velocity and displacement ground motion compared between buried model 7 and surface rupturing models 18 and 23. Station SBRC.

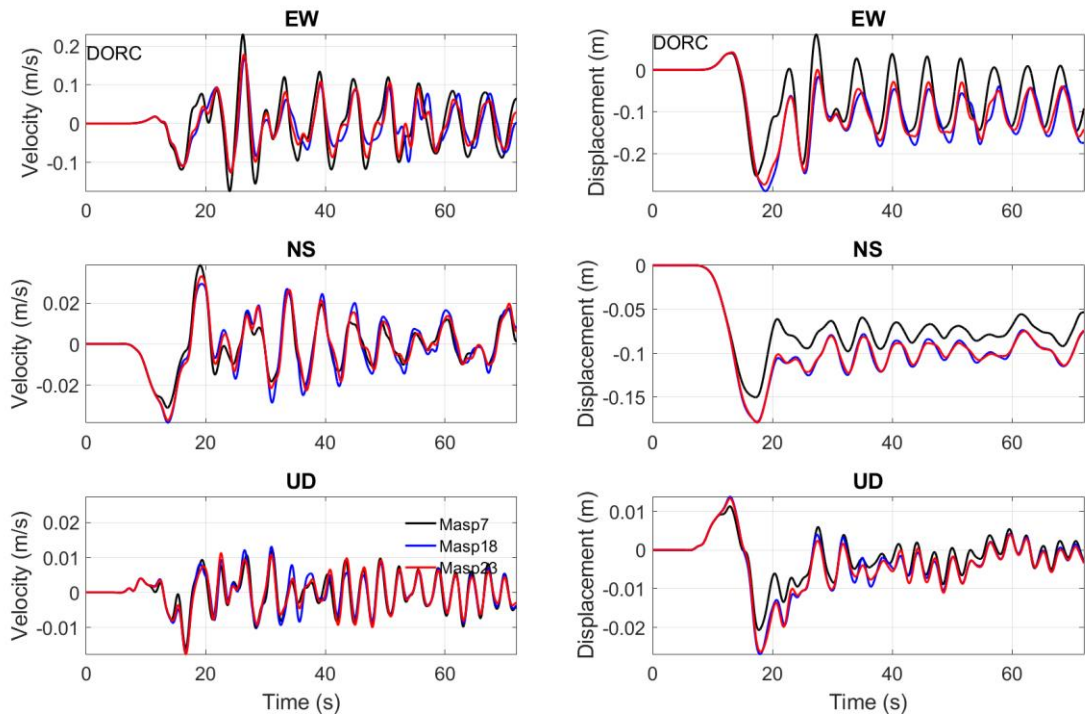


Figure A14. Three components of velocity and displacement ground motion compared between buried model 7 and surface rupturing models 18 and 23. Station DORC.

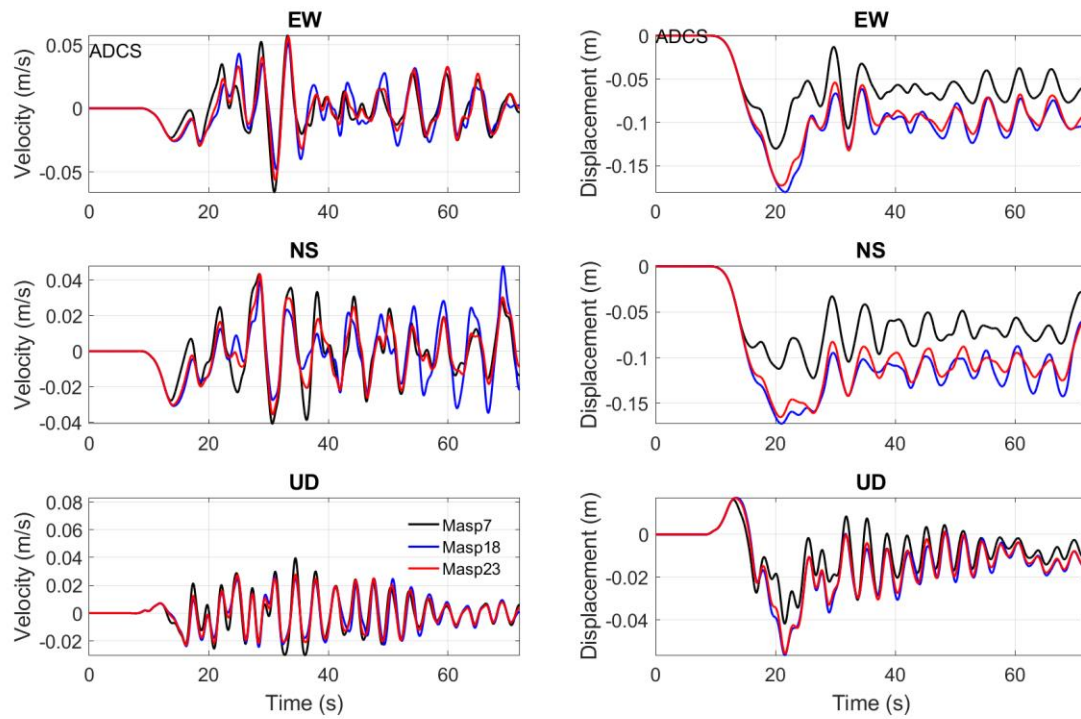


Figure A15. Three components of velocity and displacement ground motion compared between buried model 7 and surface rupturing models 18 and 23. Station ADCS.

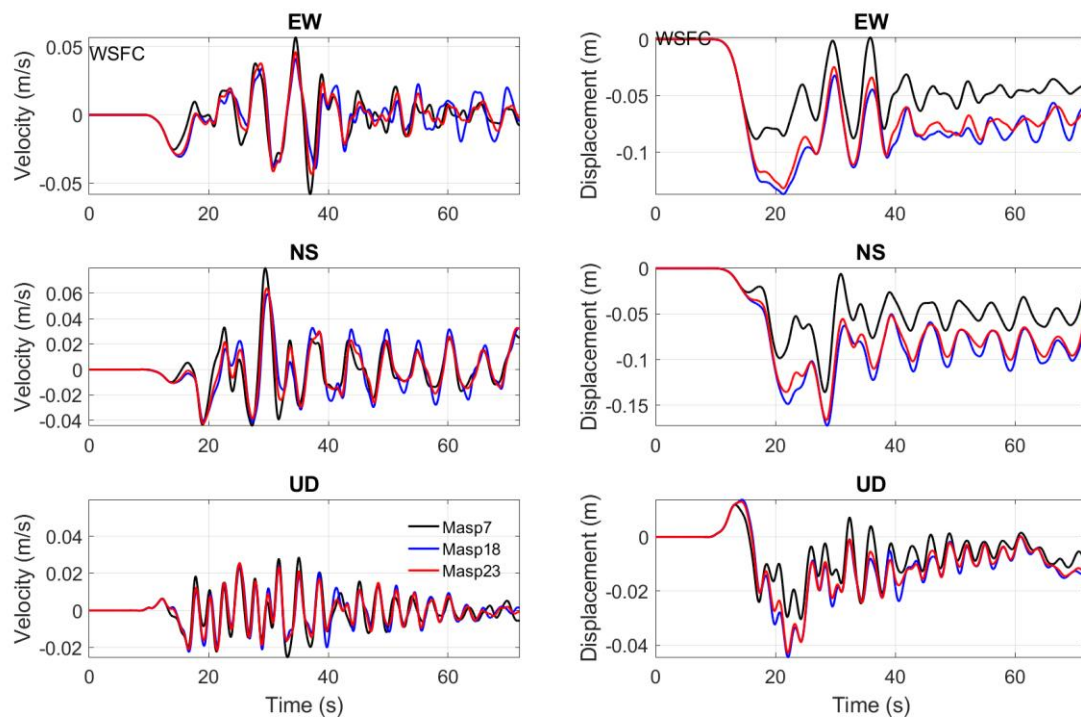


Figure A16. Three components of velocity and displacement ground motion compared between buried model 7 and surface rupturing models 18 and 23. Station WSFC.

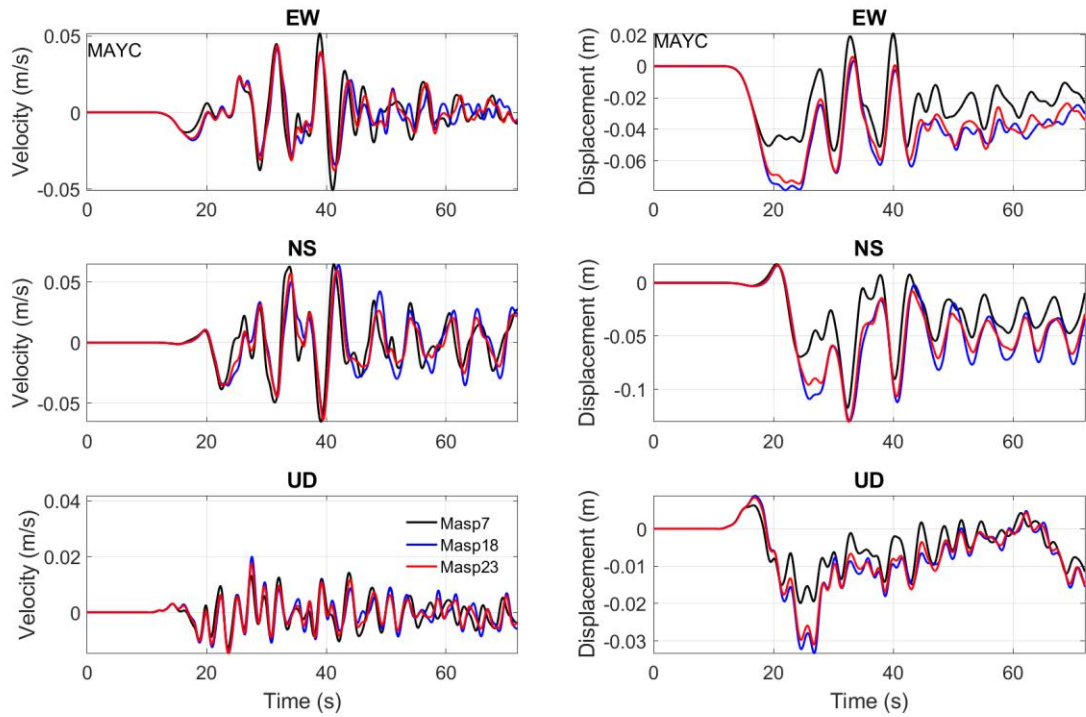


Figure A17. Three components of velocity and displacement ground motion compared between buried model 7 and surface rupturing models 18 and 23. Station MAYC.

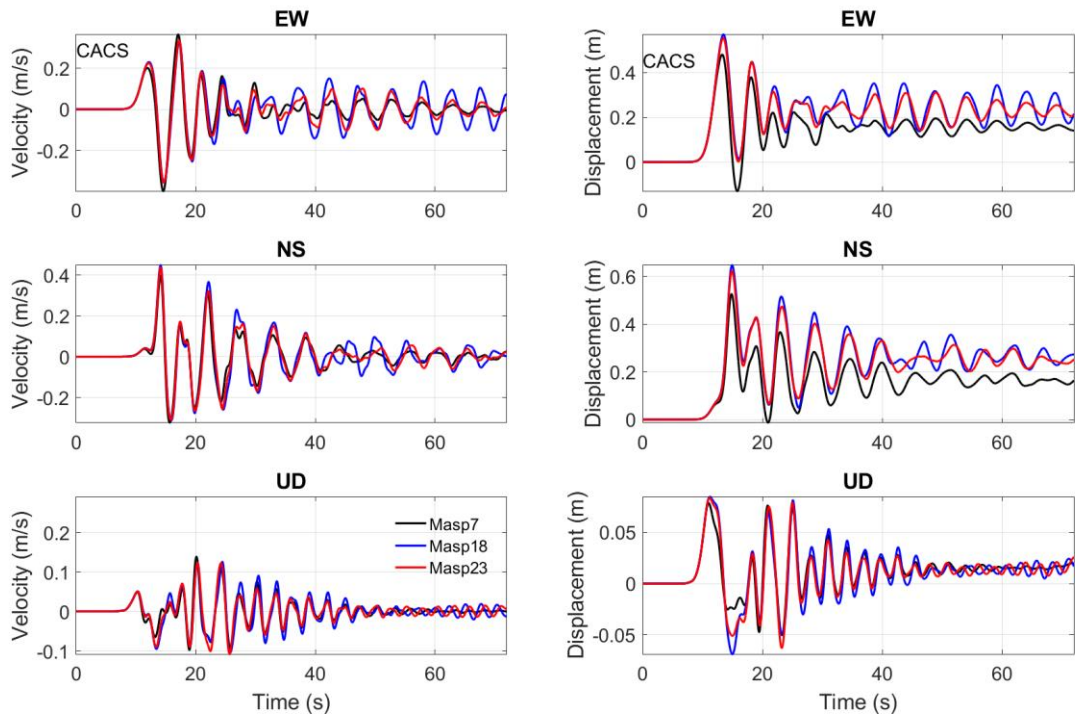


Figure A18. Three components of velocity and displacement ground motion compared between buried model 7 and surface rupturing models 18 and 23. Station CACS.

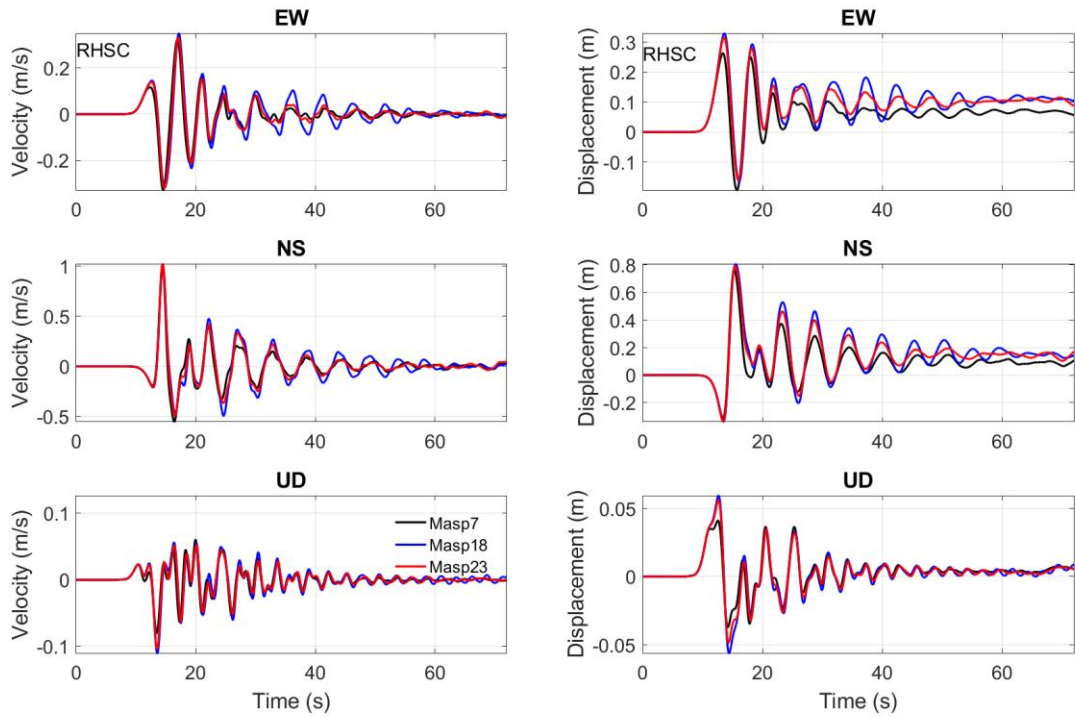


Figure A19. Three components of velocity and displacement ground motion compared between buried model 7 and surface rupturing models 18 and 23. Station RHSC.

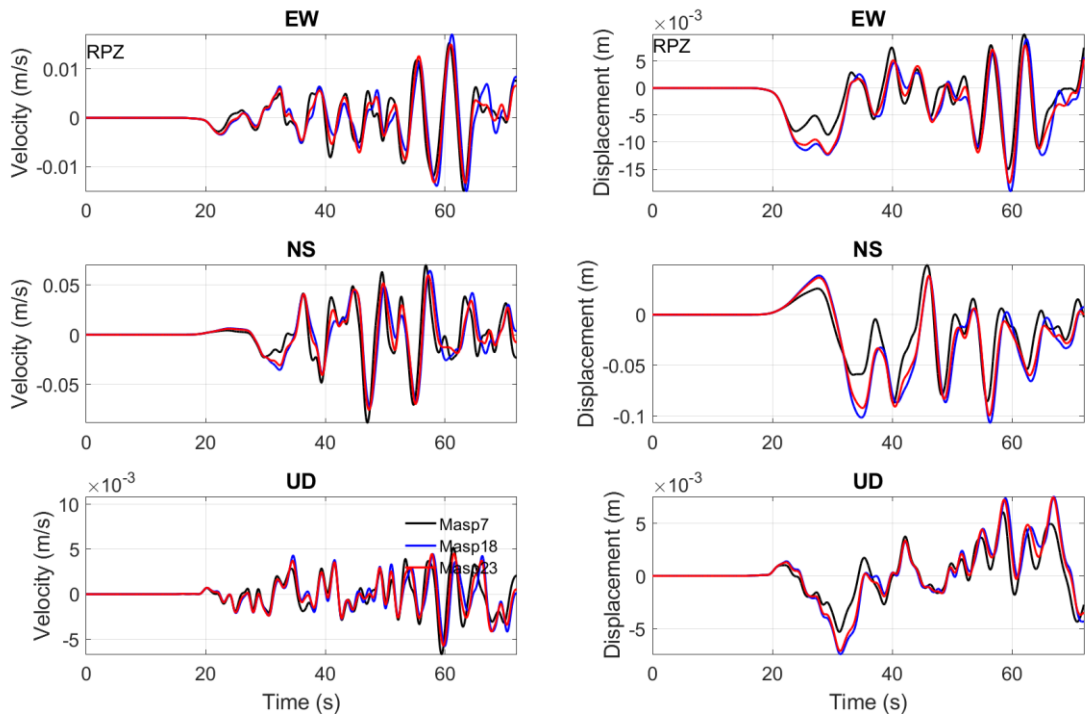


Figure A20. Three components of velocity and displacement ground motion compared between buried model 7 and surface rupturing models 18 and 23. Station RPZ.